A study of the influence of heat-treatment and gasification on the structure of microporous carbons.

Masters, Kenneth James

Award date:
1979

Awarding institution:
University of Bath

A Study of the Influence of

Heat-Treatment and Gasification on

THE STRUCTURE OF MICROPOROUS CARBONS

submitted by KENNETH JAMES MASTERS

for the degree of Doctor of Philosophy

of the University of Bath

1979

Kenneth Masters

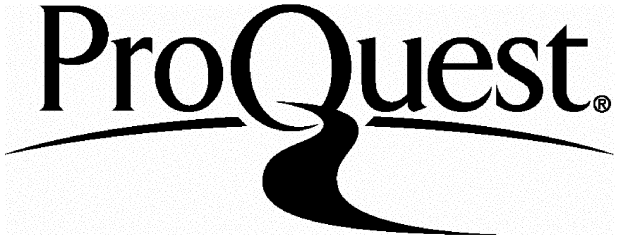

ACKNOWLEDGEMENTS

I wish to offer my gratitude to the following for their help during the course of this work.

Dr. B. McEnaney for initiating the project and encouraging its progress, Barry Chapman for his assistance with x-ray diffraction, Angela Harrington for her immeasurable patience with the typing, Mike Lock for his beautiful glassblowing, Drs. G.R. Millward (Cambridge) and J.R. Fryer (Glasgow) for their help with electron microscopy, Mr. H. Harris of NCB Stoke Orchard for ultimate analyses and Mr. Peter Wakeford and the technical staff of the School of Materials Science, for their practical assistance.

This thesis is dedicated, with appreciation, to my parents.

But nature is a stranger yet;
The ones that cite her most
Have never passed her haunted house,
Nor simplified her ghost.

To pity those that know her not,
Is helped by the regret
That those who know her, know her less
The nearer her they get.

Emily Dickinson

ABSTRACT

A study is presented of the effects of heat-treatment and gasification in CO_2 upon the microstructure of a cellulose carbon. Techniques used include, adsorption of CO_2 at 295 K, wide and small angle x-ray scattering, high resolution electron microscopy and quantitative measurement of the hydrogen evolved on heat-treatment to 1870 K.

From primary carbonisation temperatures to about 1470 K the principal effects are due to loss of hetero-elements, which cause the open micropore volume to increase. The pores in such carbons are identified as gaps between, and within, small aromatic groupings. The evolution of residual hydrogen allows these groups to coalesce and form layer-planes, which stack together to form diffracting crystallites. The process of stacking re-arranges the micropore volume to become increasingly associated with the spaces between ordered layer-plane stacks. This results in closure of closely-spaced parallel planes and reduced access for molecules to the micropore volume - causing a dramatic loss in open micro-porosity at about 1670 K. The dimensions of the retained micro-porosity increase continuously to 3000 K.

The effects of gasification are largely governed by accessibility of oxidant to the internal structure, with the internal ordering of layer-planes being of secondary importance. This results in low degrees of gasification having little effect on fine micropores, being restricted to burn-out of wide micropores to form mesopores. The presence of mesopores allows the latter stages of gasification

to occur within the structure. Pore entrances which have closed, or are prone to closure, are sufficiently inaccessible as to be unaffected by moderate gasification (less than 50% burn off). The development of mesopores is largely governed by initial accessibility of oxidant, which is in turn governed by heat-treatment temperature. Unlike micropores, mesopores are unaffected by heat-treatment to 1470 K, and probably beyond.

CONTENTS

CHAPTER 3

Preliminary Macroscopic Study

CHAPTER 4

Adsorption - Experimental and Theory

Page

CHAPTER 7

The Effects of Heat-Treatment

CHAPTER I

INTRODUCTION

CHAPTER 1

INTRODUCTION

The adsorptive properties of charcoals and active carbons have been known since the early 19th century[1], yet they continue to find increasing application in industrial and everyday life. This is partly because of their many advantages over rivals, such as ease of manufacture from a variety of source materials, stability to temperature and chemicals (except oxidants) and, being combustible, their disposal is relatively pollution free. However, such carbons still present considerable potential for further development, with carbon molecular sieves having only obtained limited success[2,3]. In order to "tailor" the adsorptive properties of carbons, a deeper understanding of the microstructure and combined effects of activation and heat-treatment are required. In addition, an upper temperature limit of ~1500 K, for processing or use, is imposed by the appearance of a rapid loss in surface area accessible to gas molecules[4-9]. An insight into this effect could result in graphitized carbons of high surface area. One can only speculate on the potential for these - fuel cell electrodes, catalyst supports for high temperature reactions and blood dialysis filters, to name a few.

It is the aim of this thesis to present a clearer understanding of the loss of accessible surface area at ~1500 K and to integrate this into the structural evolution of non-graphitizing

carbons from 770 ~ 3000 K. Cellulose was chosen for carbon preparation since it is fairly pure and produces reproducible carbon, free from unknown manufacturing processes. A small amount of work was also carried out on a commercial glassy carbon (SIGRI) and cellulose triacetate carbon. A number of complementary techniques were used since none are universally applicable or unequivocal in interpretation.

Format of Thesis

Chapter 2. The Structure of Carbon

To correctly interpret the results of this study one must have a realistic model for the carbon structure. Over the years, somewhat divergent views have arisen on this subject, so it was felt appropriate, and necessary, to review the literature on structure, in the light of recent developments.

Chapter 3. Preliminary Macroscopic Study

This study involved the use of scanning electron microscopy (SEM), mercury porosimetry and bulk shrinkage to identify any effects due to sintering or pore elimination.

Chapter 4. Adsorption - Theory and Experimental

Since a major part of this work uses adsorption, an introduction to the pertinent theory is given, together with details of experimental apparatus and technique.

Chapter 5. X-ray Studies - Theory and Experimental

The other major techniques used were wide angle x-ray diffraction (XRD) and small angle x-ray scattering (SAXS). A "readers

digest" of relevant theory is given for both techniques, together with experimental details.

Chapter 6. Elimination of Heteroelements

Many of the structural changes occurring at low HTT are due to continued secondary carbonisation. A study was made of heteroelement expulsion to separate these effects. The techniques comprised of ultimate analysis (CHO) and mass spectroscopic measurement of hydrogen evolution on heat-treatment.

Chapter 7. The Effects of Heat-treatment

Carbons were heat-treated by two methods - Isochronal (fixed time, variable temperature) and Isothermal (variable time, fixed temperature). The changes induced were examined by XRD, SAXS, adsorption and high resolution electron microscopy (HREM). The results are presented with a brief discussion.

Chapter 8. The Effects of Activation and Subsequent Heat-Treatment

Activation (partial gasification) is a common technique for modifying a carbon's porous structure. The first section of this chapter deals with the effect of activation on structure-drawing on x-ray, adsorption, HREM and SEM techniques. The second section is an adsorption and SAXS study of the effects caused by heat-treating (to 1470 K) carbons of varying activations. The Chapter concludes with a summary and discussion of activation.

Chapter 9. Low Pressure Adsorption

The use of adsorption as a structural tool is limited by the

assumption that all effects are structural in origin. One must therefore be careful to identify "non-structural" effects. It is believed that such effects can occur at low pressure, hence this point is amplified in this Chapter.

Chapter 10. General Discussion on the Effects of Heat-Treatment

An integration of the previous Chapters and general discussion of the evolution and changes occurring from 770 ~ 3000 K is given here, together with suggestions for further investigation.

CHAPTER 2

THE STRUCTURE OF CARBON

CHAPTER 2

2.1.1. THE STRUCTURE OF CARBON

The crystalline forms in which carbon can exist are many and multifarious. Reasonably well-known are the hexagonal and rhombohedral forms of graphite and cubic and hexagonal forms of diamond. Not so well-known are the recently discovered "carbyne" forms. The crystalline forms will now be described then a survey of the structure of non-crystalline carbon will be given.

Hexagonal diamond (also called Lonsdaleite)[10] is a wurtzite form which was first noted in meteorite fragments and later synthesized[11]. Cubic diamond is the commonly-met form which comprises of an extended network of carbon atoms with a tetrahedral arrangement of covalent bonds, length 0.154 nm. This structure accounts for diamond's hardness and high density (3.52 g ml^{-1}). At normal atmospheric pressure and temperature diamond is thermodynamically unstable, transforming into the most stable form of carbon-hexagonal graphite. However, since temperatures of about 2200 K are required for the transformation[12] to occur at a significant rate, diamond is kinetically stable.

Hexagonal graphite is composed of extended sheet-like layers of atoms arranged in hexagonal networks. The stacking sequence of the layers was suggested as ABAB ... by Hull[13] and later determined by Hassel and Mark[14] and Bernal[15]. This structure is shown in figure 2.1.

An alternative stacking sequence of ABCABC ... was suggested by Debye and Scherrer[16]. The existence of a fraction of this so-called rhombohedral graphite in natural graphite was found much later[17,18].

Rhombohedral graphite can also be produced by grinding natural graphite[19] but is unstable and reverts to the hexagonal form on heating.

2.1.2. Pauling's Quinoid Model

Hexagonal graphite is assumed to be completely resonating, i.e. all bonds are of equal strength and arranged at 120^{o} to each other. However, observations from electron [20] and x-ray diffraction patterns[21] of graphite single crystals seemed to suggest an orthorhombic lattice. Pauling and Lukesh[22] explained this by postulating a quinoid structure where each carbon atom forms one bond with a large double bond character and two with a lesser amount. Pauling[23] later suggested that single crystal graphite existed in the quinoid form, since this explained its high basal plane compressibility at low pressure[24]—higher than that of diamond. He also maintained that carbons with interlayer spacings of 0.344 nm were of the completely resonating type, while those with a spacing of 0.3354 nm were of quinoid form. This was because the quinoid form has a superior ability to minimise the interactions of electron density bulges of adjacent layers. Ergün [25] claimed his integrated x-ray intensities for a pyrolytic graphite also favoured a quinoid structure but Donohue[26] has pointed out serious errors in his results.

The basal plane compressibility has been adequately explained [27] in terms of the hexagonal rings buckling under pressure. This buckling also explains the high pressure phase transformations which occur in graphite. Other reasons for doubting the quinoid models are the

lack of observed a-axis anisotropy and lack of (hkl)($l \neq 0$) diffraction lines in carbons with d_{002} = 0.344 nm. The latest neutron and x-ray diffraction studies[28,29] confirm the classical Bernal hexagonal structure.

2.1.3. Carbyne forms

Since 1968 evidence has been amassing to suggest the existence of a family of polymorphic carbon forms. The first of these to be discovered was chaoite (or white carbon) which was found in a meteorite crater[30]. Since graphite occurred naturally in that area the chaoite was believed to have been produced by the impact on the graphite. A recent alternative view[31] is that the chaoite existed naturally there. Chaoite has been artifically made by heating graphite under low pressure[32,33] and is harder than B_4C.

Another allotrope, Carbon VI, has been formed by resistive or laser heating of graphite. Its structure is intermediate between Lonsdaleite and chaoite and has been suggested as a distorted form of chaoite[34].

To date, Whittaker[35] has found evidence for eight or more forms while five of these have been found by Kasatochkin et al[36]. They were all distinguished by their a_o unit cell parameter and all appear to have hexagonal symmetry. The cell parameter c_o is only known for chaoite, α carbyne, β carbyne and carbon VI, so positive identification of all types is not yet possible.

The Russian workers proposed these forms to consist of (- C ≡ C -) units, probably as chains[37], hence they were termed "carbyne"

forms. This structure is supported by the work of Kasatochkin et al[38] and the laser Raman results of Nakamizo and Kammereck[39]. It is believed that the chains are stacked in a hexagonal array so that a number of possible varieties can exist by varying the stacking relative to the triple bond positions.

Although similar crystallographically, some carbyne forms are very soft and some very hard, which indicates a wide variation of the degree of cross-linking between chains for different forms. Since if crosslinking were carried to its limits the result would be diamond, it seems that the forms may be intermediate in the graphite-diamond transition. There is some evidence for this [40,41].

Whittaker[35] has shown that graphite is unstable above 2600 K at any pressure and suggests that it transforms, via an unzipping mechanism, to the carbyne forms. He has therefore proposed a new phase diagram to take account of this (figure 2.2). Although apparently only stable at high temperature, it appears that the carbynes are metastable since recent investigations [31] have shown them to exist in many natural graphite formations, world-wide. Indeed, many samples of 'graphite' have turned out to be solely consisting of carbyne forms with no graphite. These samples were previously thought to be impure graphite.

2.2.1 Non-crystalline carbon

Introduction

The foregoing section dealt with crystalline forms of carbon but much of the carbon in use today is not crystallographically well-developed.

Franklin[42] divided non-graphitic carbons into two categories - those which develop extensive three-dimensional graphite on heating to temperatures in excess of ca. 2000 K (graphitizing, or soft carbons) and those which only form two-dimensional graphite of restricted crystallite size (non-graphitizing or hard carbons). Carbons falling into the latter category are charcoals, active carbons, carbon blacks, high or low rank coals (not the so-called coking coals), chars and glassy carbon (GC). The organic materials which form these carbons usually char or fuse but do not form a mesophase, on pyrolysis.

Franklin's discrete classification is now seen as an oversimplification, with many materials of intermediate nature being observed[43,44]. This finding, however, does not affect the general principles involved in determining whether a carbon graphitizes or not and so Franklin's classification will be adhered to, for convenience.

Non-graphitizing carbons have a variety of names, some correctly, some incorrectly, describe their structure. These are : - charcoals, amorphous, mesomorphous, isotropic, chars, paracrystalline, microcrystalline, microporous, hard, vitreous and glassy carbons. To avoid any implied structures or properties the term "hard" will be used to describe non-graphitizing carbons in general.

2.2.2. Structure of hard carbons

The first structural analyses of such carbons were carried out on carbon blacks. Because the x-ray patterns consisted of two or three diffuse bands, which appeared similar to the halos of a liquid pattern, many workers believed carbon blacks to be amorphous. Other workers,

noting that these lines corresponded to the strongest lines in graphite, concluded that carbon blacks were microcrystalline graphite.

Warren [45] used Fourier integral analysis to construct a distribution of atoms about any one atom. The resultant radial distribution function showed carbon black to be composed of individual graphite layers, which were in turn composed of a hexagonal network of carbon atoms. Two years later Hoffman and Wilm [46] noted the absence of three dimensional graphite lines {(hkl), $l \neq 0$} from the pattern for a finely crystalline carbon. Since only (hk0) reflections occurred, these must be due to lines of atoms within the layer-planes and not due to planes between the layers. In this case the Miller index l has no meaning and is often omitted - leaving the abbreviated notation (hk) for such two-dimensional reflections. Such carbons cannot, therefore, be composed of three-dimensional graphite, but only of two-dimensional layers which are roughly parallel and equi-distant, but not oriented with respect to each other in the a axis directions.

Although many workers recognised the two dimensional nature of such carbons, it remained for Warren [47] to develop the theory of diffraction by a random layer lattice. The term "turbostratic" (unordered layers) was later coined by Biscoe and Warren [48] to describe the random translation, about the a axis, and rotation, about the c axis, of layer-planes. Figure 2.3 illustrates a turbostratic crystallite [49]. Noteworthy in this model is the presence of defects, vacancies, and bends within the layer-planes.

After studying x-ray patterns for a number of chars and coal cokes, Riley and co-workers[50,51] proposed two types of structure: elementary turbostratic crystallites and a disordered cross-linked space lattice of carbon hexagons (Figure2.4). The latter structure can conveniently be made from a combination of tetraphenylene units, and is expected to be stabilized by heteroatoms, notably oxygen which is common in low-temperature chars. The two structures were not meant to be exclusive but could occur together in varying amounts depending on starting material and conditions of preparation.

The very thorough x-ray investigations of Franklin on PVDC char[52] also showed a high fraction (35%) of highly disordered carbon and she eventually visualised the structure as randomly oriented crystallites, rigidly bound together by strong crosslinks[42]. A soft carbon has much greater alignment of crystallites with fewer, or weaker, crosslinks (Figure 2.5).

Considerable fractions of amorphous carbon were also found in the analyses of Hirsch [53] and Diamond [54] of the (hk) reflections of carbonised coals. Diamond's findings [55] that half of the amorphous carbon was associated with layer-plane edge atoms suggested that such carbon constituted cross-links.

In view of the high fractions of amorphous carbon, Ergun and Tiensuu [56] questioned the assumption that the observed diffraction patterns were entirely due to trigonal atoms, stating that the diffraction patterns of small groups of tetrahedral atoms coincided with the graphitic (hk) peaks. Their conclusion that tetrahedral atoms may exist is, however, not rigorously based as the

resemblance is only limited to the (10) and (11) peaks. Further work is required to justify their decision [57].

2.2.3 Structure of Glassy Carbon

The structural study of hard carbons received impetus from the advent of glassy (vitreous) carbons[58] prepared from thermosetting resins. One of the first radial distribution analyses of glassy carbon (GC) was carried out by Noda and Inagaki [59]. Their findings pointed to small two-dimensional graphite layers linked together by tetrahedral bonds. The tetrahedral atoms do not make any regular arrangement with themselves. Furukawa [60] proposed a structure consisting of a three-dimensional network of tetrahedral, planar double, linear triple and conjugated C - C bonds, with no more than three hexagonal rings grouped together. Furukawa's model is considered most appropriate for carbons of low heat-treatment temperature (HTT) i.e. < 1000 K, where it is identical with Noda and Inagaki's model.

Kakinoki's model [61] of equally sized tetrahedral and trigonal regions, cross linked by oxygen, was later discredited as being based on incorrect oxygen analysis [62].

A rather complex model based upon the existence of Sp^3, Sp^2, Sp atoms, (- C ≡ C -)n and (C = C =)n chains was proposed by Khomenko et al [63] for vitreous carbons heat-treated from 1773 K to 3273 K. The 1773 K carbon was believed to consist of Sp^3 and Sp^2 atoms whilst heat-treatment to 3273 K caused the appearance, disappearance then re-appearance of chain(carbyne and carbene) carbon. The existence of Sp^3 carbon at high temperature was explained by

postulating strong local compressive stresses due to anisotropic thermal expansion[42]. It is possible that at very high temperatures some carbyne chains may be formed (see section on carbyne forms) since the vapour pressure of carbon becomes significant and carbon chains are known to exist in the vapour[64]. Despite these findings the amount of non-Sp^2 carbon is believed to be small. Since Khomenko's work was based on x-ray radial distribution analysis, it is unfortunate that no mention was made of the many corrections which must be made[65], or the effect of termination errors.[66,67]

A thorough radial distribution analysis of a 2073 K GC by Wignall and Pings[68] gave no evidence for tetrahedral atoms with all the peaks being satisfactorily indexed to graphite. The same conclusion was reached by Mildner and Carpenter[69] using neutron beam scattering. This technique is capable of higher spatial resolution than with x-rays but could only detect a peak at 0.142 nm (trigonal) but none at 0.154 nm - which would correspond to tetrahedral bonding. They placed an upper limit of 8% for the content of tetrahedral atoms in their 2273 K GC.

Saxena and Bragg[70] studied the x-ray K emission band for diamond, pyrolytic graphite (c axis parallel to incident electrons) and heat-treated GC. They found the peak x-ray wavelength of GC lay between those for diamond and graphite and moved towards graphite, with HTT. Their conclusions that GC contains both trigonal and tetrahedral atoms and that the latter transform to the former with heat-treatment are open to question for the following reason. The peak profile for a crystal is orientation dependent[71] and thus a polycrystalline material would give a composite peak which, in

this case, falls between that for graphite in parallel and perpendicular orientation. The latter orientation gives a peak close to that for diamond, hence the observed GC peak need not indicate any diamond-like structures. The peak's shift with HTT could be caused by annealing of defects, increase in crystallite size or increased alignment of aromatic rings - all of which could increase electron delocalisation and thus stabilise the energy levels. Such changes would be expected to shift the K band towards the more stable Sp^2 wavelength. X-ray photoemission studies[72] on the same GC sample also suggested both tetrahedral and trigonal atoms - the latter in preponderance.

This wealth of conflicting data perhaps indicates that our concept of clearly defined Sp^2 or Sp^3 atoms may not be the best. In a severely distorted trigonal structure, atomic bonds may be sufficiently bent to produce apparent hybridisations between Sp^2 and Sp^3. Sp^3 atoms are not essential for the formation of three-dimensional, non-graphitizing structures, since 3-dimensional cage-like structures can be built from tetraphenylene units (Figure 2.4) as suggested by Riley[51]. Such structures can be quite rigid and are entirely composed of trigonal atoms, so may be envisaged as being bridging groups between adjacent aromatic layers in low temperature carbons. Moreover, the rupture of the non-aromatic σ bonds would enable the phenyl rings to assume more planearity and eventually combine to extend the graphitic layers - possibly introducing a bend in the newly-formed layer-plane. This mechanism of layer-plane growth agrees well with that proposed by Diamond and Hirsch[73] for carbonisation of coals and would represent layer evolution up to about 1700 K.

2.2.4. The Impact of High Resolution Electron Microscopy on Structure

The advent of high resolution electron microscopes (HREM) has considerably aided our understanding of carbon microstructure. Lattice fringe images obtained by this technique indicate layer-planes to be considerably larger than the values obtained by line broadening methods. This simple observation confirmed the x-ray results of Maire and Mering[74] whose radial distribution analyses show layers to be at least twice as large as that indicated by (hk) profile analysis. Their view of the coherent scattering domain being limited by internal distortions, also suggested by Ergun[75], was vindicated by the considerable bending and twisting of the lattice fringes. The view of a polymeric structure made from a folded network of layers, where folds constitute sources of strain, or crystallite boundaries from a diffraction viewpoint, was suggested by Ergun and Schehl.[76,77] Their Fourier transform analysis of the (hk) reflections also shows the hexagonal rings to be distorted - a surprising finding considering their sample was a 3273 K glassy carbon, but no doubt indicating the extreme difficulty of straightening out bent interweaved layer-planes. A similar model has been suggested by Braun and Fitzer[78] and Rousseaux and Tchoubar.[79] The latter workers' analysis also shows the layer-planes to be longer in one 'a' direction than the other, i.e. the layers were more like ribbons than sheets.

From an intuitive interpretation of lattice fringe images, temperature dependence of specific heat,[80] and its ability to intercalate potassium,[81] Jenkins, Kawamura and Ban[82] proposed a model of intertwined graphitic ribbons (Figure 2.6) for GC. This model is essentially the same as that proposed for carbon fibres[83] but without preferred orientation. Jenkins' model should be viewed

with caution since lattice fringe images (on which his model relies heavily) are two dimensional representations of a three dimensional structure. Oberlin[84,85] has demonstrated the possibility of misinterpretations in such images.

Ban, Crawford and Marsh[86] used similar techniques as Jenkins et al to study PVDC carbons but claimed PVDC carbon had a different structure from the phenolic carbons studied by Jenkins et al. It is hard to identify any significant differences between the lattice fringe images of PVDC and phenolic resin carbons or indeed between any hard carbons, except carbon fibres, of the same HTT.

Ban's structural model (Figure 2.7) is, however, more realistic than Jenkins' due to a closer packing of ribbons and, more importantly, a continuous variation in stacking heights. Jenkins' model shows remarkable uniformity of L_c. Ban's model is supported by Ergun's[87] finding that the number of stacks with n layer-planes decreases exponentially with n.

2.2.5. DISCUSSION

An important point which is missing in all the models described so far - except that of Ban et al , in which it is intuitive - is that the building unit in hard carbons is not the crystallite (i.e. layer-plane stack) but the layer-plane.

In the mechanism of carbonisation of hard carbons there is no reason why the growth of one layer should be influenced by the growth of a layer adjacent or above it. Such growth is largely dictated by the original polymer's molecular orientation and carbonisation

mechanism[88]. One therefore obtains a tangled network of individual layer-planes which, in certain regions, overlap and stack up to produce a coherently scattering domain. Such a view also explains why the interlayer spacing rarely falls below the turbostratic value of 0.344 nm since this is a result of a random distribution of layer-plane a-axes in the stack (Figure 2.8).

One can also see why the stack height distribution has such a statistical nature - the probability of a high stack decreases with stack height. The ultimate crystallite sizes in a and c directions are clearly decided during the primary carbonisation stage. Growth of crystallites is limited to annealing of defects within and between layer-planes so that the formation of three-dimensional graphite, without a major re-orientation of the layer-planes, is impossible. Such carbons are therefore non-graphitizable. Disordered carbon may be visualised as being concentrated at layer edges and folds. There seems little need to invoke the concept of restraining cross-links which remain to high temperature, as the tangled network structure effectively prevents three dimensional ordering of layers. The existence of microporosity in such carbons is now seen as due to the inability of the layer-planes to pack together perfectly. Micropores can therefore be described as the space within the tangled layer-plane network and as a result will constitute a very high surface area - as is found to be the case.

The situation for soft carbons is different as the basic building unit here is the crystallite. This can be formed during carbonisation as a result of the increased mobility of forming aromatic layers. The observation of anisotropic flow lines[89] in the mesophase implies

preferred orientation of the evolving crystallites and so prevents the formation of a tangled microstructure. Defects will become in-grown and these will place an ultimate (though large) limit on crystallite size. The build up of defects, at crystallite boundaries, seems to limit the re-crystallization of even a well-formed pyrolytic graphite[90] .

2.3.1. Porous Structure of Carbons

Carbons can exhibit a variety of pore sizes and it is useful to classify them according to size. A study of active carbons and charcoals by Dubinin and co-workers[91] suggested the existence of a trimodal distribution of pore sizes. The three types have since been classified by the IUPAC[92] so :

Macropores - widths larger than 50 nm

Mesopores (previously termed transitional or intermediate) 2 - 50 nm

Micropores - smaller than 2 nm.

It has recently become expedient to further divide micropores into supermicropores (largest) and ultramicropores (smallest). There is currently disharmony on the demarcation size with Dubinin[93] proposing ultramicropores as having a *radius* of less than 0.6 - 0.7 nm, whilst Everett and Powl [94] suggest them to have a *width* less than 0.8 nm (or an available slit width of 0.53 nm, after subtracting electron orbital extensions). The classification of Everett and Powl will be used throughout this thesis since it is consistent with the physical basis of distinction between the two

pores, which became apparent from this work.

2.3.2. Origins of Porosity

Macropores

These are usually associated with morphological features, for example, a macroporous precursor which chars will form a macroporous carbon pseudomorph. Carbons which fuse prior to, or during, carbonisation (cokes) often exhibit a small macroporosity due to shrinkage cracks, and bubbles retained from the plastic stage. Macropores can occur in graphitizing and non-graphitizing carbons.

Mesopores

Mesopores are generally uncommon in carbons which have not been activated, since the precursor materials are usually fairly uniform on this scale. Mesopores, formed by partial gasification, are quite important in commercial active carbons since they may constitute a useful surface area for adsorbing very large molecules, as well as providing transport channels to micropores.

Micropores

Because of their size micropores provide the major contribution to total surface area. They are only found, in significant proportions, in non-graphitizing carbons - this being a direct result of the latter's disordered atomic structure (see page 17). Because of its origins microporosity is largely unaffected by the nature of precursor (provided it is non-graphitizing), though it can be affected by any manufacturing process which affects the microstructure (such as stretching or oxidation during carbonisation).

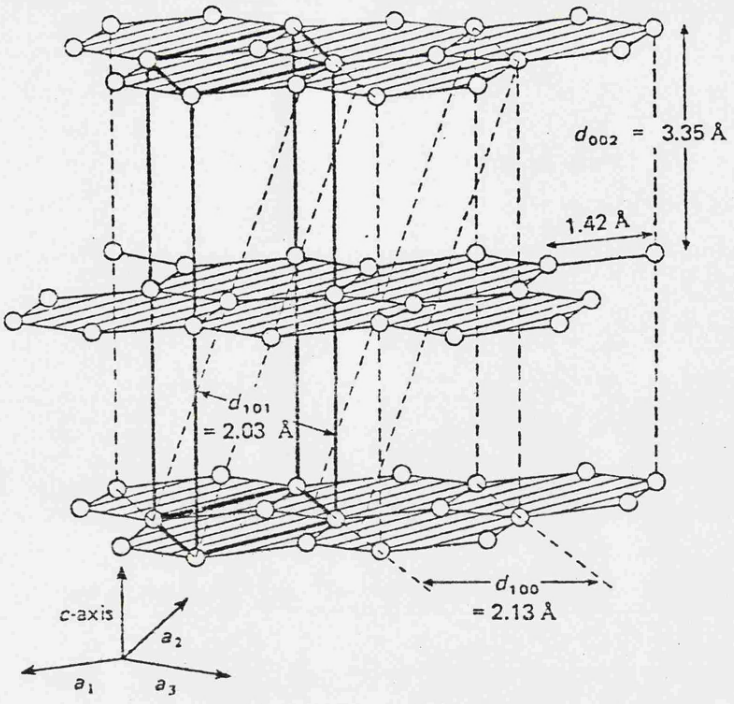

Fig. 2.1

Perfect graphite lattice (unit cell outlined)

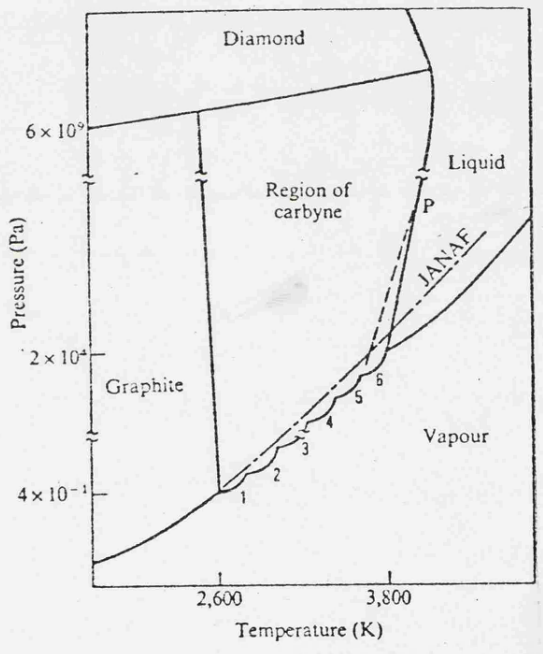

Fig. 2.2

Modified carbon phase diagram.

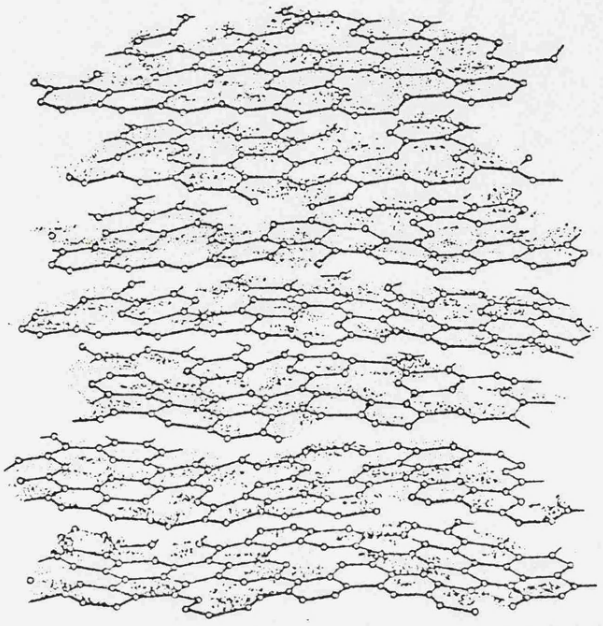

Fig. 2.3

Turbostratic carbon

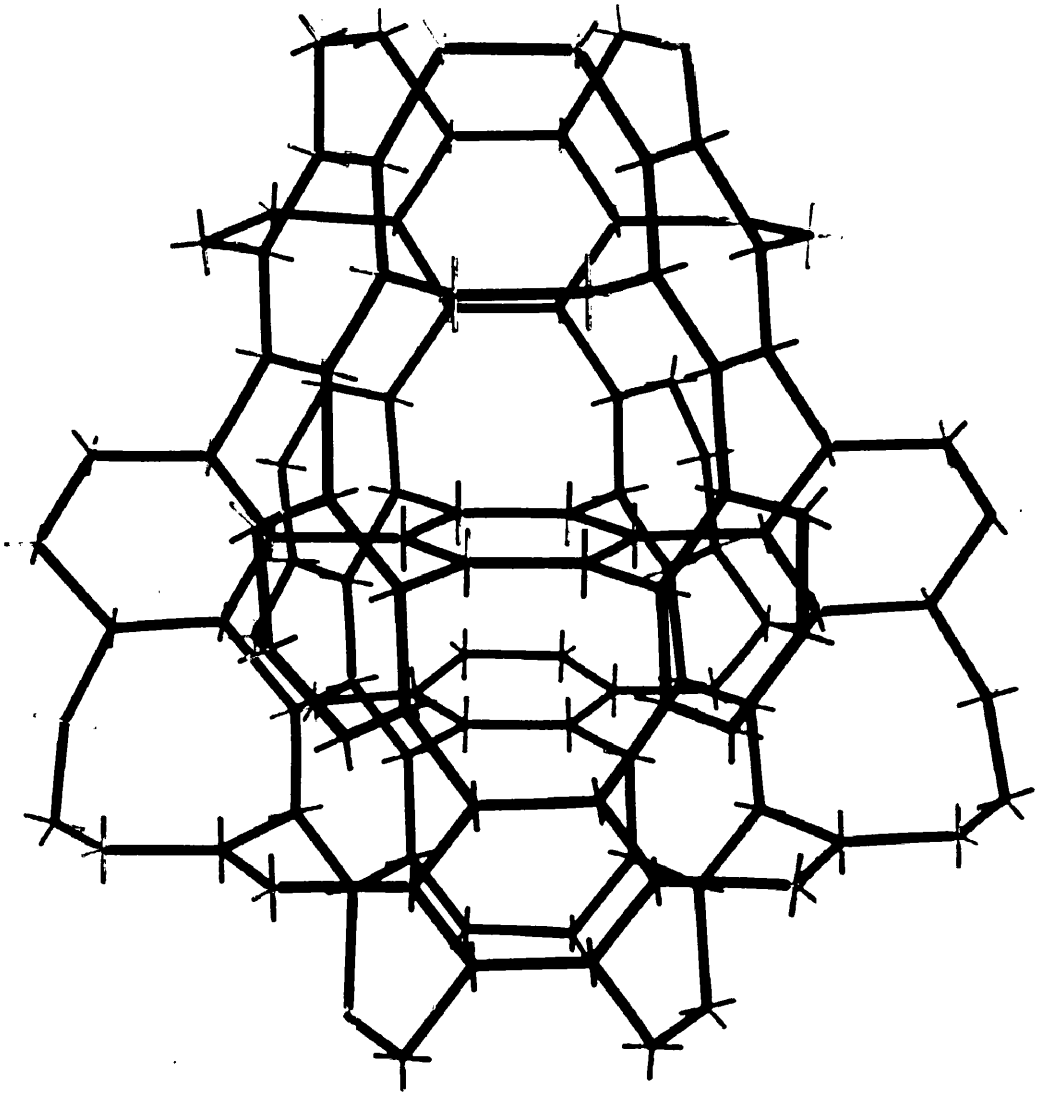

Fig. 2·4 3-D Tetraphenylene structure.

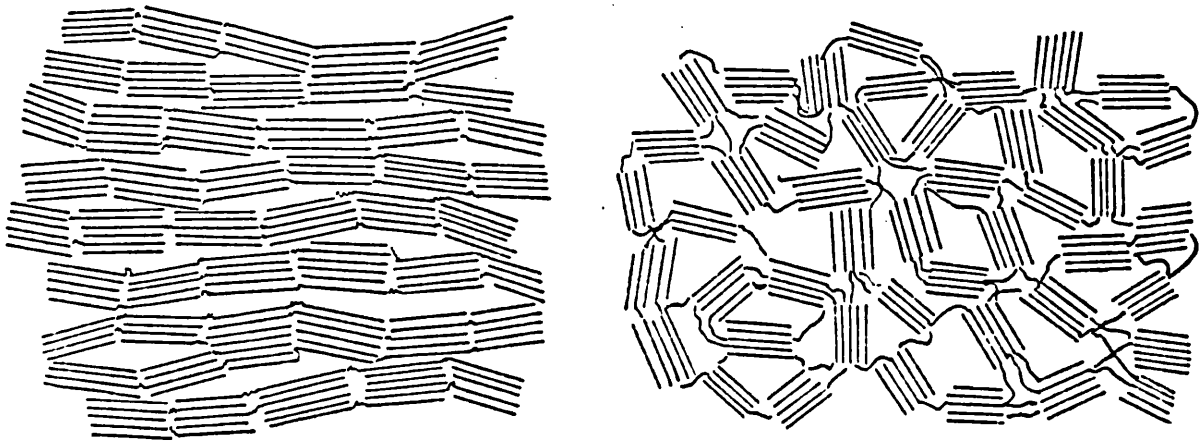

Graphitizing. Non-graphitizing.

Fig. 2·5 Franklin's models.

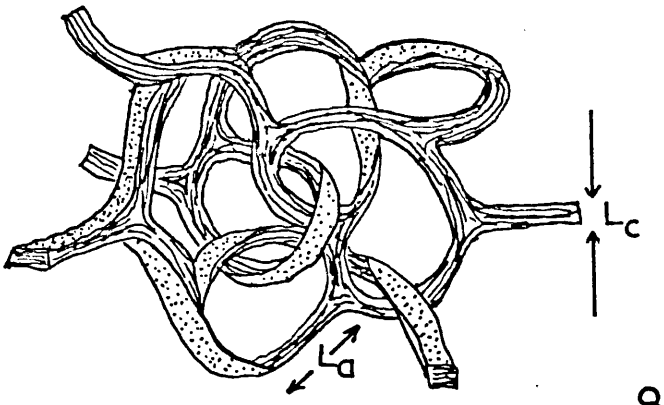

Fig.2.6 Model due to Jenkins et al.[82]

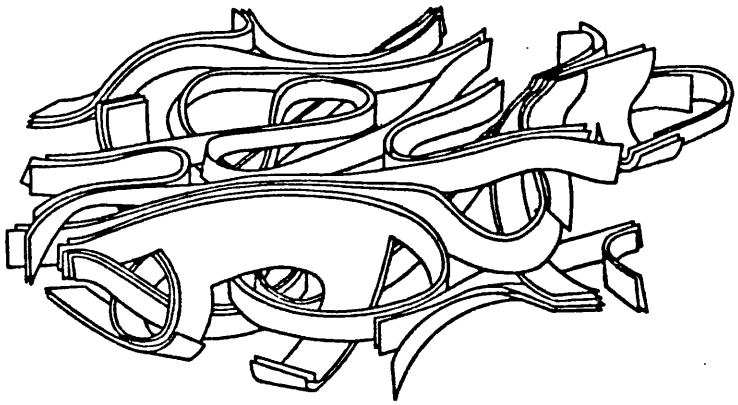

Fig.2.7 Model due to Ban, Crawford & Marsh (ref. 86)

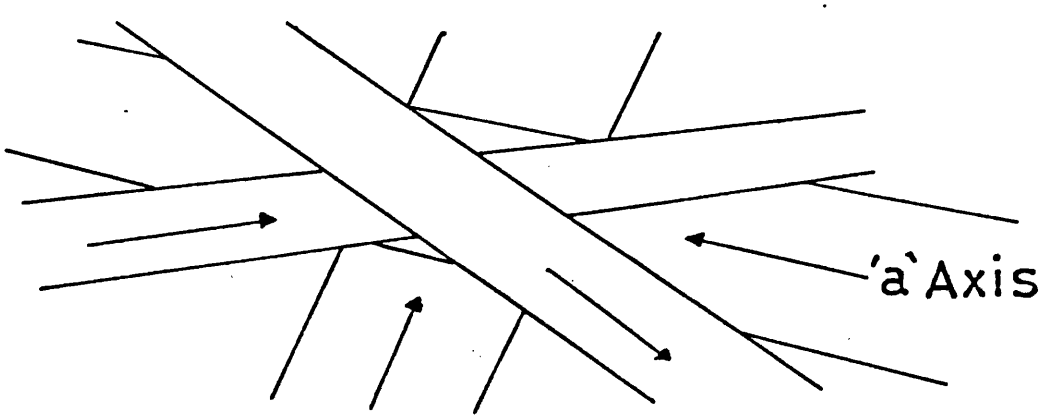

Fig.2.8 Random stacking of layers constituting a crystallite.

CHAPTER 3

PRELIMINARY MACROSCOPIC STUDY

CHAPTER 3

Preliminary Macroscopic Study

The loss of the adsorption capacity of active carbons upon heat-treatment has been described by some as a sintering process. The onset of sintering is frequently noted at about half the absolute melting point (the Tamman temperature) and this corresponds to about 1700 K for graphite (although graphite sublimes rather than melts). It is possible, therefore, that the observed pore closure effect may be due to a sintering and closing off of macropores. To investigate this question carbons of HTT 1170, 1470, 1670 and 1870 K were examined by Mercury Porosimetry , Scanning Electron Microscopy (S.E.M.) and bulk shrinkage.

3.1.1. Mercury Porosimetry

Since mercury has a negative contact angle with most solids, pressure must be exerted to force it into a porous body. The pressure required will be related to the pore radius by the Laplace equation. Inserting the values for the contact angle and surface tension, we obtain : -

$$R = \frac{7,500}{P}$$

where R is the pore entrance radius in nm and P is the pressure in kg cm^{-2}.

By measuring the amount of mercury absorbed against the pressure exerted, a pore size distribution can be obtained.

3.1.2. Experimental

Samples of powdered carbon (ca. 1 g) were examined in a Carlo Erba 1520 mercury porosimeter. The carbon was evacuated by a rotary pump for about one hour before filling the dilatometer with mercury. The pressure exerted varied between 1 and 1500 kg cm^{-2}, which corresponds to a pore radius range of 7,500 to 5 nm. The curves were corrected for mercury compressibility by running a blank and subtracting this.

3.1.3. Results

The results are presented as a plot of percentage total volume contained within pores smaller than a radius R against R (figure 3.1). There is little difference between the samples and they certainly show no macropore closure effects. The small variation up to 1000 nm is probably due to differences in packing of the powders as a large proportion of particles passed a 100 μm sieve. Most of the pore volume (~ 80%) is in the range 0.5 - 5 μm with little evidence for mesoporosity. The large size of the mercury molecule prevents micropores being penetrated. One must be cautious with this technique at high pressure as damage to specimens, such as fracturing closed pore walls, can occur and this would distort results.

3.2.1. Scanning Electron Microscopy

S.E.M. is a convenient technique for examining macro and large mesoporosity since it is capable of high magnification coupled with good resolution and an excellent depth of field, also

there is no limit to specimen thickness.

3.2.2. Results

Micrographs obtained with a Cambridge Instruments Stereoscan S4 are shown in figs. 3.2 and 3.3 for carbons of HTT 1170 and 1870 K. The difference in morphology is due to the 1170 carbon having been ground to powder, whilst the 1870 sample is the surface of a pellet. Nevertheless, it is evident that a macroporosity in the range 1 - 10 μm is present in both carbons, and this has not closed off. The 1870 carbon also does not show any evidence of sintering, such as neck growth or corner rounding. The pore sizes visible are in close agreement with those from mercury porosimetry. A higher resolution JEOL 100 CX electron microscope was used in scanning mode at 40,000 X, but could not identify any further porosity down to ~20 nm.

3.3.1. Bulk shrinkage

Any pore elimination due to sintering would cause an increase in bulk density, hence it is useful to have information on the volume changes accompanying carbonisation and heat-treatment.

3.3.2. Experimental

The diameters of a series of cellulose pellets made under identical conditions - see Appendix A(1) - were measured before and after carbonisation. Carbons of HTT >1170 K were separately heat-treated for 10 mins. (Appendix A(4)), then re-measured.

3.3.3. Results

The total shrinkage is plotted against HTT as shown in figure 3.4. It is clear that very little shrinkage occurs beyond 1270 K. The slight *swelling* noted at high HTT is within the limits of experimental error and can be traced to variation during the carbonisation stage (i.e. up to 1170 K). The same lack of shrinkage was found for the longitudinal direction, but these results are not presented here because one cannot take account of the release of stress, locked in from the compression stage.

The lack of shrinkage in the temperature region of adsorption loss would seem to preclude any pore elimination effects.

3.4 General Conclusions

The macroporosity in these carbons results from a pseudomorphic structure of the original cellulose fibres. There seems little evidence for the existence of mesoporosity in these unactivated carbons. Heat-treatment appears to have a negligible effect on macropores, so we may safely conclude that the loss of adsorptive capacity is due to changes occurring on a microstructural scale.

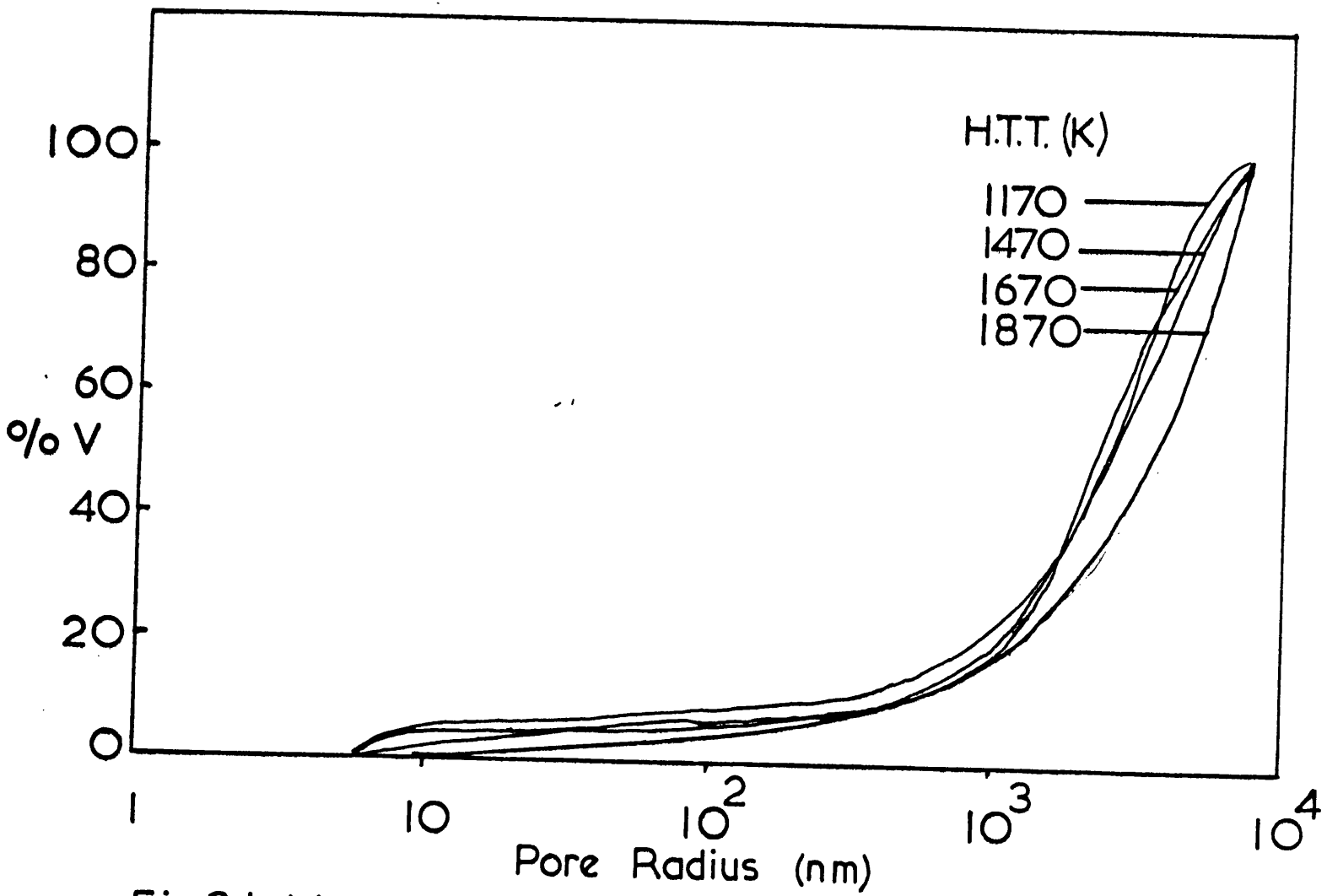

Fig.3.1 Mercury Porosimetry Curves for Heat-treated Carbons.

Fig.3.2 1170 K 10μm

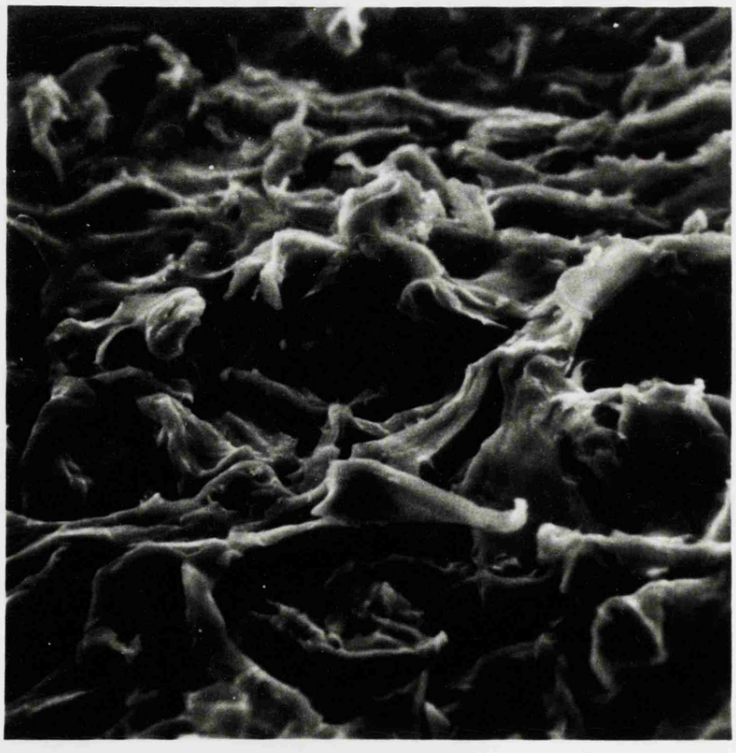

Fig.3.3 1870 K 10μm

Scanning Electron Micrographs.

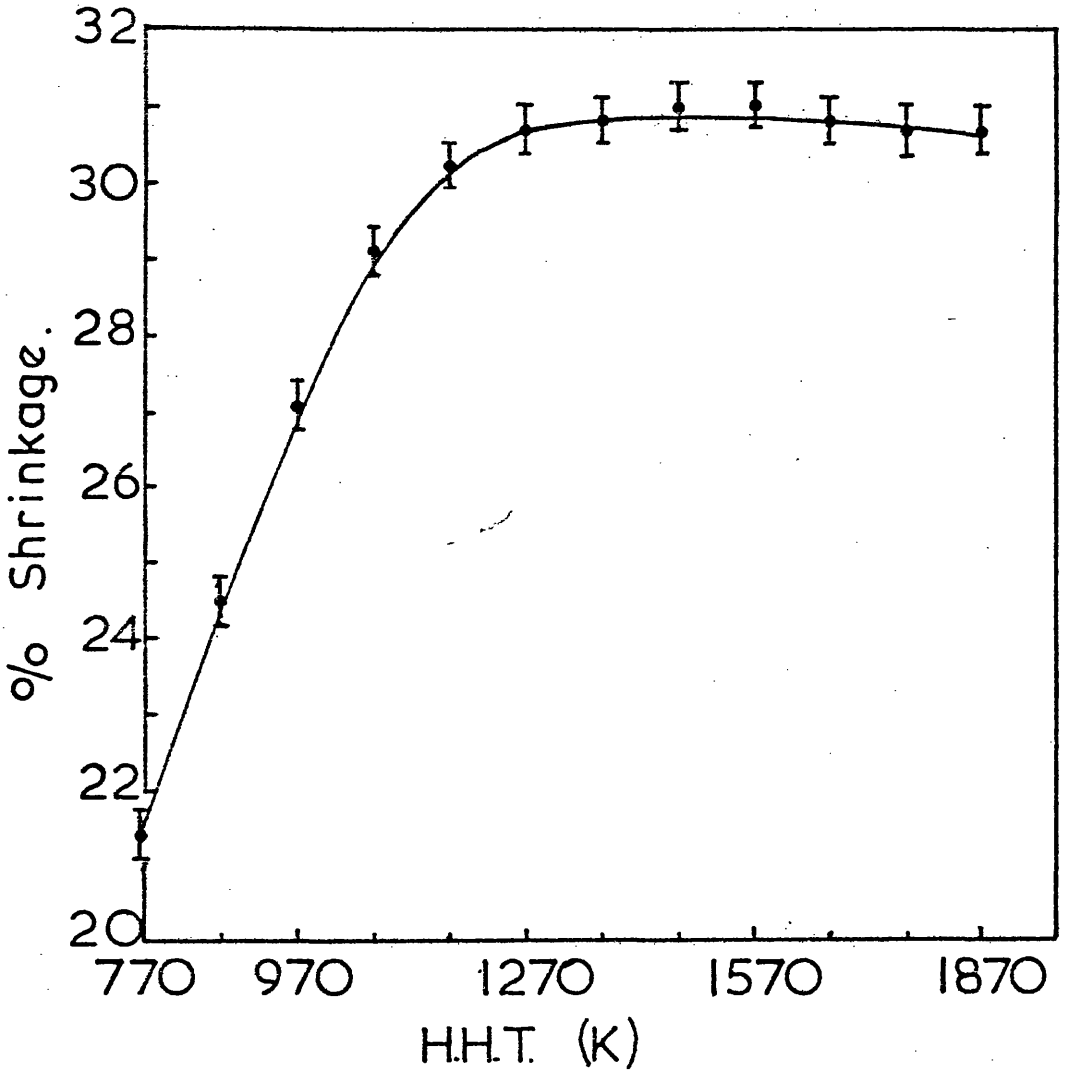

Fig.3.4 Bulk Shrinkage on Carbonisation & Heat-treatment.

CHAPTER 4

ADSORPTION—EXPERIMENTAL AND THEORY

CHAPTER 4

ADSORPTION

4.1 Introduction

The adsorption of gases and vapours is a very useful technique for investigating microstructural changes in carbons of low HTT (< 1700 K).

Initial studies were carried out with nitrogen at 77 K in a Micromeritics Orr Surface area analyser, model 2100 D. It was found that adsorption failed to reach equilibrium after long periods of time. This was attributed to the small pore entrances presenting a large energy barrier, over which entering molecules must pass. At low temperatures the molecules' kinetic energy is low, which results in a statistically small proportion of molecules which can enter, hence adsorption is slow. This effect, known as activated entry, or diffusion, can be somewhat alleviated if higher adsorption temperatures are used. Carbon dioxide at 177 K was then used, an acetone/liquid nitrogen slush bath being used to obtain the temperature. This system, however, also failed to reach equilibrium after eight hours and equilibration overnight was not found possible because of instrumental instabilities and melting of the slush bath. In addition to these problems the Orr analyser could only deal with one sample at a time; therefore a McBain spring type adsorption apparatus, capable of running four samples for long times, was constructed.

Initially it was conceived to use benzene as adsorbate, this being a standard vapour in use by Russian workers, and capable of use at water bath temperatures - allowing long unattended equilibration times. In practice, however, very small uptakes were found for unactivated

carbons. Since micropore entrances seem to be slit shaped [95,96] [97,98] the flat benzene molecule must presumably require a high degree of orientation to be adsorbed - this being the cause of the long equilibration times.

Various workers[2,99,100] have used carbon dioxide at 298 K and suggested this to be well suited to carbons. Carbon dioxide at 295 K was tried and found to give good uptakes, and equilibration times (for most carbons) of less than three hours, hence this was used throughout the study.

4.2.1. Adsorption balance design

The apparatus, shown in figure 4.1 and photograph 4.2 , was constructed from pyrex glass and attached by clamps to a framework, which was secured to a solid wall. PTFE 'O' ring sealed taps (J. Young and Co.) were used throughout to avoid outgassing problems due to absorption of organic vapours by vacuum grease. The sample hangdown tubes were attached by cup and socket 'O' ring joints - these allowing considerable movement of tubes, so as to avoid contact between the helical spring and tube walls.

Adsorptive pressures were measured by a pirani gauge (LKB 3294 B Autovac)[101] for pressures of 10^{-3} to 10 Torr and a mercury manometer for the range 1 Torr to atmospheric, the apparatus not being capable of withstanding higher pressures. The pirani gauge head was glass blown into the system - this being neat and leak free. Apart from low pressure measurements the pirani was indispensable in checking for outgassing or leaks.

The manometer had one limb capable of being evacuated then closed off by tap O. The whole manometer was isolatable from the system by tap N, so as to reduce the possibility of contamination of system and samples by mercury vapour. Tap N was only opened when pressure measurements were made and closed at other times. The amount of mercury was chosen so that both levels could be sighted by a cathetometer up to a pressure of 270 Torr, after which only one level could be sighted up to 780 Torr. The cathetometer could be swiveled in a horizontal plane to sight the sample and reference marks as well as the manometer.

The one litre bulb, G, was incorporated to allow very small amounts of adsorptive to be introduced into the system. A by-pass tube, F, allowed the pressure to be further adjusted. The adsorptive mainly used was carbon dioxide (Air products, high purity) which was dried by passage through a column of 3 A molecular sieves, J. The column was connected, via a needle value, I, and 3 mm copper tubing to the inlet, H. Prior to use the whole gas line and column were evacuated to exclude air, then the column charged up to allow time for drying. The column was wrapped with heating tape [102] to allow the sieves to be periodically regenerated by heating under vacuum, in situ.

The pumping system consisted of an Edwards rotary pump, A, backing a water cooled diffusion pump B. The diffusion pump oil used was DC 702 silicone. A liquid nitrogen trap, D, and water cooled baffle valve, E, were included to reduce oil vapour backstreaming. A by-pass line, C, was included to protect the diffusion pump whilst large quantities of gas were

being pumped away.

The rotary pump had a separate power failure protection system which, on power failure, would isolate the vacuum system and allow the rotary pump back to atmospheric. The delay time between the two events was adjustable.

The maximum sensitivity of spring balances is set by the hangdown tube length since, for a given length, any increase in sample weight must be offset by a reduction in spring sensitivity. The tube lengths were 0.65 m which allowed a 0.4 g sample on a spring of sensitivity ~60 cm g^{-1}. A realistic estimate of the minimum movement detectable by the cathetometer is $\pm$ 0.003 cm, hence the minimum detectable weight change is $\pm$ 5 x 10^{-5} g.

The helical springs used[103] were made from pyrex and supplied in 0.3 m (unextended) lengths. These could be cut to yield springs of any desired sensitivity. Their advantages over silica equivalents were their considerably lower cost, greater robustness, ease of repair and flexibility of spring sensitivity. Their chief disadvantage is their low dimensional stability i.e. they are prone to creep under stress. This problem seems to have been solved, however, by following the practice of Chipallatti and Giles[104] and annealing the springs under a 0.5 g load at 470 K for 8 hours. After such treatment no significant creep could be detected over the period of an isotherm (ca. one week); sensitivities also remained constant over six months.

To allow the maximum possible sensitivity springs to be used the sample supension fibre had to be kept to a minimum (5 - 10 cm). This resulted in the spring protruding into the thermostated water-bath and being obscured from the cathetometer. To circumvent this problem the pyrex support fibres were made with a kink in an appropriate place for attachment to the spring. This left an upward pointing extension, the top of which could be sighted (see inset R). Perfect parallelism of the upward and downward sections of the fibre was achieved by hanging it by its sample hook and momentarily playing a small flame onto the kink. Gravity pulls the two sections into line. A fiducial reference fibre was suspended within the spring. Checking this allowed any movements of the cathetometer to be detected and allowed for.

Carbon pellet samples (ca. 0.4 g) were attached to the support fibre by a fine wire loop. Powder samples were contained in aluminium foil buckets.

Samples were thermostated by immersion of the hangdown tubes into a deep perspex water bath. The temperature was controlled by a Techne tempette TE 1^{105} thermostat which was stable to $\pm$ 0.2 K over a complete run.

Outgassing was achieved by wrapping heating tape around the vicinity of the sample and evacuating to a pressure of less than 10^{-4} Torr. The temperature was controlled by a variac to about 480 K. Outgassing was conveniently carried out overnight.

Corrections for buoyancy were not possible since the effective sample density varies with heat-treatment and activation. This is due to differing amounts of closed porosity. Without an independent means of measuring the density, in carbon dioxide, realistic corrections are impossible. Unfortunately, the largest effect is seen in carbons of high HTT since their density is lowest - this also coincides with low adsorptive capacity such that the measured adsorption on these carbons is somewhat underestimated.

4.2.2. Operating procedure

Samples were outgassed under vacuum by wrapping heating tape around the specimen area of the hangdown tubes. Completion of outgassing was indicated by a cessation of spring extension, and checked by closing off the system for 15 minutes and looking for a rise in pressure (>0.01 Torr) on the pirani gauge. This latter check was important since leaks were not uncommon.

When ready, the heating tape was removed and the tubes submersed in the water bath and this brought up to temperature. Only when the samples were thermostated, and being pumped, were the zero pressure extensions measured. This is necessary because the springs were not separately thermostated and differences in temperature would alter the spring extensions. An increase in temperature will cause a spring to contract due to a change in its elastic constants[106]. Because a mercury manometer is not a frictionless piston, a little agitation of the tubes, prior to sighting, ensures correct levels are measured. Slight variations of the two levels from equal

height, at zero pressure, were corrected for.

Equilibration times varied considerably and true stability had to be indicated by constancy of extension over two or more hours. Activated carbons and ones of HTT $<$ 1470 K reached equilibrium after 2 hours whilst carbons of HTT = 1570 K required 12 hours. Continuing adsorption on 1470 K carbons could be detected after one week.

Sample weights were found by outgassing, then sealing off under vacuum and cooling. Samples were individually removed and quickly weighed on a balance, to four decimal places. Due to adsorption from the air, the first stable reading was taken. Errors of this kind have little effect, due to the large weight of carbon, but would be significant for specimens left to the atmosphere for a few hours.

A. Rotary pump.

B. Oil diffusion pump.

C. By-pass line.

D. Liquid nitrogen trap.

E. Baffle valve.

F. By-pass line.

G. 1 Litre volume.

H. Inlet connection.

I. Needle valve.

J. 3 Å Drying column.

K. CO_2 cylinder connection.

L. Hangdown tubes.

M. Pirani head.

N. Manometer isolation tap.

O. Limb evacuation tap.

P. Mercury manometer.

Q. Fiducial reference fibre.

R. (Inset) Sample support fibre.

S. Samples.

T. 'O'-Ring joints.

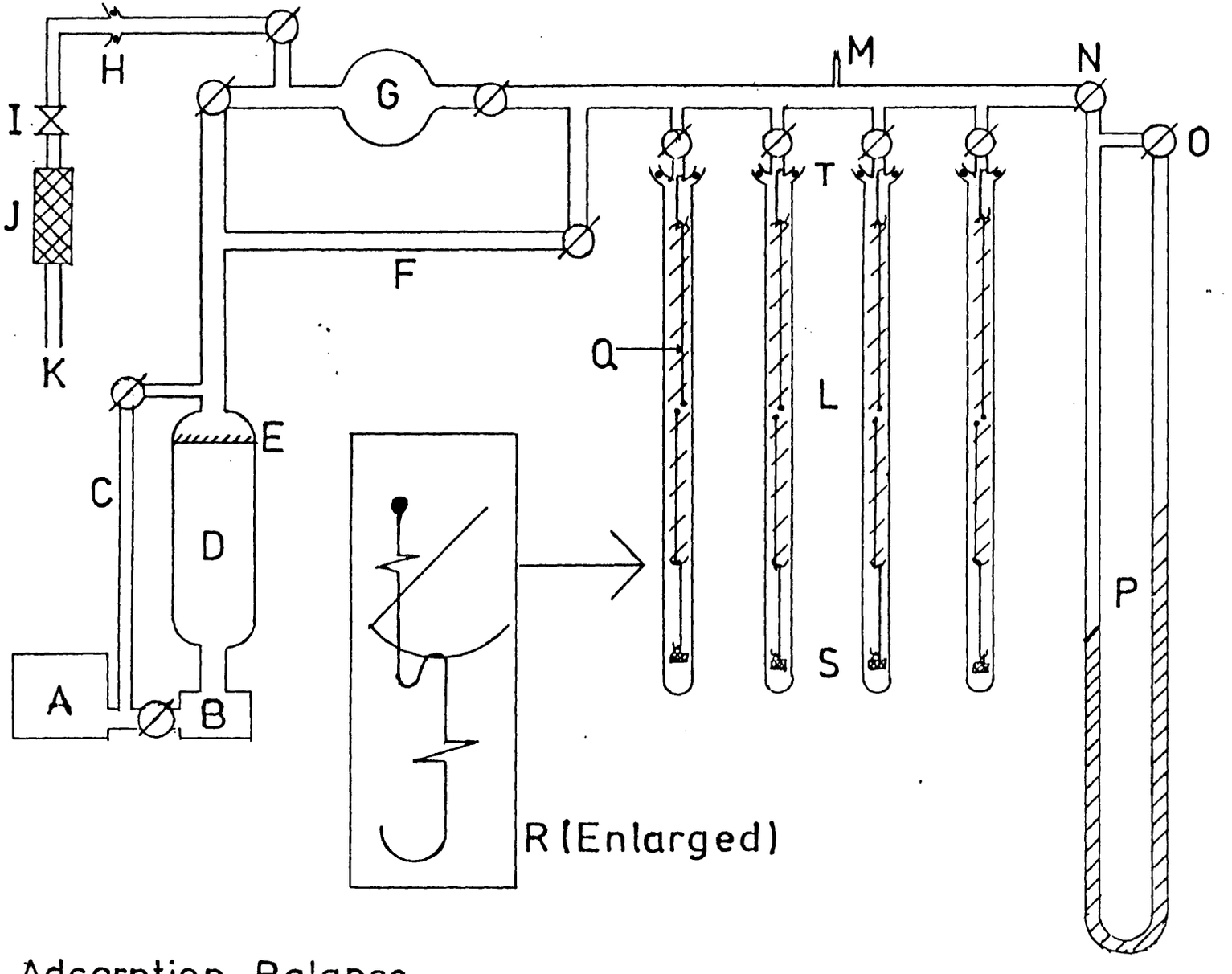

Fig. 4.1 Adsorption Balance

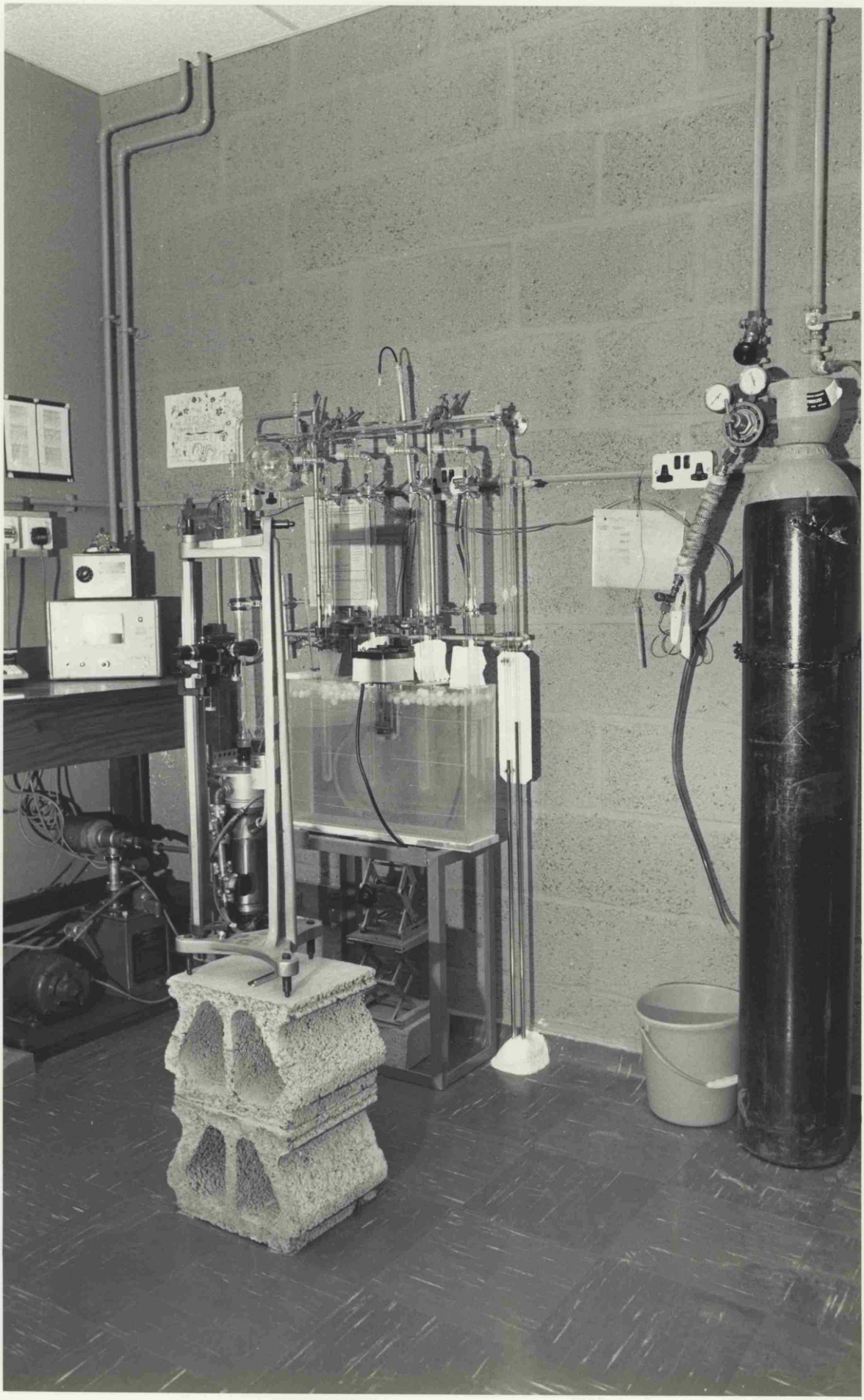

Fig. 4.2 Adsorption Balance.

4.3.1. Treatment of Adsorption Data

The first treatment of adsorption was by Langmuir[107] who used a kinetic argument to derive an equation which fits the Type I isotherm in the BDDT classification[108]. He made the assumptions (1) that the solid surface was a two dimensional array of energetically homogeneous sites, (2) that no interaction occurred between adsorbate molecules and (3) that adsorption ceased on completion of a monolayer. In physical adsorption none of these assumptions are really correct but Langmuir's equation still finds application in chemisorption.

Langmuir's approach to determining the monolayer capacity is clearly very limited but was extended to cope with multilayer adsorption by Brunauer, Emmett and Teller[109].
The resultant B.E.T. equation allows monolayer capacities for a much wider range of adsorbents to be found and can yield surface areas if the adsorbate molecule's occupied area is known. The B.E.T. equation is derived for open, plane, surfaces but can be modified to cope with porous adsorbents where the pore width restricts the maximum number of layers. Despite this modification, the B.E.T. theory is rather suspect when applied to very fine pored adsorbents. DeBoer and Custers[110] first pointed out that a molecule in a crevice of molecular dimensions could have a heat of adsorption six times as large as on a plane surface. Such an effect is due to the overlap of adsorption forces from opposite walls[111].

The result of such an overlap of forces is to cause enhanced low

pressure adsorption with the adsorbate acting more as a liquid or compressed gas (depending on temperature) than a localised layer. This effect, termed micropore filling, is believed to be the cause of B.E.T. surface areas which exceed the maximum theoretically possible [112-114].

There are currently two approaches to adsorption in microporous solids - the deBoer 't' plot and the Polanyi potential theory as developed by Dubinin and co-workers.

4.3.2. The deBoer t Plot

The t plot is a means by which an isotherm is replotted with different co-ordinates so as to allow deviation from the idealised situation of adsorption on a plane, open, surface to be observed. It is possible to obtain values of micropore volume and surface area of 'open' surfaces as shown by Sing [115]. These values, and the approach in general, are subject to much controversy as various 'standard' isotherms exist [116] which differ so as to considerably alter the values obtained. Dubinin [93,117] criticize it as only having been applied to super-microporous absorbents (r >0.6 nm) and not ultramicroporous ones. Marsh and Rand [118,119] criticize its use by Mikhail et al [120] to obtain pore size distributions as assuming an unrealistic mechanism of adsorption.

An approach which was derived specifically for microporous adsorbents and does not assume a mechanism for adsorption is the Dubinin theory of volume filling of micropores, which is based on the Polanyi potential theory. Since this approach was exclusively used in this study it will be described in more detail.

4.3.3. The Polanyi Potential Theory

Polanyi's view[121] of the adsorption forces can be likened to a gravitational field surrounding the solid's surface. The field of attraction is characterised by an adsorption potential, ε, which is defined as the isothermal work done, by the adsorption forces, on transferring a molecule from the free gaseous phase to a particular point above the surface. It should be noted that the term potential used here does not refer to intermolecular potential such as the Lennard-Jones type potential. The surface is therefore visualised as being surrounded by equipotential surfaces as shown schematically in figure4.3.

As one moves away from the surface the volume, V, enclosed by an equipotential surface increases as its potential value decreases. Eventually the potential falls to zero and the volume enclosed by $\varepsilon = 0$ becomes the total (limiting) adsorption space, V_o.

Clearly, the way in which V changes with ε will depend on the particular adsorbent's porosity or surface heterogeneity. A plot of V vs. ε is therefore called a "characteristic curve". Provided only London type dispersion forces are involved, and because these are temperature independent, such a curve should be the same for different temperatures of measurement. Temperature invariance of the characteristic curve is a fundamental postulate of the potential theory.

The thermodynamic adsorption potential, ε, is found so :

If a gas is isothermally and reversibly compressed the change in Gibbs free energy is given by

$$dG = Vdp - SdT \qquad 4.1$$

at const. T

$$\left.\frac{dG}{dp}\right|_T = V \qquad 4.2$$

if the gas is ideal

$$\left.\frac{dG}{dp}\right|_T = \frac{RT}{p} \qquad 4.3$$

Integrating,

$$G = RT \ln P + C. \qquad 4.4$$

If the standard, reference, state is taken as the bulk liquid with a saturated vapour pressure of P_o

$$G^o = RT \ln P_o + C \qquad 4.5$$

If the adsorbed phase is taken as being identical to the bulk liquid the free energy change, which ε is defined as, is found from

$$G^o - G = -\Delta G = RT \ln P_o/p = \varepsilon. \qquad 4.6$$

The assumption that the adsorbed phase behaves as bulk liquid is only really valid when $T < T_c$, where T_c is the critical temperature. If the adsorption volume is in pores where

considerable potential overlap occurs then P_o can probably be used as the reference state up to T_c, since the majority of adsorbate will experience forces sufficiently large to liquify it. If wide pores exist there will be a mixture of liquid and compressed gas which will change in proportion as T approaches T_c. In the latter case a number of methods have been proposed for determining ρ_a - the adsorbate density[122,123,124,125], but the particular formula used must ultimately depend on the particular adsorbent. This is demonstrated by the semi-empirical method of Dubinin, Kadlec and Zukal[126]. Since all measurements in this study were carried out at $T < T_c$, values of P_o and ρ_a were taken from values for the liquid phase[127]. Values were used in 0.1 K intervals to compensate for experimental temperature fluctuations.

When $T > T_c$ the concept of a liquid phase loses its meaning. Berenyi[122] suggested the adsorbate density would be the maximum to which the gas could be compressed i.e. the molar volume given by the Van der Waals constant b. Dubinin and Nikolayev[123] also assume ρ_a to be constant but equal to the molar volume at T_c. Conversely, Dubinin, Kadlec and Zukal[126] suggested that ρ_a varies with T in the same manner as below T_c - hence could be obtained by a series of measurements at temperatures well below and close to T_c, on the same absorbent.

The value of P_o used for $T > T_c$ was suggested by Berenyi as being kTb^{-1}, where the constant k depends on the units used.

Nikolayev and Dubinin, after analysing much experimental data, arrived at

$$\varepsilon = RT \ln \frac{P_c T^2}{P T_c^2} \qquad 4.7$$

where P_c is the critical pressure.

P_o can also be obtained[126] from an extrapolation of a plot of saturated vapour fugacities vs. T^{-1}.

Knowing values for ε and V, the characteristic curve could be constructed but was of little use for determining structural information until further developed by Dubinin and co-workers.

4.3.4. The Dubinin Theory

Dubinin recognised that the characteristic curves for active carbons fell into two extreme categories. The first (type A) possessed micropores of size commensurate with that of the sorbate molecule. The second (type B) possessed large pores and gave curves similar to non-porous materials. Dubinin and Radushkevich also noted that the type A curves resembled the positive branch of a Gaussian distribution, from which they proposed two equations to fit the two types of curve :

$$V = V_o \exp(-k\varepsilon^2) \qquad \text{Type A} \qquad 4.8$$

$$V = V_o \exp(-k\varepsilon) \qquad \text{Type B} \qquad 4.9$$

V_o is the limiting volume of the adsorption space which, for type A carbons, is taken as being equal to the micropore volume. The significance of V_o for type B carbons is not so easily

defined as it includes adsorption on open surfaces. k is a constant which depends upon the adsorbent and adsorbate.

Dubinin has shown that all the characteristic curves for different vapours on the same adsorbent can be shifted to superimpose each other if ε is divided by a constant, β, which depends on the vapour. Affinity coefficients, β, can be found by adsorbing a series of vapours onto a characterised adsorbent and taking one (usually Benzene) as standard with $\beta = 1$. It is also found that β can be approximated from the ratio of molar volumes, or better still, parachors for the given and standard vapour. k can therefore be factorised so: -

$$k = \frac{B}{\beta^2} \qquad 4.10$$

where B is now only dependent on the adsorbent.
Equation 4.8 now becomes, in linear form : -

$$\ln V = \ln V_o - \frac{B}{\beta^2} \{RT \ln(P_o/p)\}^2 \qquad 4.11$$

for $T < T_c$.

Equation 4.11 is known as the Dubinin-Radushkevich (D-R) equation. A plot of $\ln V - \ln^2(P_o/p)$ should yield a straight line which intercepts the ordinate at $\ln V_o$, hence the micropore volume can be found.

4.3.5. Significance of B

B is a shifting parameter which allows characteristic curves for different adsorbents to be superimposed.

The dimension of B/β^2 are $(\text{energy})^{-2}$ so the two parameters are often combined so : -

$$B/\beta^2 = \frac{1}{E^2} \qquad 4.12$$

where E is called the characteristic energy for the particular sorbate/sorbent system. 4.8 becomes

$$V = V_o \exp - \left(\frac{\varepsilon}{E}\right)^2 \qquad 4.13$$

E is thus seen as being a particular value of ε for which the fraction of volume filling, V/V_o, is 1/e i.e. $V/V_o = 0.368$. Its relationship to the mode of the distribution of volume with adsorption potential is found so : -

$$\frac{dV}{d\varepsilon} = - 2 V_o \frac{\varepsilon}{E^2} \exp - \left(\frac{\varepsilon}{E}\right)^2 \qquad 4.14$$

Equation 4.14 has the form of a Rayleigh distribution and its profile is solely determined by E (see Figure 4.4). The maximum of the distribution is found from $d^2V/d\varepsilon^2 = 0$, from which differentiation of 4.14 gives : -

$$E = \sqrt{2}\, \varepsilon_{max}. \qquad 4.15$$

ε_{max} is the mode of the distribution.

E not only determines the peak position but also the breadth of the distribution as can be seen in figure 4.4. Although it is not possible to directly relate pore sizes to ε values, distributions described by 4.14 often prove of value in observing structural changes.

4.4.1. Limitations of the Dubinin-Radushkevich equation

A linear D-R plot can only be expected over a wide pressure range if the distribution of volume with potential follows a Rayleigh distribution over its whole range. Many systems yield linear plots over restricted ranges and, depending on the pressure range examined, different values of V_o may be obtained. Since the D-R plot is used as an extrapolation device, to find V_o, the region at high relative pressure (low ε) should be used, if low pressure deviations occur.

The nature of the deviations from linearity are often characteristic of a particular structure of adsorbent and so can offer a useful tool for structural investigations.

4.4.2. Marsh and Rand D-R Plots

Marsh and Rand[100,128] identified three types of deviation which were attributed to particular distributions of potential (see Figure 4.6).

Type A

This showed two linear sections with the low pressure (high ε) end deviating down. Such plots are found in zeolites, non-activated carbons and generally homogeneous carbons.

Type B

This plot is curved over the whole range of pressure. Marsh and Rand suggested this was a result of a log-normal type of distribution. This deviation is found in activated carbons and implies a structure closer to the aforementioned type B carbons than type A.

Type C

This latter class was only observed for nitrogen and argon on certain activated carbons. There is evidence for a type A deviation with a high pressure upturn superimposed. Marsh and Rand concluded that this shape was due to a bimodal distribution of potential. Bearing in mind that this type occurred only in the systems where P/P_o approached unity, it seems likely that the upturn is due to capillary condensation in messopores - which are frequently present in activated carbons. The "type A" deviation may be due to a loss of large micropores into mesopores which fill by multilayer adsorption until constricted sufficiently to allow capillary condensation.

4.4.3. Dubinin-Astakhov equation

The specificity of the D-R equation can be seen when one remembers that the only variable in the Rayleigh distribution is E, which not only controls the distribution's maximum but also its breadth, w, by

$$w = E^2(2\Gamma - {}^{3}/_{2}\,\Gamma^2) \qquad 4.16$$

where Γ is the gamma function.

The Rayleigh distribution assumes homogeneous adsorbents to be predominantly of low ε_{max} and vice-versa. Deviations may be expected for the real cases where this relation does not occur.

Equation 4.13 is, in fact, an example of a Weibull function[129] which takes the form

$$F(A) = 1 - \exp\{-(\varepsilon/E)^n\} \qquad 4.17$$

The exponent n, which was previously assumed equal to either 1 or 2, is now seen as a variable which predominantly affects the distribution breadth (and to some extent ε_{max}). For very homogeneous solids n will be high so that as $n \to \infty$ the characteristic curve tends to a step function and its differential - the potential distribution - tends to a Dirac delta function, as shown in figure 4.5.

The distribution half-height breadth is given by

$$w = E^n \left(n\,\Gamma - \frac{n+1}{n}\,\Gamma^n\right) \qquad 4.18$$

4.18 is the general case of 4.16

The position of intersection for distribution curves of different n is at $\varepsilon = E$ i.e. $V/V_o = 1/e = 0.368$.
ε_{max} tends towards this point, as n increases, by the following

$$E = \left(\frac{n}{n-1}\right)^{1/n} \varepsilon_{max} \qquad 4.19$$

4.19 is the general form of 4.15

Equation 4.17 as applied to adsorption takes the form : -

$$F(A) = 1 - V/V_o = 1 - \exp\{-(\varepsilon/E)^n\} \qquad 4.20$$

$$\therefore \quad V = V_o \exp -(\varepsilon/E)^n \qquad 4.21$$

Equation 4.21 is known as the Dubinin-Astakhov (D-A) equation. Its use can help with the understanding of the Marsh-Rand deviations[130] as variation of n predominantly affects data at high values of ε - which is where most deviations occur (except type C).

Type A plots can be linearised by using a value of $n > 2$. This type of structure is therefore of a type which is more homogeneous than required by the D-R equation. Such carbons would have a narrow pore size distribution.

Type B plots require a value of $n < 2$ for linearity. As mentioned before, this implies a wide pore size distribution or considerable multilayer formation on open surfaces. For $n = 1$ we have the particular form of the D-R equation for type B carbons (equation 4.9).

4.4.4. Stoeckli's equation

An alternative approach to the generalisation of the D-R equation has been proposed by Stoeckli[131]. In this he assumes the D-R equation to have general validity but that adsorption by a heterogeneous system is described by a summation

of individual distributions, each obeying the D-R equation and characterised by a value of B ($B = \beta^2/E^2$).

By assuming a Gaussian distribution of B with micropore volume the summation could be evaluated as an integral to give :

$$V = V_o \exp\{-B_o Y\} \exp\{Y^2\Delta^2/2\} \{1 - \text{erf}(x)\}/2 \qquad 4.22$$

where

$Y = (T/\beta)^2 \ln^2(P_o/p)$, $x = (y - B_o/\Delta^2)\, \Delta/2^{\frac{1}{2}}$,

$\text{erf}(x) = -\text{erf}(-x)$ and is the error function, B_o and Δ are respectively the maximum and half width of the Gaussian distribution of B.

Stoeckli critisies the Dubinin-Astakhov equation as implying a variable distribution of ε yet this is what his approach does. It does no more than allow a wider distribution of potential to be treated than the D-R equation is capable of. Equation 4.22 is also only able to cope with systems equal to or more heterogeneous than those which fit the Rayleigh distribution e.g. highly activated carbons. It cannot cope with carbons of high homogeneity, unless negative values of Δ are used. Since the Stoeckli equation offers no more than the D-A equation, the extra computation necessary hardly seems worthwhile.

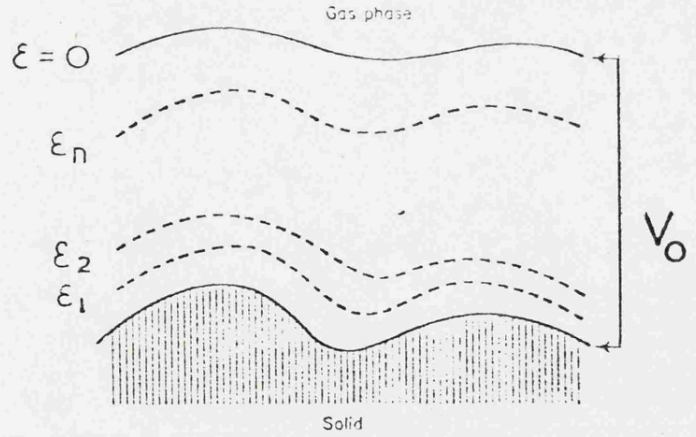

Fig.4.3 Schematic representation of Polanyi Adsorption Space.

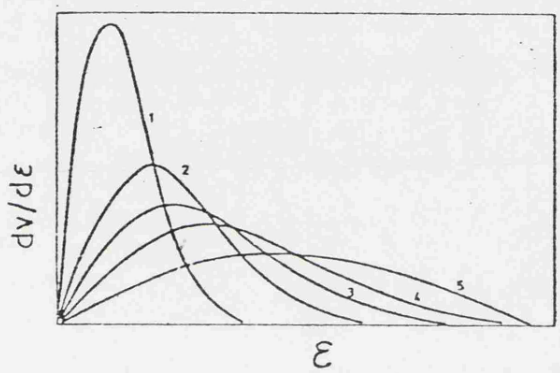

Fig.4.4 Pore volume distributions for n = 2, of varying E. 1= low E, 5= high E.

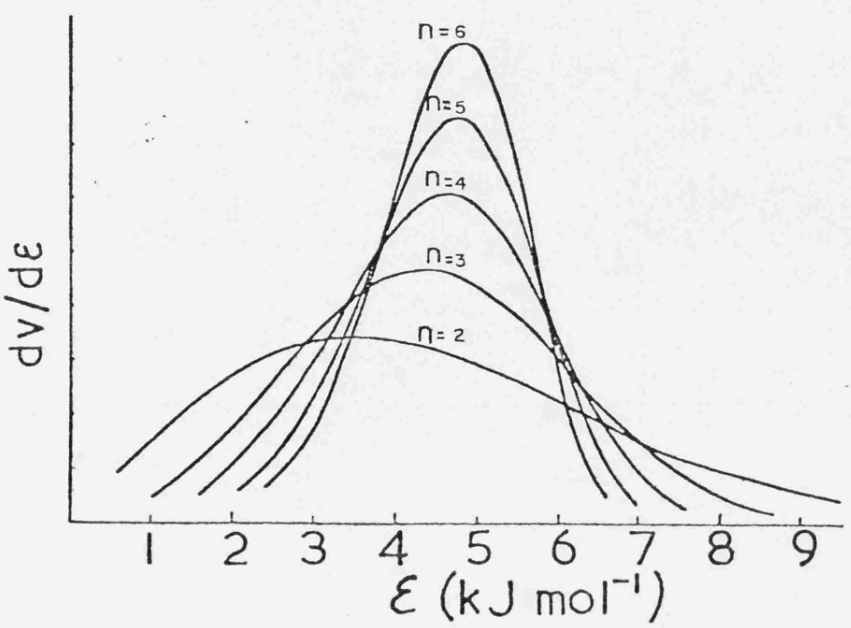

Fig. 4.5 Volume distributions for E=5 kJ mol^{-1}, n variable.

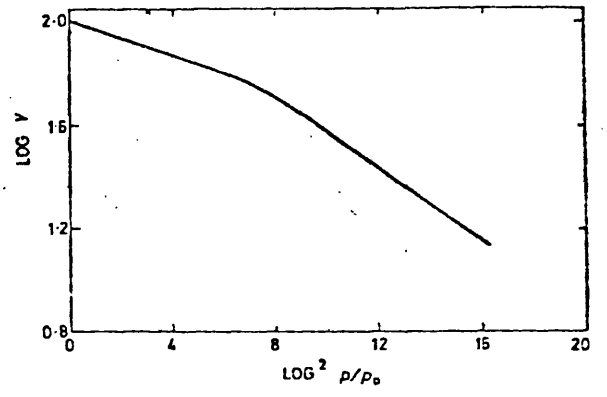

Type A.

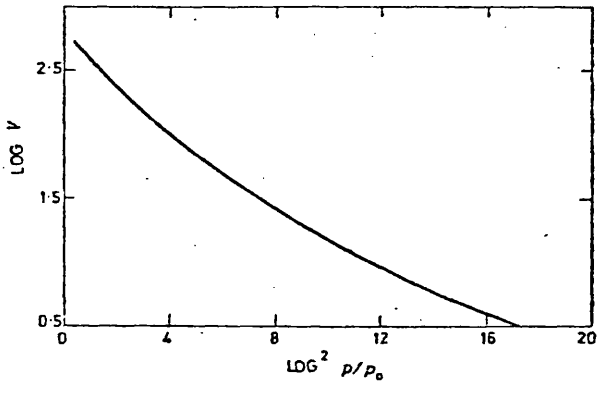

Type B.

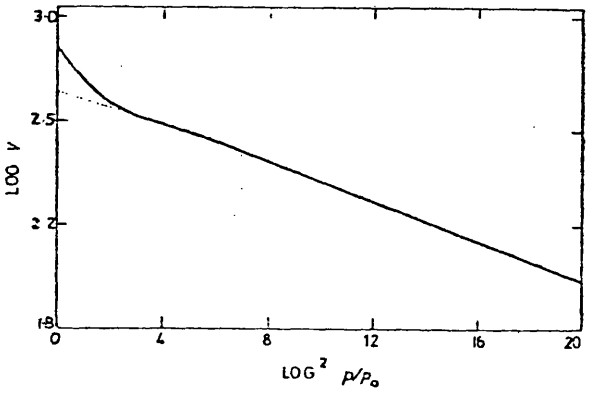

Type C.

Fig. 4.6 Marsh & Rand Type D-R Plots.

CHAPTER 5

X RAY STUDIES – THEORY AND EXPERIMENTAL

CHAPTER 5

5.1.1. Theory of small angle x-ray scattering

When a beam of x-rays pass through an inhomogeneous material some of the radiation will be scattered to the side of the transmitted beam. This phenomena is the same as the well known Rayleigh scattering of light caused by fluctuations in refractive index, except that the scattering of x-rays is caused by fluctuations in electron density on a much smaller scale.

The intensity and angular distribution of the scattering will depend on the magnitude of the fluctuations and the size of the regions over which they extend. The intensity has its maximum at $\theta = 0$ and decreases as θ increases, approaching zero as the phase difference between the most widely separated atoms of the particle becomes of the order of 2π. A useful guide to the extension of the scattering is therefore given by

$$\theta_1 = \frac{\lambda}{2D} \qquad 5.1.$$

where θ_1 is the limiting angle for detection and D the largest particle diameter. A more thorough description of small angle x-ray scattering (SAXS) will now be given and it will be shown how useful parameters relating to structural heterogeneity can be obtained.

If $\rho(\bar{x})$ is the electron density at a point defined by a vector $(\bar{x})$, measured from an arbitrary origin, the amplitude, F(h), of radiation scattered will be the Fourier transform[132] of $\rho(\bar{x})$, i.e. :

$$F(h) = Fe(h) \int_V \rho(\bar{x}) \exp(i\, h.\bar{x})\, dVx \qquad 5.2$$

where $h = 4\pi\sin\theta/\lambda$, 2θ being the angle between incident and scattered rays, dVx is the element of volume V situated at $\bar{x}$, $i = (-1)^{\frac{1}{2}}$, $Fe(h)$ is the amplitude of scatter by a single electron.

The intensity of scatter, $I(h)$, is then :

$$I(h) = F^{+}(h)F(h) = Ie(h) \int_V \int_V \rho(\bar{x})\, \rho(\bar{x} + \bar{r})\, dVx \exp(ih.\bar{r})dVr \qquad 5.3$$

$F^{+}(h)$ is the complex conjugate of $F(h)$, $\bar{r}$ is a vector connecting two points in the solid defined by their vectors $\bar{x}$ and $(\bar{x} + \bar{r})$. $Ie(h)$ is the intensity of scatter from a single electron at a distance d from the sample, given by the Thompson equation :

$$I_e(h) = 7.90 \times 10^{-26}\, I_o\, d^{-2} P \qquad 5.4$$

where I_o is the incident beam intensity, P is the polarisation factor, $(1 + \cos^2 2\theta)/2$, which is essentially unity for SAXS.

The essential problem now is that we do not know the form of the $\rho(\bar{x})$ distribution and so cannot evaluate the integrals. To avoid this problem the density distribution is characterised by what Debye and Bueche[133] call a correlation function and Porod[134,135] terms a characteristic function - $\gamma(r)$.

5.1.2. Correlation Function

Consider a heterogeneous solid as having an average electronic density $\bar{\rho}$, on which are superimposed local variations, η, which will be positive or negative such that they average out to be $\bar{\rho}$. If we have two points, 1 and 2, separated by a distance, r, and take the product of their fluctuations $(\eta_1\eta_2)$, we may obtain a large number of values for the product by moving the points around, but keeping r fixed. The average value can be designated $(\eta_1\eta_2)_{av}$. This average will depend on the distance r such that when $r = 0$, $(\eta_1\eta_2)_{av}$ will equal $\bar{\eta}^2$, which is the average amplitude of fluctuation over the whole solid. For large values of r the average product will be zero since η_1 and η_2 will vary independently.

In general then, $(\eta_1\eta_2)_{av}$ will be a function of r which will begin with $\bar{\eta}^2$ for $r = 0$ and go to zero in some, as yet undetermined, fashion with increasing values of r. The correlation function is used to determine the fashion in which $(\eta_1\eta_2)_{av}$ changes with r :

$$(\eta_1\eta_2)av = \gamma(r)\ \bar{\eta}^2 \qquad 5.5$$

for a two phase material $\gamma(r)$ may be thought of as being the probability that points 1 and 2 lie in the same phase when separated by a distance r.

If we define $\rho(\bar{x})$ in terms of the average electronic density, $\bar{\rho}$, and its density fluctuation $\eta(\bar{x})$ then

$$\rho(\bar{x}) = \bar{\rho} + \eta(\bar{x}) \qquad 5.6$$

and 5.3 becomes :

$$I(h) = Ie(h) \int_V \int_V (\bar{\rho} + \eta(\bar{x}))(\bar{\rho} + \eta(\bar{x}+\bar{r}))\exp(ih\cdot\bar{r})\, dVx\, dVr \qquad 5.7$$

when 5.7 is factorised the term $\eta(\bar{x})\eta(\bar{x} + \bar{r})$ is dominant so that

$$I(h) = Ie(h) \int_V \int_V \eta(\bar{x})\eta(\bar{x} + \bar{r})\, dVx\, \exp(ih\cdot\bar{r})dVr \qquad 5.8$$

from 5.5 it can be seen that :

$$\int_V \eta(\bar{x})\ \eta(\bar{x} + \bar{r})\ dVx = \gamma(\bar{r})\ \bar{\eta}^2 V \qquad 5.9$$

thus 5.8 becomes :

$$I(h) = Ie(h)\bar{\eta}^2\ V \int_V \gamma(\bar{r})\exp(ih\cdot\bar{r})dV_r \qquad 5.10$$

If the material is isotropic $\gamma(\bar{r})$ will only depend on the magnitude of $\bar{r}$ and at large $\bar{r}$, tend to zero, thus 5.10 may be simplified and reduced from a volume integration to an infinite one dimensional one :

$$I(h) = 4\pi Ie(h)\bar{\eta}^2 V \int_0^\infty r^2\gamma(r)\ \frac{\sin(hr)}{hr}\ dr \qquad 5.11$$

For a two phase system it is easily shown that the mean fluctuation, $\bar{\eta}$, is related to the total density difference, $\Delta\rho$, between the two phases by :

$$\bar{\eta}^2 = \Delta\rho^2\ C(1 - C) \qquad 5.12$$

where C is the volume fraction of one of the phases, thus :

$$I(h) = 4\pi Ie(h)\Delta\rho^2 C(1 - C)\, V \int_0^\infty r^2\gamma(r)\,\frac{\sin(hr)}{hr}\,dr \qquad 5.13$$

Debye, Anderson and Brumberger[136] have shown that the surface area per unit volume, S/V, of the two phases can be found from :

$$S/V = -4\, C(1 - C)\, \gamma'(0) \qquad 5.14$$

where $\gamma'(0)$ is the gradient of the correlation curve at $r = 0$. Using equations 5.13 and 5.14 they also showed that at large scattering angles the intensity decreases proportionally to h^{-4} and that it is directly related to the surface area :

$$\lim_{h \to \infty} I(h) \simeq \frac{Ie(h)2\pi\Delta\rho^2 S}{h^4} \qquad 5.15$$

The h^{-4} dependence was first deduced by Porod[134,135] and so is referred to as Porod's Law.

Clearly, use of 5.15 to obtain values of surface area is difficult because the incident beam intensity and irradiated volume are required. Because these values are often not easily obtained experimentally, Porod introduced a normalisation procedure to avoid these measurements.

Porod multiplied 5.13 by h then Fourier inverted it to yield the correlation function :

$$\gamma(r) = 1/\left[2\pi^2 Ie(h)V\ \Delta\rho^2\ C(1 - C)\right] \int_0^\infty h^2 I(h)\ \frac{\sin hr}{hr}\ dh \qquad 5.16$$

Since $\gamma(r)$ and $\sin(hr)/hr$ tend to unity as r tends to zero, 5.16 becomes :

$$2\pi^2 Ie(h)\Delta\rho^2 V\ C(1 - C) = \int_0^\infty h^2 I(h)\ dh \qquad 5.17$$

substituting 5.17 into 5.15 gives :

$$S/V = \pi\ C(1 - C)\ \lim_{h\to\infty} I(h)h^4 \Big/ \int_0^\infty h^2 I(h)\ dh \qquad 5.18$$

Porod also showed how to obtain a linear parameter, ℓ_c, which he called the distance of heterogeneity and defined as

$$\ell_c = 2\int_0^\infty \gamma(r)\ dr \qquad 5.19$$

ℓ_c is the average length of all lines contained in the particles and thus (as indicated by 5.19) is obtained by integration of 5.16

$$\ell_c = 1/\left[2\pi Ie(h)V\ \Delta\rho^2\ C(1 - C)\right] \int_0^\infty hI(h)\ dh \qquad 5.20$$

5.20 is made easier for use by substitution of 5.17 to give :

$$\ell_c = \pi \int_0^\infty hI(h)\ dh \Big/ \int_0^\infty h^2 I(h)\ dh \qquad 5.21$$

137
Kuroda has shown that for spherical particles ℓ_c is related to the mass averaged diameter, $\bar{D}$, by :

$$\ell_c = 3/4\ \bar{D} \qquad 5.22$$

Use of equations 5.18 and 5.21 both involve integrations over the whole scattering curve. This is difficult since only a limited angular range is measurable. At low angles there is not so much of a problem since h^2 is small and inaccuracies therefore not too important. Guinier's approximation is frequently used for this range. At high angles, however, measurements must be made with high accuracy. Again we are limited, this time by the presence of the (002) Bragg reflection (in carbon). A method due to Gerold[138] is used in this region, which improves the accuracy.

If the scattering particles are random in size and shape, Debye, Anderson and Brumberger[136] have shown that the correlation function assumes an exponential form :

$$\gamma(r) = \exp\ (-\ r/a) \qquad 5.23$$

a is termed the correlation distance.

Use of 5.23 now allows equation 5.13 to be integrated to yield

$$I(h) = \frac{8\pi I_e a^3 \Delta\rho^2\ C(1 - C)\ V}{(1 + h^2a^2)^2} = \frac{A}{(1 + h^2a^2)^2} \qquad 5.24$$

The parameter, a, can be determined by a plot of $I(h)^{-\frac{1}{2}}$ against h^2 when

$$a = (\text{slope}/\text{Intercept})^{\frac{1}{2}} \qquad 5.25.$$

In the case of an exponential correlation function 5.14 becomes

$$S/V = \frac{4\,C(1 - C)}{a} \qquad 5.26$$

and 5.19 becomes

$$\ell_c = 2a \qquad 5.27$$

If the heterogeneity is truly random the methods of Debye and Porod should yield the same results. Such agreement has been found for the surface area of a carbon black by Williams[139] and ℓ_c for carbon fibres by Johnson and Tyson[140].

If the volumetric fraction of one phase is known then, in addition to S/V, the mean chord intercept length in the matrix, ℓ_m, and a similar length for the pores, ℓ_p, can be found from :

$$\ell_m = a/C \qquad 5.28$$

$$\ell_p = a/(1 - C) \qquad 5.29$$

where C is now the volume fraction of pores.

The method of Debye et al clearly offers a method of obtaining useful parameters from a system, without the need for absolute intensity measurements or time consuming integrations over undetermined regions.

Such a technique is also useful when experimental apparatus is such that very low angle measurements are not possible, as was the case in this study. The only condition to be satisfied is that the scattering particles be random in size and shape. This can be checked by the linearity of the $I(h)^{-\frac{1}{2}} - h^2$ plot.

5.1.3. Slit Corrections

It must be pointed out that the equations derived so far are valid only for point collimated beams (e.g. in pin-hole cameras) but much use is made of slit collimated radiation since this affords the higher incident intensities as required for counter systems.

Unfortunately, slits distort the scattered profile (see Riley)[141]. Whilst correction procedures exist they are tedious and can often introduce errors. It is fortunate, therefore, that the slit length (also called height) distorts (or "smears") the profile in a predictable way.

At high angles the slit collimated intensity, $J(h)$, follows a h^{-3} dependence since, as shown by Guinier and Fournet[142]:

$$\lim J(h)h^3 = \frac{\pi}{2} \lim I(h)h^4 \qquad 5.30$$

5.15 therefore becomes :

$$\lim_{h\to\infty} J(h) \simeq \frac{I_e(h)\pi^2\Delta\rho^2 S}{h^3} \qquad 5.31$$

Porod's equation 5.18 becomes :

$$S/V = 4\,C(1-C)\lim_{h\to\infty} J(h)\,h^3 \Big/ \int_0^\infty hJ(h)\,dh \qquad 5.32$$

and 5.21 becomes :

$$\ell_c = 2\int_0^\infty J(h)\,dh \Big/ \int_0^\infty hJ(h)\,dh \qquad 5.33$$

Williams[139] has shown that the Debye equation 5.24 becomes :

$$J(h) = \frac{8\pi^2 I_e(h)\,\Delta\rho^2 C(1-C)\,V\,a^2}{(1+a^2h^2)^{3/2}} = \frac{B}{(1+h^2a^2)^{3/2}} \qquad 5.34$$

The slope and intercept from a plot of $(J(h))^{-2/3} - h^2$ thus yields a, as before, from 5.25.

A finite slit width also produces aberrations though not as serious as the slit length. This error is mostly important at very low angles and would require correction[143] if Porod's Method was used. At higher angles the effect is negligible and so was ignored in the present work.

5.1.4. Other methods

Besides the correlation function approach the other major method of analysing SAXS is due to Guinier[144]. He demonstrated that for spherical particles the intensity at low angles can be well approximated

by a Gaussian function of the form

$$\lim_{h\to 0} I(h) \simeq I_e(h)\, N_p \Delta\rho^2 V_p^2 \exp(-h^2R^2/5) \qquad 5.35$$

where R is the radius of the particle and Np is the number of particles of volume Vp.

To generalise for non-spherical particles he used the concept of radius of gyration, Rg, about is electronic centre of mass, so 5.35 becomes

$$\lim_{h\to 0} \simeq I_e(h)\, Np\Delta\rho^2 V_p^2 \exp(-h^2Rg^2/3) \qquad 5.36$$

and $$R = (5/3)^{\frac{1}{2}}\, Rg = 1.29\, Rg \qquad 5.37$$

If lnI(h) is plotted against h^2 the slope will yield Rg.

The application of Guinier's equation is restricted to relatively ideal systems since it involves the assumptions that the particles are non-interacting, uniform in size and of identical, known, shape. The effect of interparticle interference (which occurs in concentrated dispersions) is to depress scattering at low angles and so the value of Rg. This is important as Guinier's approximation is only valid as $h \to 0$. Measuring in this range is experimentally difficult and the corrections for interference difficult (but can be done - see Rothwell)[145]. Polydispersity (varying particle size) is often indicated by non-linear Guinier plots and the above approach then reduces to a "method of tangents".

In order to make allowance for polydispersity both Hosemann[146] and Shull and Roess[147] assumed a Maxwellian particle size distribution. In this case the scattered intensity is given by :

$$I(h) = I_e(h)\, Np\, \Delta\rho^2 \bar{V}p^2 \left[1 + \frac{h^2 \bar{R}g^2}{3}\right]^{-(n+4)/2} \qquad 5.38$$

The distribution is then defined by $\bar{R}g$ and n where $\bar{R}g$ is the mass averaged radius of gyration and n is a measure of the distribution width.

If $I(h)h^2$ is plotted against h a maximum should occur at h_m where :

$$h_m = 1/\bar{R}g \{6/(n+2)\}^{\frac{1}{2}} \qquad 5.39$$

A tangent to the point of inflection at high h should intersect the x-axis at a point h_T then :

$$\frac{h_T}{2h_m} - 1 = \frac{1}{(2(n+1))^{\frac{1}{2}}} = g \qquad 5.40$$

where g is the polydispersity. The value for $\bar{R}g$ can be obtained from 5.39 and 5.40.

Shull and Roess rearranged 5.38 to obtain

$$I(h) = K \left[h^2 + 3/\bar{R}g\right]^{-(n+4)/2} \qquad 5.41$$

Their method then involves plotting log $I(h) - \log(h^2 + \alpha)$ and varying α until a straight line is obtained. $\bar{R}g$ is then obtained from that value of α by

$$\bar{R}g = (3/\alpha)^{\frac{1}{2}} \qquad 5.42$$

A method for generalising Guinier's equation by using a discrete distribution was developed by Jellinek and Fankuchen[148]. In this case

$$I(h) = K\sum M(Ri)Ri^3 \exp(-h^2Ri^2/3) \qquad 5.43$$

An analysis of the $\log I(h) - h^2$ plot in terms of 5.43 then yields a distribution of the mass fraction of particles of radius Ri - M(Ri).

Kuroda[137] carried out such an analysis for two carbon blacks and found a bimodal distribution. This, together with a discrepancy between electron microscope results and those of Hosemann's approach led him to suggest that the Maxwellian distribution was inappropriate for such carbons.

If the incident beam intensity is known, together with $\Delta\rho$, both the specific area and particle size distribution can be obtained by a method due to Elkin, Shull and Roess[149]. The method is based upon the above equations and the interested reader is directed to the original paper or Hosemann and Bagchi's book[150].

The treatment of data to yield particle size distribution has seen some recent advances with the work of Vonk[151,152]. His method has been applied

to carbons by Wang et al[153] but requires considerable computation and has, as yet, not been proven effective on well characterised materials. It also relies upon a number of not-altogether valid assumptions.

Because most of the above methods are only applicable to dilute systems, require measurement at low angles or involve invalid assumptions they were not used in this study. The data obtained in this work was treated by the method of Debye and co-workers, modified to cope with slit collimated radiation. It is felt that this approach is well suited to the study of carbon microstructure.

5.2.1. Wide angle x-ray diffraction

X-ray diffraction (XRD) is a useful technique for examining the degree of order and perfection of the atomic arrangements within a carbon.

The diffraction patterns observed for non-graphitized carbons (as in this study) are composed of a few broad, asymmetric peaks which frequently overlap one another (see figs.5.1 and 5.2). Such a pattern suggests a turbostratic carbon of small crystallite size.

For the cellulose carbons examined here only three peaks were observable. The strongest occurs at about $2\theta \simeq 22^{o}$ and corresponds to the (002) reflection. The second, somewhat weaker one, occurs at 43.5^{o} and is very asymmetric with a tail extending to higher angles. This peak corresponds to a combination of the (10) and (004) reflections. Because of their closeness, and low intensity, resolution was not possible therefore L_a and d_{10} were not obtained. The third peak occurs at $2\theta = 79^{o}$, and is very weak, only being of useable intensity for the 2500 K glassy carbon. This is due to the (11) peak with, perhaps, some contribution from the (006) (but this seems unlikely).

The (002) peak is comparatively easy to analyse but would yield misleading results if used in its raw form. The peak is, in fact, modified by the following effects :

1, Compton, or incoherent, scattering

2, Small angle scattering (SAXS)

3, The Lorentz effect.

4, The polarization effect.

5, Variation of the atomic scattering factor across the peak.

To obtain the pure diffraction profile allowance must be made for these effects. A graphical method was proposed by Short and Walker[154], which was found to be quick and useful for internal comparison of isochronally heat-treated carbons. Unfortunately, this method was found inadequate when applied to activated carbons, where high precision and accurate background compensation are essential for meaningful results to be obtained. The adopted procedure will now be described.

5.2.2. Compton scattering

Compton, or incoherent, scattering is due to the exchange of energy and momentum between an incident photon of wavelength λ and an electron. The electron is expelled from the atom and the photon has, after the collision, a slightly smaller energy, ie. a longer wavelength λ'. The wavelength change is given by

$$\Delta\lambda = \lambda' - \lambda = \frac{h}{mc} (1 - \text{Cos } 2\theta) \qquad 5.44$$

where h is Planck's constant, m is the mass of an electron and c is the speed of light. $h/mc = 0.02426$ Å.

Because of the changed wavelength the Compton radiation will not constructively interfere to enhance the Bragg reflections and so constitutes a background intensity which increases with angle. The wavelength change is, unfortunately, so small that it cannot be filtered out by conventional pulse height analysis although Ergun[155,156] claims to have experimentally eliminated it from Ag Kα by use of balanced filters.

Quantum mechanical calculations show that the intensity, in electron units, is given by

$$I_{inc} = R\ (\ Z - F) \qquad 5.45$$

where Z is the sample's atomic number and F depends on the element and scattering angle. R is the Breit-Dirac recoil factorwhich was established by Breit[157] by taking into account the recoil velocity of the electron after collision. R is commonly taken as $(\lambda/\lambda')^3$ but as pointed out by Keating and Vineyard[158] and Ergun[159] this only applies to intensity detectors, whilst for photon counters (e.g. proportional counters) the correct form is $(\lambda/\lambda')^2$. Breit showed that R was given by :

$$\frac{1}{R} = \left[\frac{\lambda'}{\lambda}\right]^2 = 1 + \frac{2h\lambda}{mc}\left(\frac{\mathrm{Sin}\theta}{\lambda}\right)^2 \qquad 5.46$$

for Cu Kα ($\lambda = 1.54$ Å).

$$1/R = 1 + 0.0744\left(\frac{\mathrm{Sin}\theta}{\lambda}\right)^2 \qquad 5.47$$

The values of F used were those obtained by Keating and Vineyard [158] for carbon in the covalent state and R was calculated from 5.47.

It should be pointed out that the data given in the International Tables for x-ray crystallography[160] appears to be in error as I_{inc}/R is quoted but no wavelength is given. From 5.46 it can be seen that R is wavelength dependent and examination of the original sources shows the quoted values are, in fact, only I_{inc}, which do not include the Breit-Dirac factor.

As with coherent radiation the Compton scattering is affected by the polarisation effect so that the observed intensity is given by :

$$J_{inc} = C\left(\frac{1 + \cos^2 2\theta}{2}\right)\frac{I_{inc}}{R} \qquad 5.48$$

where C is a constant which converts electron units to experimental units. Values of $\{(1 + \cos^2 2\theta)I_{inc}\}/2R$ are tabulated in appendix B.

To find C we note that the (coherent) atomic scattering factor decreases with angle whilst the incoherent scattering increases (cf. Equation 5.45). The intensity was therefore measured at a high angle, devoid of Bragg reflections, and assumed to be wholly incoherent. This angle was taken as 100^0 2θ but even at this angle the SAXS can still contribute up to 60% of intensity, hence this was subtracted, as shown later. C is therefore given by :

$$C = \frac{R}{I_{inc}}\left(\frac{2}{1+\cos^2 2\theta}\right)(J_{Tot} - J_{SAXS}) \qquad 5.49$$

or, for carbon at $100^{o}2\theta$, using $CuK\alpha$

$$C = 0.42\ (J_{Tot} - J_{SAXS}) \qquad 5.50$$

5.2.3. SAXS Correction

The tail-end of the SAXS approximates to Porod's law and even though a gradient of -3 is not obtained it still gives a linear lnI vs ln2θ plot. Such plots were made for the angular region up to $8^{o}2\theta$ (to avoid interference from the (002) peak) and extrapolated to the higher angles. From these plots the intensity of SAXS over the whole (002) profile could be found and subtracted. The intensity at 100^{o} 2θ was used for correcting the Compton scattering.

5.2.4. Lorentz factor

The Lorentz factor is necessary because the intensity of a reflection is proportional to the time during which the crystallites are in a position to reflect. The relative rates in which the reflecting orientation is passed through varies with angle such that reflections at small and large Bragg angles are enhanced with respect to the others.

The actual form of the factor used depends upon the experimental mode employed but for diffractometers considerable dispute exists amongst various workers. D.J. Johnson[161] empirically uses $Sin2\theta$ claiming this to be most realistic, whilst R.H. Bragg[162] uses $Sin^{2}\theta$, as do a few others. The problem was extensively examined by Pike and Ladell[163,164] who suggested $Sin^{2}\theta Cos\theta$ as the correct form. Wilson[165] also suggests this form and points out that it makes some allowance for absorption. The Lorentz factor

was therefore taken, in this work, as $Sin^2\theta Cos\theta$.

5.2.5. Polarization factor

When the incident radiation is unpolarized the component parallel to the reflecting planes is fully reflected but the amplitude of the perpendicular component is reduced by a factor of $Cos\theta$, or its intensity by $Cos^2\theta$. This is due to the polarising effect of reflection. The polarisation correction factor is therefore $(1 + Cos^2\theta)/2$.

5.2.6. Variation of atomic scattering factor

The efficiency with which an electron reflects an x-ray photon varies with the angle between the incident and reflected beams such that at $\theta = 0$ the scattering of an atom, in electron units, is equal to the number of electrons in it, i.e. its atomic number. As the angle increases the scattering power decreases, hence its atomic scattering factor, f, decreases. The intensity of reflection will be obtained from f^2. Tables of f are available [166] and were used in this study. Because of its breadth, account should be taken of the variation of f^2 across the profile of the (002) peak.

To summarise, the correction procedure amounted to :

1, subtraction of SAXS and incoherent scattering

2, Multiplication by $(1 + Cos^2 2\theta)f^2/Sin^2\theta Cos\theta$

The angular dependent factors are tabulated in Appendix B.

Saxena and Bragg[162] initially claimed corrections for broadening and displacement due to low specimen absorption were unnecessary but this was later revoked[167]. Such corrections are very difficult to apply in this work since the effective specimen thickness is unknown. Because the overall trends would remain unaffected, no absorption correction was made. Instrumental broadening was also ignored as peaks are very wide[168].

Having reconstructed the corrected (002) profile the interplanar c spacing is found from

$$d_{002} = \lambda/2 \, \mathrm{Sin}\theta \qquad 5.51$$

whilst the crystallite size, perpendicular to the layer-planes, is given by the Scherrer equation[169]

$$L_c = \frac{57.3 \, K \, \lambda}{\beta \, \mathrm{Cos} \, \theta} \qquad 5.52$$

where K is the Scherrer constant, which depends upon the particular reflection, and was taken as 0.89 for the c-axis dimension, according to Warren[48]. β is the peak width at half height, in 2θ degrees.

Determining the peak's position presents a problem since the actual peak is rounded and rather flat, hence the peak position is uncertain. Various centroid definitions exist[165] from which it was decided to use the midpoint of the profile at half breadth - this being well defined. A slight asymmetry of the profile results in this position giving a slightly larger interlayer spacing than from positions higher up the peak, but the effect is small (ca. 0.001 nm).

5.3 X-ray experimental

Both wide and small angle diffraction data were obtained with a Philips PW 1050 goniometer diffractometer. The detector was a xenon filled proportional counter linked to a PW 4620 ratemeter and pulse height discriminator. The radiation used was nickel filtered copper Kα(0.1542 nm) generated in a Philips PW/1010/80, operated at 40 kV and 20 mA. Soller slits together with 1^{o} divergence, 0.1^{o} receiving and 1^{o} anti-scatter slits were used. In order to permit measurements at lower angles various combinations of narrower slits were tried but resulted in an unacceptable loss in intensity, and only allowed an angle of 1^{o} to be achieved. Bearing in mind the high angle to which SAXS was observed the above slits were therefore found to be the optimum. A blank trace, with no specimen, was used to correct the small angle data for direct beam, parasitic and air scatter. The minimum angle of measurement was 2.5^{o} 2θ.

The specimens were in the form of "as made" cylindrical solid pellets. The x-ray beam was reflected from a flat circular surface. This was found to be more reproducible than with powder specimens.

For high accuracy work a chart speed of 0.5 cm/min and scan speed of 0.5^{o}/min were used. Scales were changed to maintain a high signal.

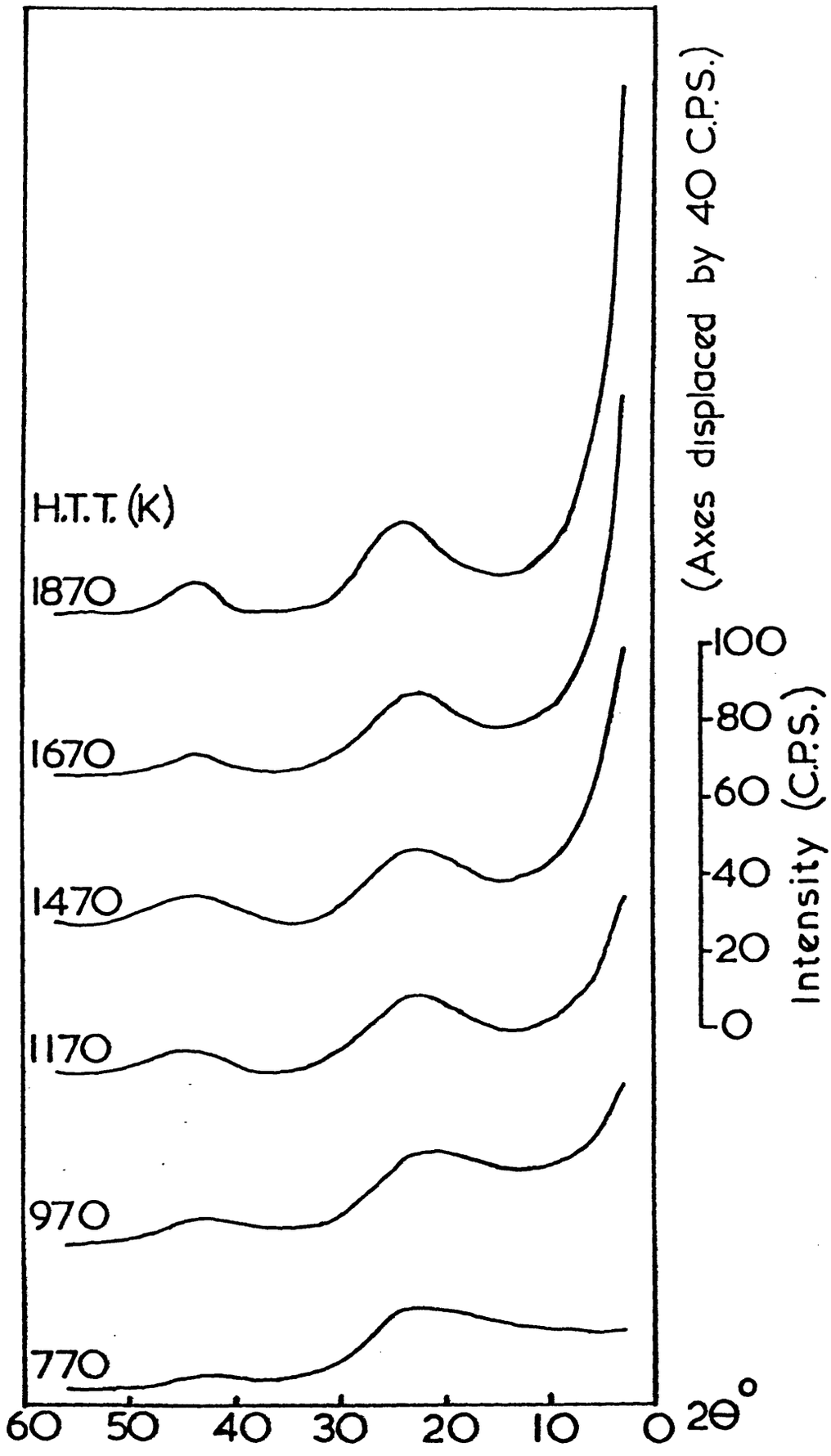

Fig. 5.1 Uncorrected X.R.D. Patterns for Heat-treated Carbons.

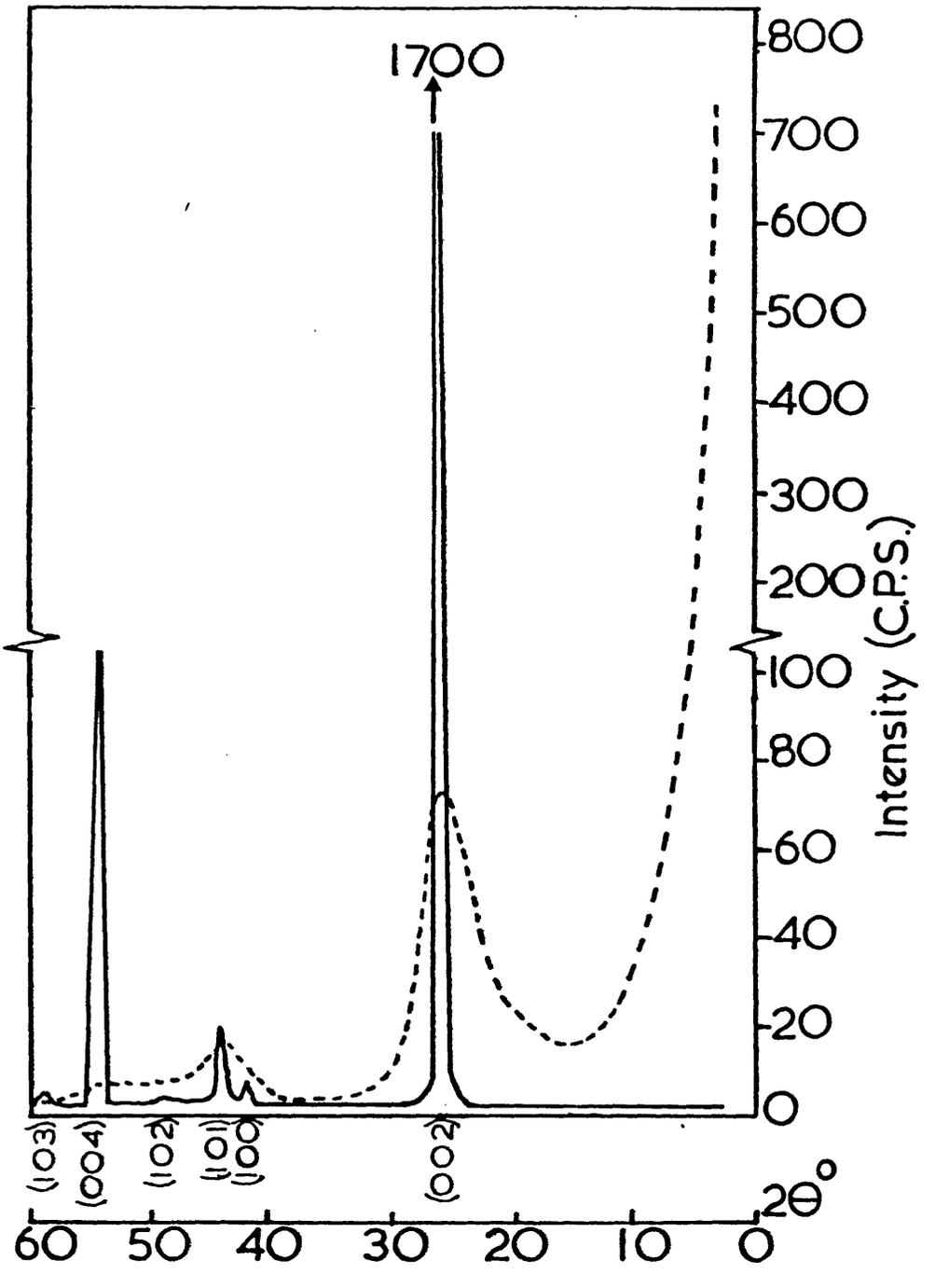

Fig. 5.2 Uncorrected X-Ray Diffraction Patterns for Graphite (solid line) & 2500 K G.C. (dashed).

CHAPTER 6

ELIMINATION

OF

HETEROELEMENTS

CHAPTER 6

ELIMINATION OF HETEROELEMENTS

Many of the structural changes which form the basis of this study occur in the latter part of secondary carbonisation. It is useful to be able to differentiate between changes caused by continued loss of heteroelements and changes occurring in the basic carbon structure. This requires knowledge of the limiting temperature at which carbonisation can be considered complete. Thermogravimetry indicated that weight loss continued beyond 1270 K therefore two methods were used to evaluate heteroelement expulsion at higher temperatures - elemental (CHO) analysis and mass spectroscopic evolved gas analysis.

6.1.1. Elemental Analysis

The results of a CHO analysis for heat-treated carbons are given below in table 6.1.

Table 6.1

HTT(K)	1270	1470	1570	1670	1770	1870	Precision
Weight % C	96.9	97.8	98.7	99.6	99.7	99.7	± 0.15
Weight % H	0.28	0.10	0.03	0.03	0.01	ND	± 0.05
Weight % O	0.86	0.61	0.53	0.15	0.06	0.01	± 0.05
Atomic % H	0.28	0.10	0.03	0.03	0.01	-	± 0.05
Atomic % O	0.054	0.038	0.033	0.009	0.004	-	± 0.003

Table 6.1 shows the loss of hydrogen to be progressive but appears to have reached completion by 1670 K. On an atomic basis there is somewhat less oxygen than hydrogen, the oxygen tending to be less affected by HTT than hydrogen. Some of the oxygen may be chemisorbed as a surface oxide which would explain its apparent

insensitivity to HTT. The reduction after 1570 K may be due to a lower accessible surface area capable of chemisorbing oxygen or a reduction in active sites where chemisorption could occur. This trend agrees with that found by Dovaston[170] for the loss of surface oxides from cellulose triacetate carbons, on outgassing to ∿ 1200 K. His values are about 3 x as large as would be expected if the loss were wholly CO, but this may be a result of the different carbon or loss of material other than oxides.

If the oxygen is indeed present as surface oxide its rôle in structural transformations is unlikely to be significant. This together with its lower atomic concentration suggests hydrogen to be the heteroelement of most importance in the latter part of secondary carbonisation. Because the CHO analysis is limited in sensitivity it was decided to study heteroelement expulsion further by evolved gas analysis.

6.2 Evolved Gas Analysis

6.2.1. Experimental

The apparatus used to analyse the gases evolved on heat-treatment is shown in figures 6.1 and 6.2. The sample pellet (0.4 - 0.5 g) was contained within a graphite susceptor (K) which was heated by a radio frequency (R.F.)induction coil (I). This enabled very rapid heating and cooling rates to be used. The susceptor was supported on a graphite rod within a vacuum-tight, water-cooled, pyrex tube. The evolved gases were sampled by taking a bleed, via a 1 m capillary tube and Edwards needle valve, into the mass spectrometer (M.S.), a 180^{o} magnetic type Vacuum Generators

Micromass 1. The M.S. was pumped by a water-cooled diffusion pump backed by a rotary pump. A polyphenyl-ether diffusion pump oil (Santovac 5) was used to minimise creep into the system and also because the breakdown products are electrically conducting. Prior to use the mass spectrometer UHV system was baked out ($\sim$ 500 K) overnight.

6.2.2. Mode of Operation

Operation under flowing argon was impractical since the M.S. sensitivity is considerably reduced by the heavy dilution of components. Two methods of operation under vacuum were tried : -

1. Continuous pumping by rotary pump with stream sampling.
2. Sealing the system and recording the pressure rise.

Method 1. was found to be unreliable since the pumping speed varies considerably with pressure and this was not always predictable or easy to calibrate. Sensitivity was also low after the initially vigorous evolution decreased. Method 2. was more sensitive to small evolution rates and was easily calibrated, so was adopted.

A blank run with no sample showed the degassing from the graphite susceptor to be only $\sim$ 1% of the quantities normally evolved from samples. Addition of hydrogen to this system gave a constant pressure, showing negligible reaction between graphite and hydrogen at $\sim$ 1 Torr and 1500 K, and negligible sampling loss.

Unfortunately, operation under vacuum caused a number of problems which restricted the scope of this work.

1. At pressures between 0.05 and $\sim$ 5 Torr, the R.F. field caused a blue discharge in the specimen tube. This caused difficulty with temperature measurement by optical pyrometry. This problem was most pronounced at temperatures less than 1400 K. The apparatus was changed to accommodate a Pt/Pt + 13% Rh thermocouple in the susceptor. The e.m.f. was measured by a battery-powered Wheatstone bridge, mains-powered potentiometers being interfered with by the R.F. power. This system was satisfactory with the sample resting on the tip (to prevent tip discharges) and served as a check on the optical pyrometer.

2. An upper limit for measurement of $\sim$ 1700 K was encountered because the evolution of gas was so low. The low tube pressure, combined with the high intensity R.F. field, caused a dense bright discharge which upset the electronics and caused rapid heat transfer to the sample tube - with a resultant high thermal stress on the glass. If the power was not quickly reduced this could, and on one instance did, fracture the sample tube.

3. When the system was sealed at a given temperature, the pressure would increase initially then reach a steady value. This pressure did not, however, correspond to the total amount of hydrogen which was capable of evolution at that temperature since, on evacuation and re-sealing, more hydrogen was evolved (see figure 6.3). The second amount was typically 10 - 30% of the first amount. This suggests that the hydrogen-carbon reaction is reversible and comes to equilibrium. To complicate the evaluation of kinetic data it was found that, as the system pressure rose, the sample temperature decreased due to increased thermal conduction by gas. This effect was

most noticeable both at the initial stages of pressure increase and evacuation. For instance, at 1400 K, sudden evacuation could result in the sample temperature rising by 50 K.

4. The proximity of mass peaks for CO^+, N_2^+, O_2^+ and CH_4^+, O^+, OH^+,N^+ prevented their resolution and individual measurement. The signal in these mass ranges was found to increase with hydrogen evolution in the lower temperature regions which suggests some of the oxygen present may arise from the original cellulose or that some hydrogen is evolved as CH_4 and higher hydrocarbons (perhaps acetylenes ?). Work was begun on chromatographic separation of these gases, prior to M.S. analysis, but this was ceased through lack of time.

Because of the above problems and the special significance of hydrogen content it was decided to concentrate on obtaining a cumulative hydrogen yield as a function of HTT. The following procedure was followed to obtain this data from 1170 K upwards.

a. At 1170 K the system was pumped until no significant pressure rise was found on sealing the system.

b. The system was closed and the temperature raised by about 50 K (more at high temperature where the pressure rise was less). The final temperature was adjusted to be the same as the highest reached during the initial pressure increase stage. Since the system was calibrated at room temperature (after the run), the power was switched off when the plateau was reached, and the sample cooled. The rapid cooling effectively quenched the hydrogen–carbon equilibrium. Because the gas near the susceptor cooled, the

pressure dropped to a constant level, which was used as a measure of the amount evolved. Any hydrogen re-adsorbed on cooling would be evolved in the next stage.

c. The system was evacuated then re-sealed and the temperature brought up to its previous value.

This sequence was repeated until negligible hydrogen was evolved (twice was usually enough but more frequently below 1400 K). The temperature was then increased and the cycle repeated. Large temperature intervals could not be used since the pressure in the M.S. would rise above 10^{-4} Torr, which was the limit imposed for linear response and filament lifespan.

6.2.3. Calibration

At the end of a run the system was calibrated at room temperature by either of two methods. 1., A stream of hydrogen from a jet type flowmeter could be injected into the system. The flowmeter was itself calibrated against a bubble-flow meter (built from a microburrette). 2., A known volume of gas could be injected from a pulse-meter (see figure 6.4). The pulse-meter is similar to a gas proportioning valve but built to withstand vacuum and avoid internal leakage during operation. It could also be by-passed via a flow-through position. The volume loop enclosed 1.1 ml. Good consistency was found between both methods.

6.2.4. Results and Discussion

Hydrogen was found to be rapidly evolved for the first 5 minutes then the rate decreased, sometimes requiring more than 30 minutes

(at low temperatures) to cease. This, together with further evolution after evacuation, suggests the hydrogen is in dynamic equilibrium with the carbon. This equilibrium shifts towards the gas phase with increasing temperature. This is suggested by the necessity for frequent evacuations to remove the hydrogen at low temperature whilst most of the hydrogen is evolved in the first stage at higher temperatures.

Because equilibrium was reached more rapidly for the second and subsequent stages, it seems likely that the first stage is lengthened due to the time needed to break C-H bonds such as in reaction (A) : -

$$C - H \longrightarrow C^* + \tfrac{1}{2}H_2 \qquad - (A)$$

Once liberated the hydrogen seems to equilibrate with the carbon in a more labile form, possibly as a chemisorbed surface complex (reaction (B)) : -

$$C + \tfrac{1}{2}H_2 \rightleftharpoons C \ldots H \qquad - (B)$$

This implies that the carbon atoms at the originally hydrogen rich sites re-arrange to become more stable, e.g. reaction (C)

$$C^* + C^* \longrightarrow C - C \qquad - (C)$$

The time period for the initial breakdown (A) would be about 20 - 30 minutes and seems quite constant for all temperatures since equilibration times were similar at 1300 K and 1600 K. Because the evolution rates are similar for carbons whose pores are open

(1300 K) as well as carbons whose pores are closed (1600 K) it seems unlikely that diffusion of gas, at these temperatures, out of pores is a controlling step in the observed rates. Adding support to this is the finding that if the sample was cooled and pumped no hydrogen would be evolved, but on heating to the previous temperature evolution rapidly returned. If diffusion control existed one would expect the hydrogen to be removed from the pores during evacuation. A simple calculation showed that if all the hydrogen evolved in a typical stage existed in gas form within the microporous structure, the pressure inside the micropores would need to be ~ 5 atmospheres. It seems more likely that the hydrogen exists in a chemically bound form. These conclusions agree with the finding by Berkowitz and Den Hertog[171] that sample comminution had no effect on hydrogen evolution rate up to 1070 K, i.e. that the experimentally measured rates directly equate with the formation rates.

The similarity of evolution rates for different temperatures does not necessarily imply a temperature-independent rate of decomposition since far more hydrogen would be evolved from a virgin sample heated for a given time at 1600 K than at 1300 K. This suggests that there is a range of effective bond strengths such that the activation energy for liberation of hydrogen, which remains at 1600 K, is greater than for hydrogen which is stable only to 1300 K.

The cumulative hydrogen yielded on heating from 1170 to 1750 K is shown in figure 6.5 and clearly shows secondary carbonisation to cease between 1600 and 1700 K. No further hydrogen could be detected beyond 1750 K. These results agree well with those obtained by CHO analysis, table 6.2, bearing in mind the concentrations are at

the limits of detection for the latter technique. The % H values obtained by EGA were calculated assuming % H = 0 at 1870 K and that a final 0.01% was evolved from 1770 to 1870 K.

Table 6.2

HTT (K)	1270	1470	1570	1670	1770	1870	Precision
CHO W % H	0.28	0.10	0.03	0.03	0.01	0	± 0.05
EGA W % H	0.32	0.09	0.05	0.015	0.005	0	± 5% of value

The importance of these findings on the structural transformations will be discussed further in Chapter 10, where they will be integrated with results from the other techniques.

A. Argon cylinder connection.

B. Hydrogen cylinder connection.

C. De-oxygenator column.

D. Drying columns.

E. Jet-type flowmeter.

F. Needle valve.

G. Pulse meter.

H. Tap.

I. Induction coil.

J. Water-cooled sample tube.

K. Graphite susceptor (sample inside).

L. Optical pyrometer.

M. Two-way tap.

N. Pirani gauge.

O. Exit gas bubbler.

P. Fore-line trap.

Q. Rotary pump.

R. Needle valve.

S. Mass spectrometer head.

T. Penning gauge.

U. Liquid nitrogen trap.

V. Oil diffusion pump.

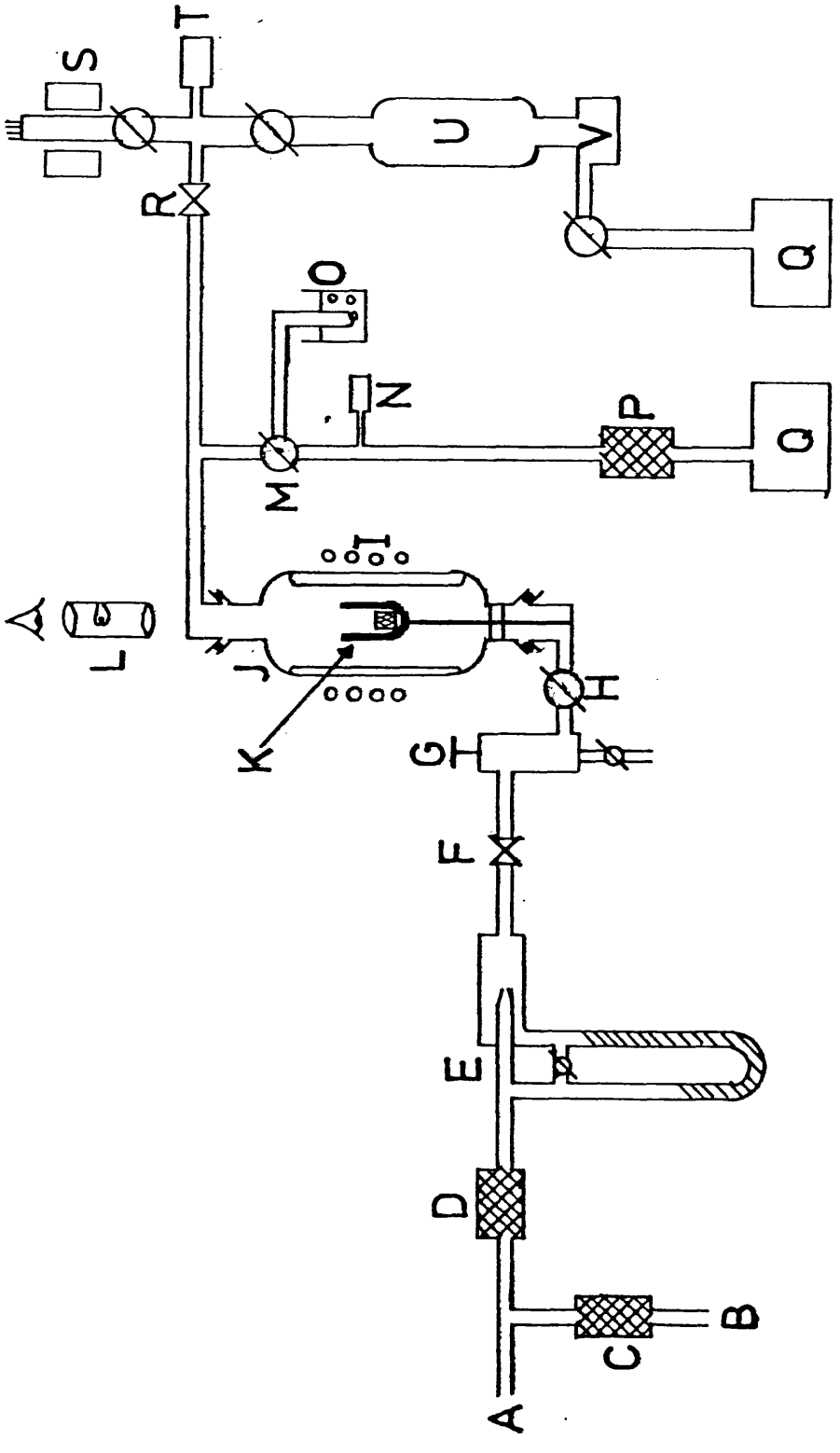

Fig. 6.1 Heat-treatment and evolved gas analysis apparatus.

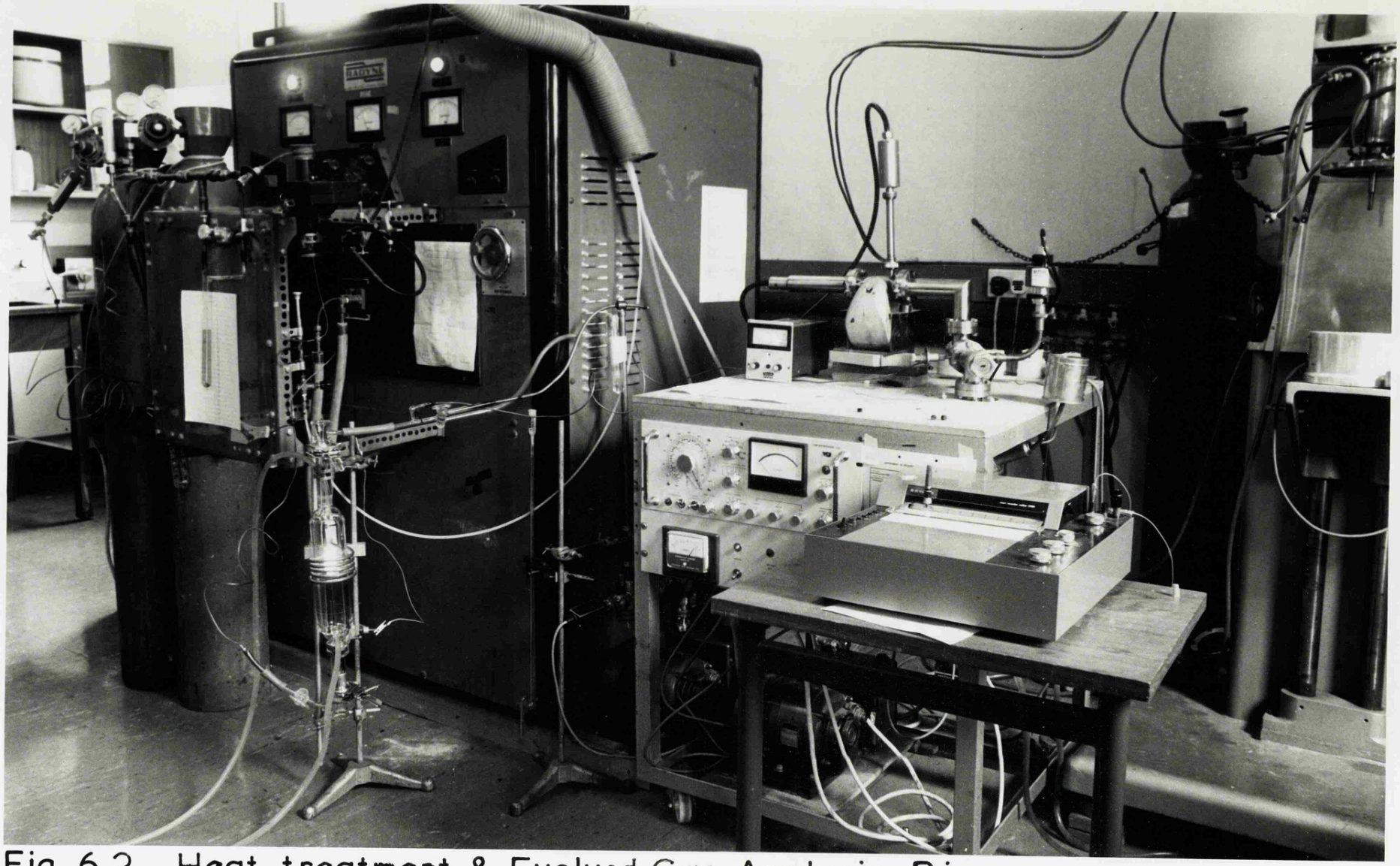

Fig. 6.2 Heat-treatment & Evolved-Gas Analysis Rig.

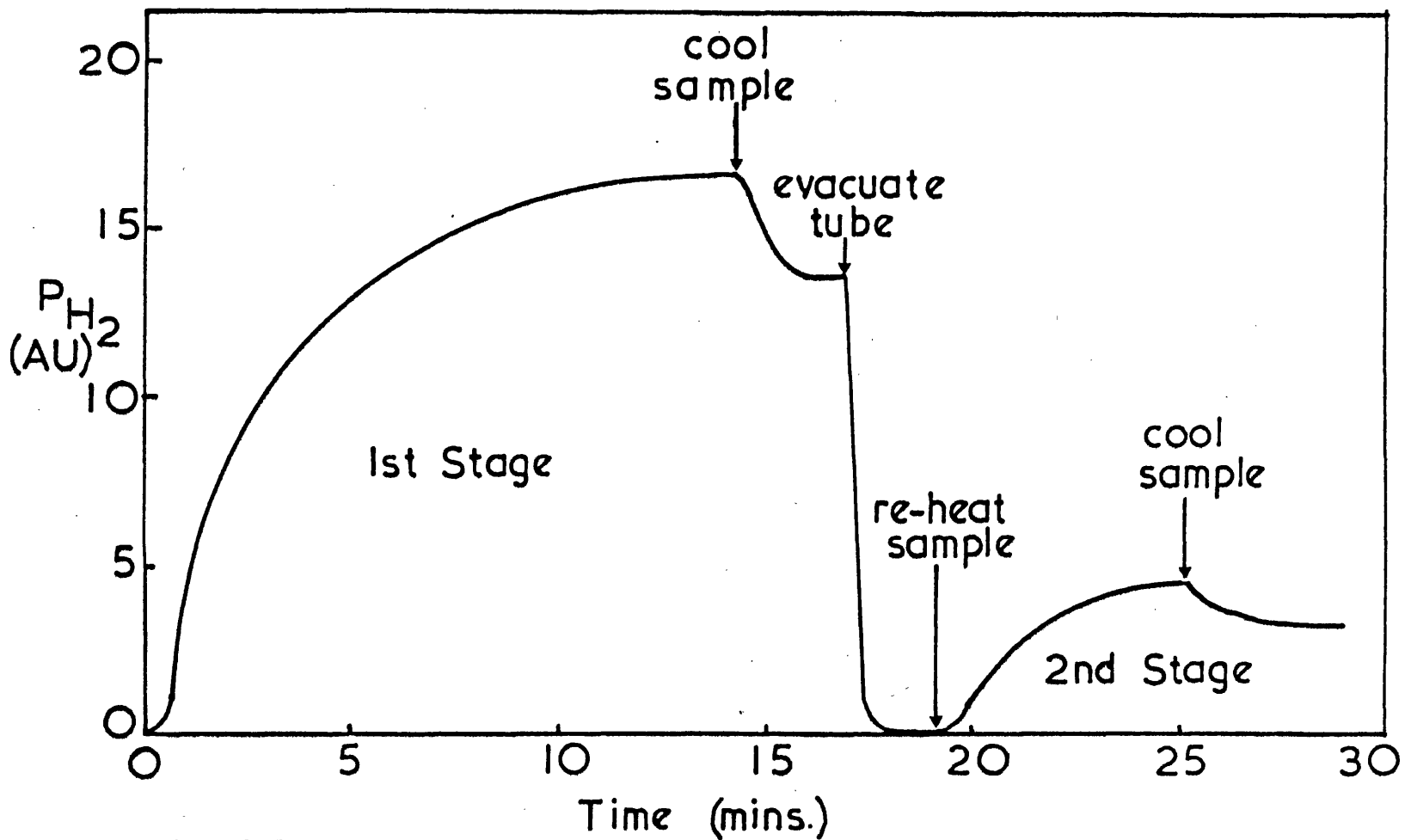

Fig. 6.3 Typical Hydrogen Evolution Curve.

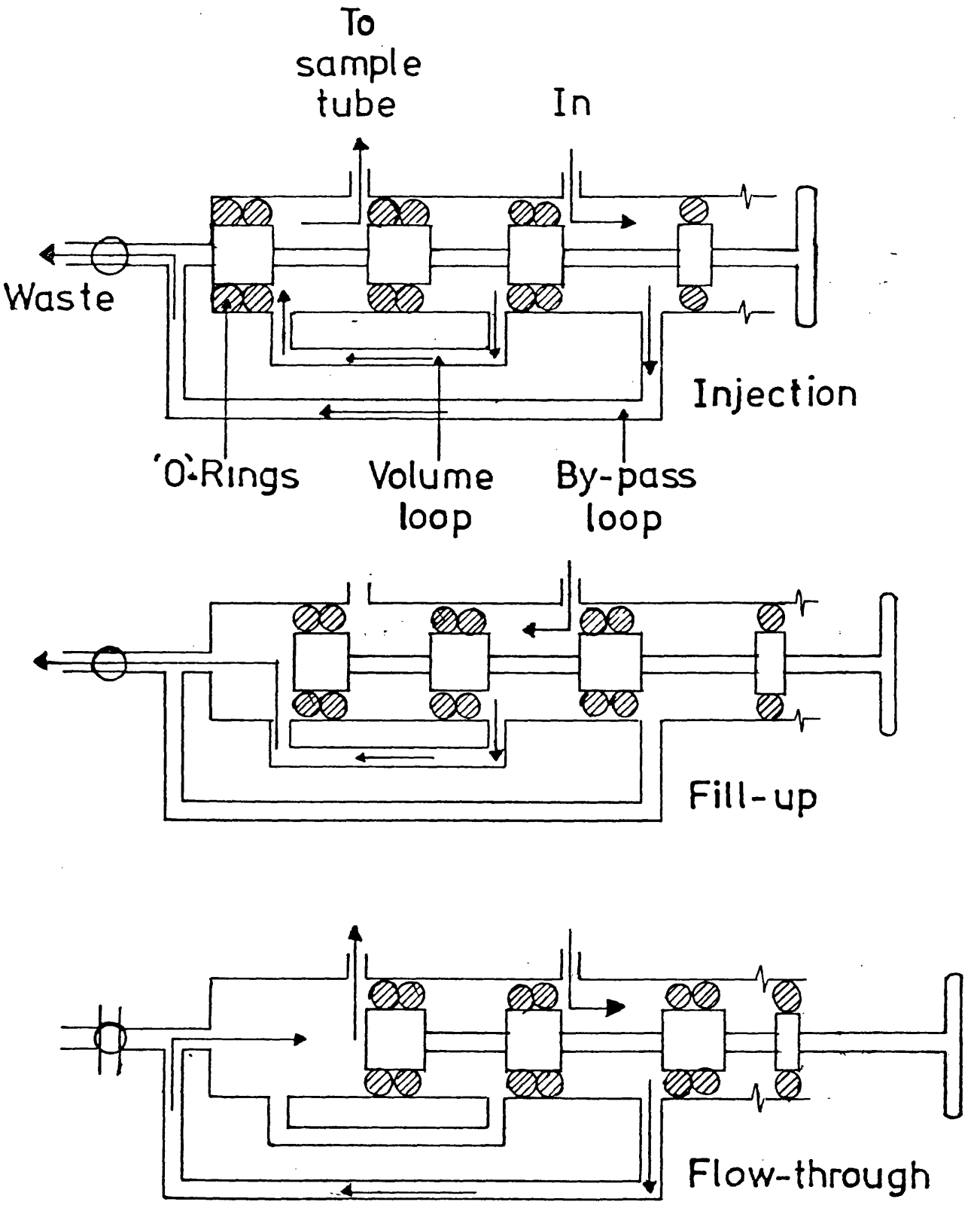

Pulse meter operation

Fig.6.4

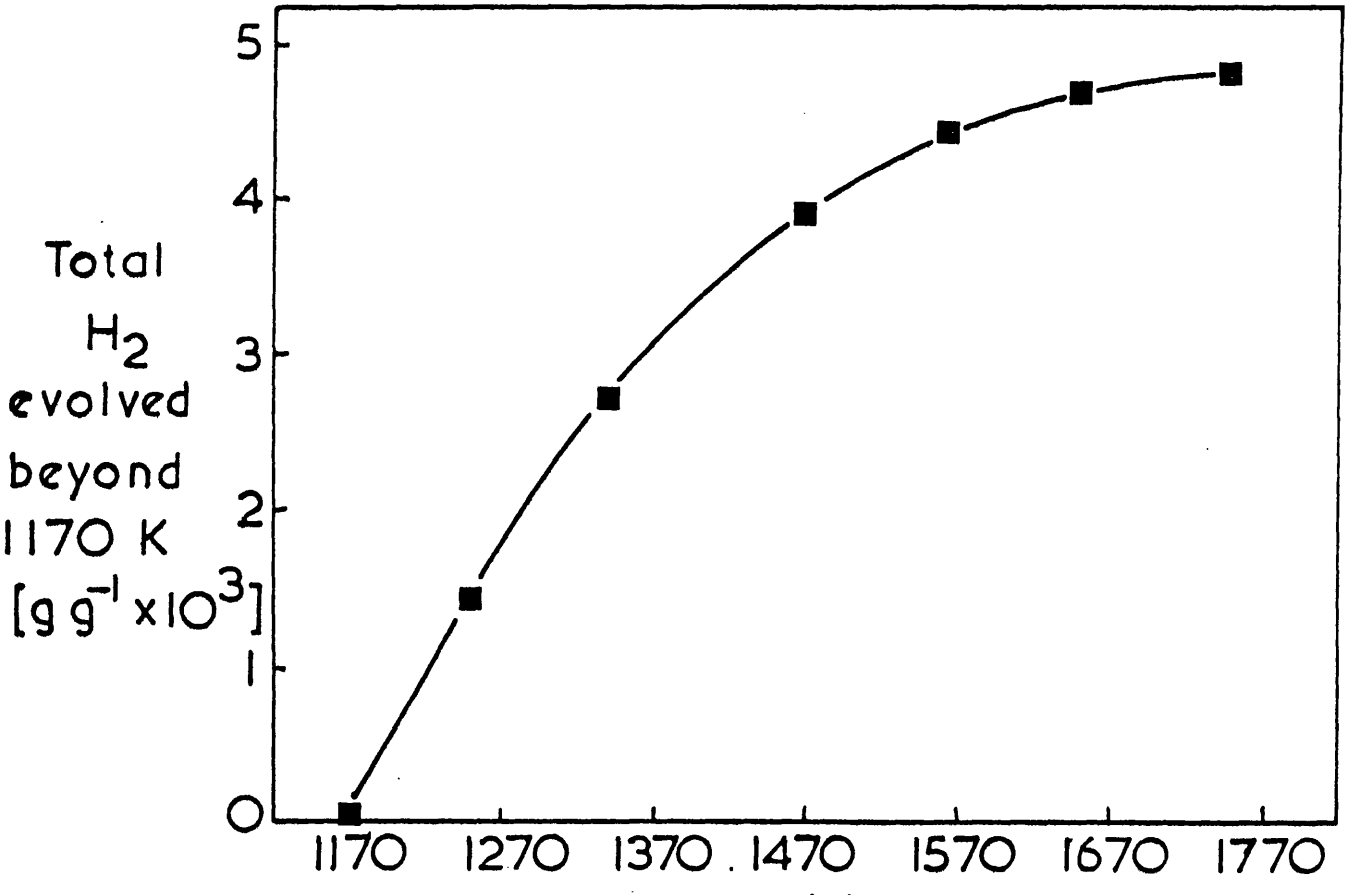

Fig. 6.5 Hydrogen evolved on heat-treating cellulose carbon.

CHAPTER 7

THE EFFECTS OF HEAT-TREATMENT

CHAPTER 7

X-RAY STUDIES OF ISOCHRONALLY HEAT-TREATED CARBONS

7.1.1.

A set of cellulose carbons were heat-treated at different temperatures for 10 minutes and the diffraction patterns recorded. The SAXS from these and a commercial glassy carbon (Sigri, HTT 2500 K) were analysed by the Debye approach, i.e. $J^{-2/3}$ - h^2 plots were made and correlation distances, a, were obtained from the slopes and intercepts. Sample plots are shown in figure 7.1, the linearity of the plots testify to the correctness of the exponential correlation function. The a values are shown in figure 7.2 and table 7.1. The a value obtained by Wignall and Pings[68] for a Beckwith 2073 K GC is included for comparison.

It can be seen that some growth in a occurs with HTT but at an increasing rate after about 1573 K. The values for the glassy carbons suggest growth continues at a linear rate, even at high temperatures.

The precursors for the Beckwith and Sigri glassy carbons are unknown, but it is unlikely that cellulose was used. The agreement with the cellulose carbons indicates an insensitivity of microstructure to the organic precursor or manufacturing technique.

The correlation distance is related to the mean chord intercept distances of the pores and matrix, ℓ_p and ℓ_m, by

$$\frac{1}{a} = \frac{1}{\ell_m} + \frac{1}{\ell_p} \qquad 7.1$$

(The Porod distance of heterogeneity, ℓ_c, is the mean of ℓ_m and ℓ_p).

To obtain mean pore or matrix lengths either absolute intensity measurements[172] or a value for the volume fraction of one phase are needed. The latter approach was used here with the volume fraction of pores, C, being defined as :

$$C = V_o/(V_o + V_c) \qquad 7.2$$

where V_o is the total open and closed micropore volume and V_c the volume of carbon, in unit weight of specimen.

The value of V_o should not include meso or macropores as these do not significantly contribute to the region of scatter which was investigated here. Adsorption measurements (see section 7.4.3) show the micropore volume to be fully developed at about 1270 K and small amounts of activation suggest it to be substantially accessible to CO_2 at 295 K. The micropore volume of 0.32 ml g^{-1} for the 1270 K cellulose carbon was therefore taken as being constant, to a first approximation, for all carbons examined. Any further change in V_o with HTT cannot be observed by adsorption due to the pore closure effect.

The volume occupied by carbon is commonly obtained from the x-ray density :

$$V_c = 1.315 \times d_{002} \qquad 7.3$$

If d_{002} is expressed in nm, then V_c is in ml g^{-1}.

Application of this approach revealed a paradox, namely, that the bulk (geometric) density of the Sigri carbon was 1.45 g ml^{-1} which, assuming an x-ray density of 2.20 g ml^{-1}, results in a *total* porosity of 0.235 ml g^{-1}. Such a discrepancy between this and the assumed value of 0.32 ml g^{-1} seems odd considering the apparent similarity of microstructure revealed by their correlation distances.

To discover where the error lay, the bulk density of a cellulose carbon was needed. Because the cellulose carbons are macroporous, the density of 1170 K carbon was determined in a mercury porosimeter. The mercury was subjected to a pressure of 1500 Kg cm^{-2} which should cause it to penetrate pores of radius larger than 5 nm. Coarse sized particles ($\sim$5 mm diameter) were used to avoid interparticle space, and the data was corrected for mercury compressibility. The resultant density should comprise solely of carbon and micropore volume since no evidence existed for mesoporosity. The density so obtained was 1.477 g ml^{-1}. If one takes the x-ray density as 2.20 g ml^{-1} the above bulk density yields a micropore volume of 0.223 ml g^{-1}, yet the D-R adsorption volume is known to be 0.3 ml g^{-1}. There are two possible explanations for this discrepancy :

(A) The micropore volume may be wrong because the D-R plots (at 295 K) were not measured to P/Po = 1.
The extrapolation appears to be reasonably valid, however, since

the D-R plots were linear over a large pressure range and deviations are generally observed only at low pressure, not high pressure. Any error in the assumption of liquid density for CO_2 would cause an underestimate of V_o since, being so close to T_c, the absorbate would tend to resemble a gas more than liquid.

(B) The *effective* volume occupied by carbon may be in error since the x-ray density assumes all the carbon to be in the form of an infinite crystal. Plainly this is not the case since XRD shows that the well-formed crystallites have a stack height of only 1 - 2 unit cells. Now, the geometric density of an isolated unit cell is three times that of one within a lattice, since none of the atoms are shared between other cells. In addition, the graphite lattice is so voluminous that if it were reduced to isolated layer-planes - which were accessible to adsorbate molecules - the volume occupied by carbon would be considerably decreased. The volume of a turbostratic crystal, as seen by adsorbate molecules, would be larger than for the same amount of carbon in the form of isolated layer-planes, because much of the turbostratic carbon is inaccessible to adsorbate. Since the value of V_c, required for ℓ_p and ℓ_m calculations, is used as the volume for a phase of *constant, finite, electron density*, the x-ray density would appear to be inappropriate for this purpose, since space accessible to adsorbate molecules cannot be classed as belonging to the carbon phase.

Because of the foregoing arguments V_c was obtained from :

$$V_c = \frac{1}{\rho_b} - V_o \qquad 7.4$$

where ρ_b is the density of carbon + micropores and was determined by mercury porosimetry as 1.477 g ml^{-1}. Taking V_o (from CO_2 adsorption) as 0.32 ml g^{-1} gives V_c = 0.357 ml g^{-1}, or a carbon density of 2.8 g ml^{-1} (cf. an x-ray density of 2.2 g ml^{-1}). This results in the volume fraction of pores, C, being 0.472. C was taken as constant for all the heat-treated carbons since very little bulk shrinkage was found for HTT $\gtrsim$ 1200 K. The following parameters were calculated and are shown in table 7.1 and fig. 7.3.

$$\ell_m = a/c \qquad 5.28$$

$$\ell_p = a/(1-C) \qquad 5.29$$

$$\text{Surface area per unit volume, } S/V = \frac{4C(1-C)}{a} \qquad 5.26$$

$$\text{Surface area per unit weight, } S/g = \frac{4C(1-C)(V_o+V_c)}{a} \qquad 7.5$$

Fig. 7.3 shows both ℓ_p and ℓ_m increase with HTT, in agreement with other workers [145,173-176]. This indicates a coarsening of pores from small finely dispersed ones to larger ones with a greater thickness of matrix between them. The reduction in surface area confirms this view.

Included in fig. 7.3 is the layer-plane stack height - L_c, as obtained from the width of the corrected (002) profile. It is interesting to note that ℓ_m approaches L_c as HTT increases. If the structure is imagined as a random orientation of layer-planes, the pores will

be the voids between adjacent layer-planes and groups of planes. L_c will be a measure of the distance between defects in comparatively well-formed stacks, whereas ℓ_m will be the distance between defects (density fluctuations)within the whole structure. If highly defective single layers or stacks exist ℓ_m will always be smaller than L_c . However, as the structure improves with heat-treatment, defects between layer-plane stacks will become annealed out, increasing both L_c and ℓ_m. The approach of ℓ_m to L_c indicates such annealing occurs most noticeably in small layer plane groups and must involve considerable grouping together of individual layer-planes. This view is supported by the constant value of interlayer spacing, d_{002},up to 1600 K which is probably a result of the production of many 'new' layer stacks of fairly wide separation, due to continuing secondary carbonisation. This appears to be complete at ~1600 K, since d_{002} then begins to decrease and L_c increase, with ℓ_m increasing still faster. These increases are probably due to the annealing out of defects within the now formed stacks. Whether ℓ_m may actually equal L_c for the Sigri carbon is difficult to say because neither parameter is known with certainty. ℓ_m may be larger because some of the space which was assumed to be void (since accessible to adsorbate molecules) may have become incorporated into a turbostratic lattice. The value of V_c would, in this case, need to be somewhat closer to the value derived from the x-ray density. If the x-ray density were used, a micropore volume of 0.278 ml g^{-1} would give coincidence of ℓ_m and L_c . Such a value is not unreasonable. L_c is also weighted towards larger stacks so that many smaller stacks may be equal in size to ℓ_m. On the other hand, L_c may be larger than measured since no correction was applied for broadening due to specimen transparency (absorption). Nevertheless, for carbons of high HTT it appears that the micropores are voids

between relatively perfect stacks of layer-planes, which constitute the pore walls.

The picture of a micropore at low HTT is less clear since ℓ_p for a 1170 K carbon is less than the c spacing. The surface areas for these carbons are also excessively high - more than the theoretical maximum of 2620 m^2g^{-1}. These values remain unrealistic for all likely values of c. These findings pose the question of whether a is solely related to the dimensions of a void-matrix system or whether it is influenced by other factors. This point will now be considered.

7.1.2. Deviations from Porod's Law

Throughout the theory of SAXS it is assumed that, A, each phase is of uniform density and, B, the phase boundaries are sharp.

Assumption A is probably not correct for the carbon phase since, if it is poorly crystalline, the population of defects will constitute electronic density fluctuations within the solid matrix. The intensity component from such fluctuations will simply add the scattering from the ideal system but, because the correlation distances are very small, the intensity will be predominantly observed at high angles (c.f. eqn.5.1).

Ruland[177] has shown the normalised intensity component from one dimensional fluctuations to be given by

$$J_F = \frac{\tau F \ell_1}{2 S} \qquad 7.6$$

where $S = \mathrm{Sin}\ 2\theta/\lambda$, τ is the surface density of electrons in the

two dimensional entities which participate in the fluctuation and $F\ell_1$ is the fluctuation of density as projected onto a straight line parallel to the direction of disorder. This form seems appropriate for the case in hand since one-dimensional fluctuations have been observed in both graphitizing[178] and non-graphitizing carbons[175,179]

If the phase interfaces are not sharp but diffuse, the result will be a reduction in scattered intensity, also at high angles. Hosemann and Bagchi[180] have shown how this effect can be represented by a convolution of the ideal density distribution (such as a Dirichlet step function) with a smoothing function. If a Gaussian smoothing function is used, the observed intensity for a system with diffuse interfaces is given by :

$$J_{obs} = \frac{I_e(h)\pi^2\Delta\rho^2 S(1 - 2\sigma^2h^2)}{h^3} \qquad 7.7$$

where S is the surface area within the volume irradiated. σ is the variance of the Gaussian distribution and will be a measure of the interfacial width.

When factorised, the first term of Eqn.7.7 will be recognised as the Porod asymptote (eqn.5.31) whilst the second term represents the loss in intensity due to the diffuse interface.

The total observed intensity for an "imperfect" porous solid may therefore be composed of a component which obeys Porod's law (i.e. decreases as h^{-3}) and two components which vary as h^{-1}, the first, due to electronic density fluctuations, being positive and the second, due to diffuse interfaces, being negative. We may therefore write :

$$J = b_1 h^{-3} + b_2 h^{-1} \qquad 7.8$$

or

$$Jh^3 = b_1 + b_2 h^2 \qquad 7.9$$

A plot of Jh^3 against h^2 should tend to a straight line which is horizontal for an ideal system, has a positive gradient if electron density fluctuations are present and a negative gradient if the interfaces are diffuse. In some cases the latter two effects may partially or completely cancel one another. If the linear region is extrapolated to cut the y-axis, the intercept will be the Porod asymptote, i.e. a measure of the well-defined surface area.

Sample plots for the isochronally heat-treated series are shown in figure 7.4, h has been replaced by $\sin 2\theta$ for convenience and J is in arbitrary units. The large positive slopes clearly indicate considerable density fluctuations to be present, with any effect due to diffuse interfaces being overshadowed. The gradients gradually decrease with HTT whilst the extrapolated intercepts increase, from zero below 1200 K. For the 2500 K Sigri carbon (Figure 7.5) Porod's law is actually attained which indicates that there are no electron density fluctuations within the solid, and the matrix/void interfaces are sharp. The slight increase above $\sin^2 2\theta = 0.022$ ($2\theta = 8.5^0$) is due to overlap from the (002) peak, this region being particularly sensitive to extraneous intensity.

If the intercept b_1 and gradient b_2 are plotted against HTT (Figure 7.7) an interesting trend is shown. The gradients (b_2) pass through a maximum at about 1270 K then decrease linearly. The initial increase

may be a result of continued secondary carbonisation, in two ways : 1, If hydrogen were to aggregate at regions of distortion, vacancies, layer-plane edges, etc (where unstable carbon atoms exist) the intensity of electron density fluctuation in these areas is reduced by the further extension of electron density away from the solid carbon. The hydrogen, in effect, blurs the definition of the defect. As hydrogen is removed during carbonisation the electron density fluctuation increases in magnitude. This process is therefore similar to the loss of a phase of intermediate electron density between solid carbon and void. 2, For larger density fluctuations (approaching conventional voids) hydrogen may be attached to the carbon surface and this, as before, will blur the interface. Removal of this hydrogen will result in the removal of a negative component which obeys h^{-1} scattering, i.e. a sharpening of interfaces occurs. The involvement of hydrogen in the transformations of this temperature region is suggested by the hydrogen evolution measurements of Chapter 6.

The decrease in slope after 1270 K must be due to the loss of small scale density fluctuations and probably becomes more rapid after 1800 K because there are none for the 2500 K carbon. The loss of small electron density fluctuations appears to be to the gain of scattering by larger ones (i.e. well defined voids) since the Porod component b_1 starts to increase at about 1270 K. For 1070 and 1170 K carbons virtually all the scattering is from electron density fluctuations and none from conventional pores.

7.1.3. Amorphous Scattering

If the structure of low-temperature carbons is characterised by

diffusely bounded, small scale, electron density fluctuations, the question arises as to whether a glassy, amorphous, structure may not be more appropriate than the one described, or one of discrete microcrystals. Silica, for instance, has a bulk density 17% less in its glassy state than in its crystalline state. If this is the case for carbon, the scattering which follows the h^{-1} law would be of the diffuse gas type and so be given by $J = Af^2$ where A is the amount of amorphous carbon and f its coherent atomic scattering factor. A plot of $f^2(2\theta)^3$ against $2\theta^2$ (Figure 7.6), shows a curve whose gradient increases only gradually at high angles and so may be approximated by a straight line, with a negative intercept on the y-axis. Inspection of the $Jh^3 - h^2$ plot for the 1070 K carbon shows that extrapolation of the low angle points gives a negative intercept, while extrapolation from higher angles gives a zero intercept. The observed plots for low HTT carbons could therefore be a combination of the ideal Porod asymptotic shape (e.g. 2500 K Sigri GC) and the amorphous scattering curve, with the Porod proportion increasing with HTT.

This explanation of diffuse scattering in terms of amorphous carbon has been used by Franklin[52] and Short and Walker[154], but was criticised by Ruland[181] who suggested that it was more likely to be due to imperfections, especially vacancies, in the structure of the graphitic layers. Whilst not dismissing the possibility of scattering from single layer-planes, he points out that a similar effect is produced by an imperfect stacking of layers, as well as variation of size and perfection within a given stack. The latter argument is largely one of semantics since the borderline between a layer-plane within a disordered group of planes and an apparently isolated

one is ill-defined. Ergun[159] also points out that production of amorphous carbon (with no repetitive interatomic distances) is unlikely during a carbonisation process. It will be shown in section 8.7.2. that the existence of a discrete amorphous phase is unlikely.

7.2.1. X-Ray Study of Isothermally Heat-treated Carbons

In order to find out more about the mechanism of pore coarsening, a set of cellulose carbons were heat-treated at various temperatures for 2, 5, 10 and 30 minutes. Temperatures selected were 1270, 1470, 1570 and 1670 K (the heating program is given in Appendix A(5)).

7.2.2. SAXS

The correlation distances (figure 7.8) show that pore growth is very rapid, with significant differences in a being achieved after only 2 minutes. The subsequent rate of growth appears to be small at 1270 K but gradual at 1470 K.

It is known (see Chapter 6) that hydrogen continues to be evolved up to 1670 K, so the initially rapid growth observed at all temperatures is probably due to the loss of hydrogen from layer-planes, which enables them to pack together. The apparent lack of change for the 1270 K carbons may be a result of the removal of hydrogen which causes an increased definition of electron density fluctuations and so offsets the loss of fluctuations caused by the better packing of layers.

Because the kinetics of hydrogen evolution would be faster after 1470 K the growth in a ceases more rapidly but there appears to be further growth at longer heating times. This may suggest the existence of a second mechanism which occurs at higher temperatures, is much slower, and does not depend on heteroelement expulsion.

7.2.3. X.R.D.

Whilst the correlation distances are profoundly affected by HTT and to a lesser extent HTt, the XRD parameters (Table 7.2) are relatively unaffected by both. The interlayer spacing, d_{002}, varies little for all carbons, while L_c only increases for the two highest heat-treatment temperatures. These findings agree with those for isochronally heat-treated carbons where little growth of L_c occurred before 1570 K, whilst a showed a steady increase.

Since SAXS is strongly influenced by electron density fluctuations within disordered carbon, whilst XRD is biased towards ordered regions, we may deduce that up to ~ 1570 K, the predominant changes occurring are in disordered regions. These changes are probably a result of continuing secondary carbonisation, which is producing ordered layer-planes from a tangled network of misorientated, defective, aromatic groupings. Such a change may be imagined as a dissociation of a tetraphenylene type structure (see figure 2.4) and re-grouping of the aromatic units to form crude layer-planes. The packing in newly formed stacks will be faulty, thus the statistical value of L_c and d_{002} will change little in this region. When carbonisation is nearing completion (~ 1570 K), L_c may begin

to increase, since the process is then one of increasing perfection of the formed layer stacks.

7.3 General Discussion

To summarise, low HTT carbons appear to be composed of a random network of highly defective layer-planes whose crystallites are small due to a high concentration of bends and kinks. Electron density fluctuations are more due to gaps between individual layers, and vacancies within layers, than to gaps between large layer stacks ("crystallites"). These fluctuations may be considered as being micropores which are not yet fully developed. The definition of such voids is blurred due to hydrogen bonded to surface atoms.

As HTT increases, hydrogen is lost, resulting in previously hydrogen-rich regions of intermediate density becoming more defined as matrix/void regions. Vacancies and defects begin to be annealed out from within planes which allows them to stack more efficiently, resulting in an increase in L_c as measured by x-rays. Many stacks are still defective since ℓ_m is less than L_c, but the two approach and, perhaps, meet each other by about 2000 K. The finding that the carbon matrix of 2500 K GC has no density fluctuations within it suggests these layer stacks are substantially perfect. The difference between L_c and ℓ_m may therefore be due to L_c being biased towards the large crystallites.

The annealing of small gaps between layer-planes results in the creation of larger voids together with larger crystallites.

This is schematically represented in figure 7.9. The latter system bears more resemblance to a conventional porous system and so scatters in obeyance with Porod's law (as seen by the 2500 K Sigri GC).

The pores in this model would be expected to be needle-shaped which agrees with Perret and Ruland's findings[176]. Whilst Rothwell's[145] finding that the pores assume a spherical shape with increasing HTT has been shown to be incorrect[176], we may conclude that his findings suggest an increase in the pores' minor axes with a lesser effect on their major axes. This agrees with the proposed mechanism of growth as being due to a translational packing of layers along the C-axis.

It can be seen from figure 7.9 that many of the spacings, which constitute ultramicropores, are reduced to turbostatic values, as a result of the pore coarsening effect. These changes are of notable significance for the access of adsorbate molecules to the internal structure and will be discussed further in Chapter 10 and Section 7.6.

TABLE 7.1

X-Ray Data for Isochronally Heat-treated Carbons

XRD			SAXS				
HTT(K)	d_{002}(nm)	L_c(nm)	a(nm)	ℓ_p (nm)	ℓ_m (nm)	$S/V(m^2ml^{-1})$	$S/g(m^2g^{-1})$
970	0.372	0.804	-	-	-	-	-
1070	0.355	0.866	0.155	0.294	0.328	6431	4354
1170	0.358	0.871	0.176	0.333	0.373	5664	3835
1270	0.360	0.857	0.200	0.379	0.424	4984	3375
1370	0.357	0.848	0.210	0.398	0.445	4747	3214
1470	0.360	0.894	0.239	0.453	0.506	4171	2824
1570	0.359	0.895	0.247	0.468	0.523	4036	2732
1670	0.358	0.947	0.283	0.536	0.600	3522	2385
1770	0.354	0.995	0.332	0.629	0.703	3003	2033
1870	0.352	1.033	0.365	0.691	0.773	2731	1849
2070(ref 68)	-	1.5	0.52	0.985	1.101	1917	1298
2500	0.347	1.812	0.689	1.305	1.460	1447	979

TABLE 7.2

X-Ray Parameters for Isothermally Heat-Treated Carbons

		XRD		SAXS
HTT (K)	HTt(mins)	d_{002}(nm)	L_c(nm)	a (nm)
1270	2	0.359	0.893	0.199
	5	0.362	0.902	0.201
	10	0.360	0.886	0.201
	30	0.363	0.849	0.201
1470	2	0.362	0.902	0.219
	5	0.358	0.881	0.226
	10	0.358	0.903	0.228
	30	0.358	0.895	0.245
1570	2	0.359	0.891	0.250
	5	0.359	0.883	0.250
	10	0.358	0.932	0.246
	30	0.363	0.927	0.271
1670	2	0.362	0.932	0.268
	5	0.360	0.954	0.264
	10	0.361	0.911	0.265
	30	0.357	0.950	0.278

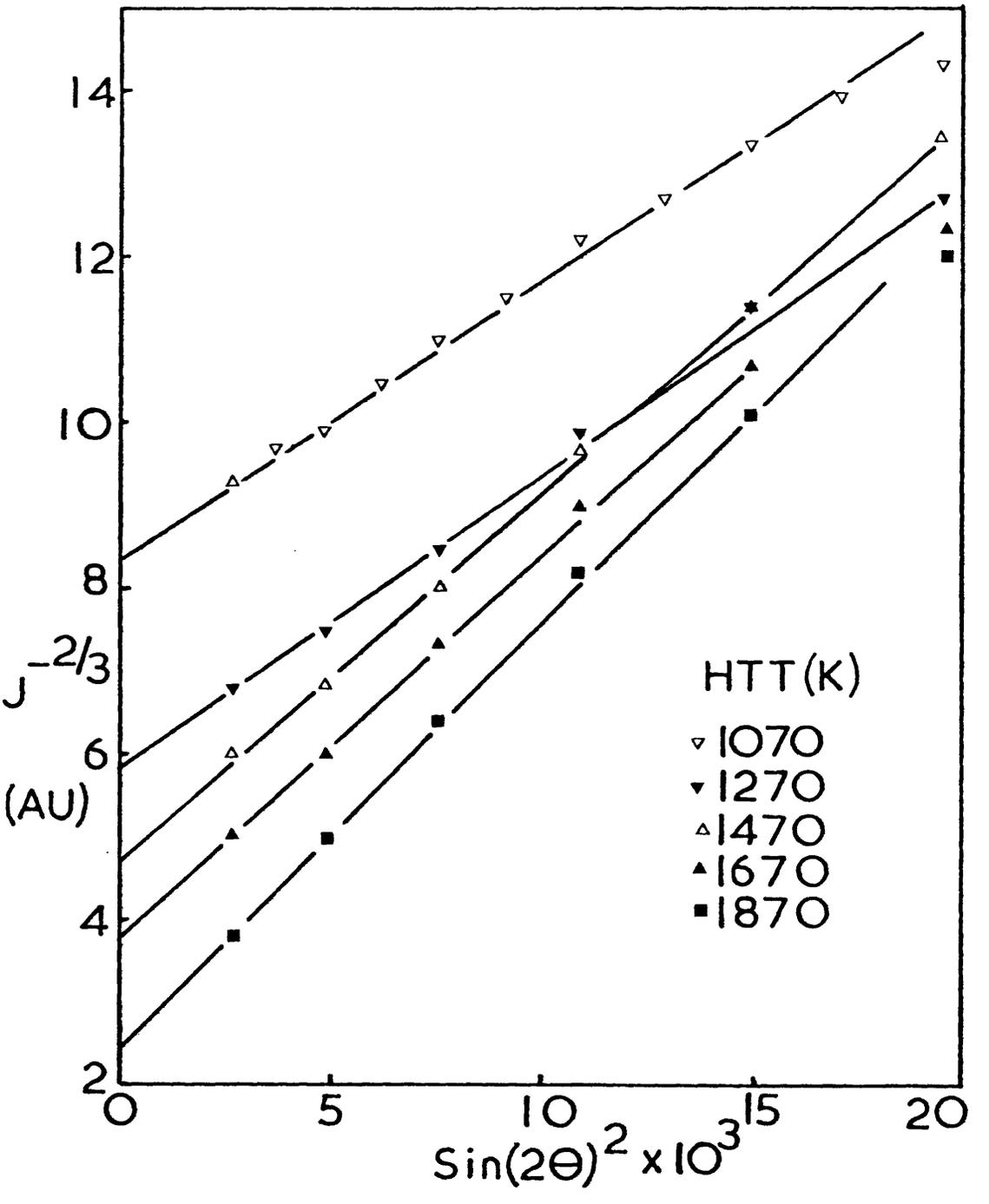

Fig.7.1 Debye Plots for Isochronally Heat-treated Carbons.

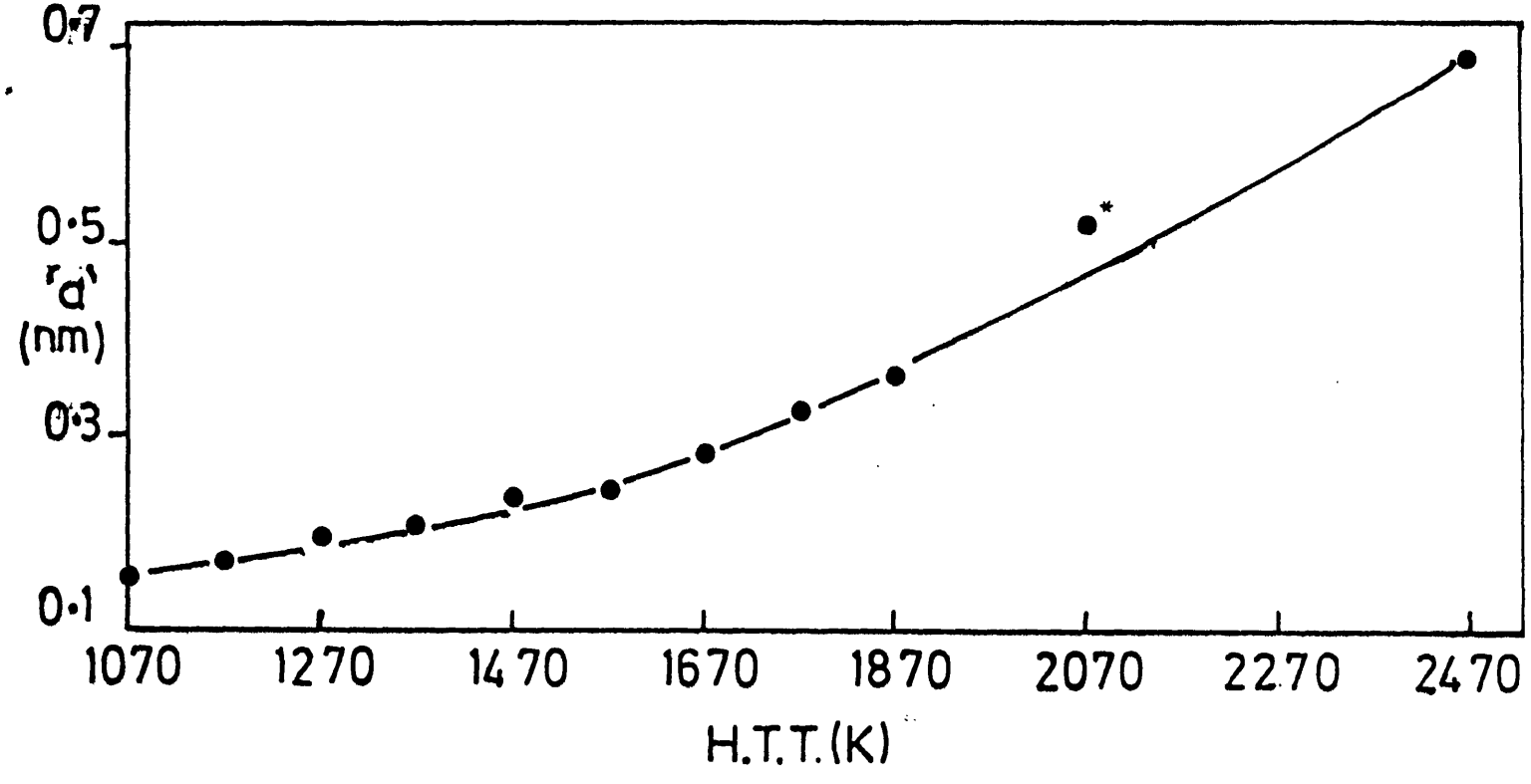

Fig. 7.2 Correlation distances for isochronally heat-treated carbons (*Ref. 68)

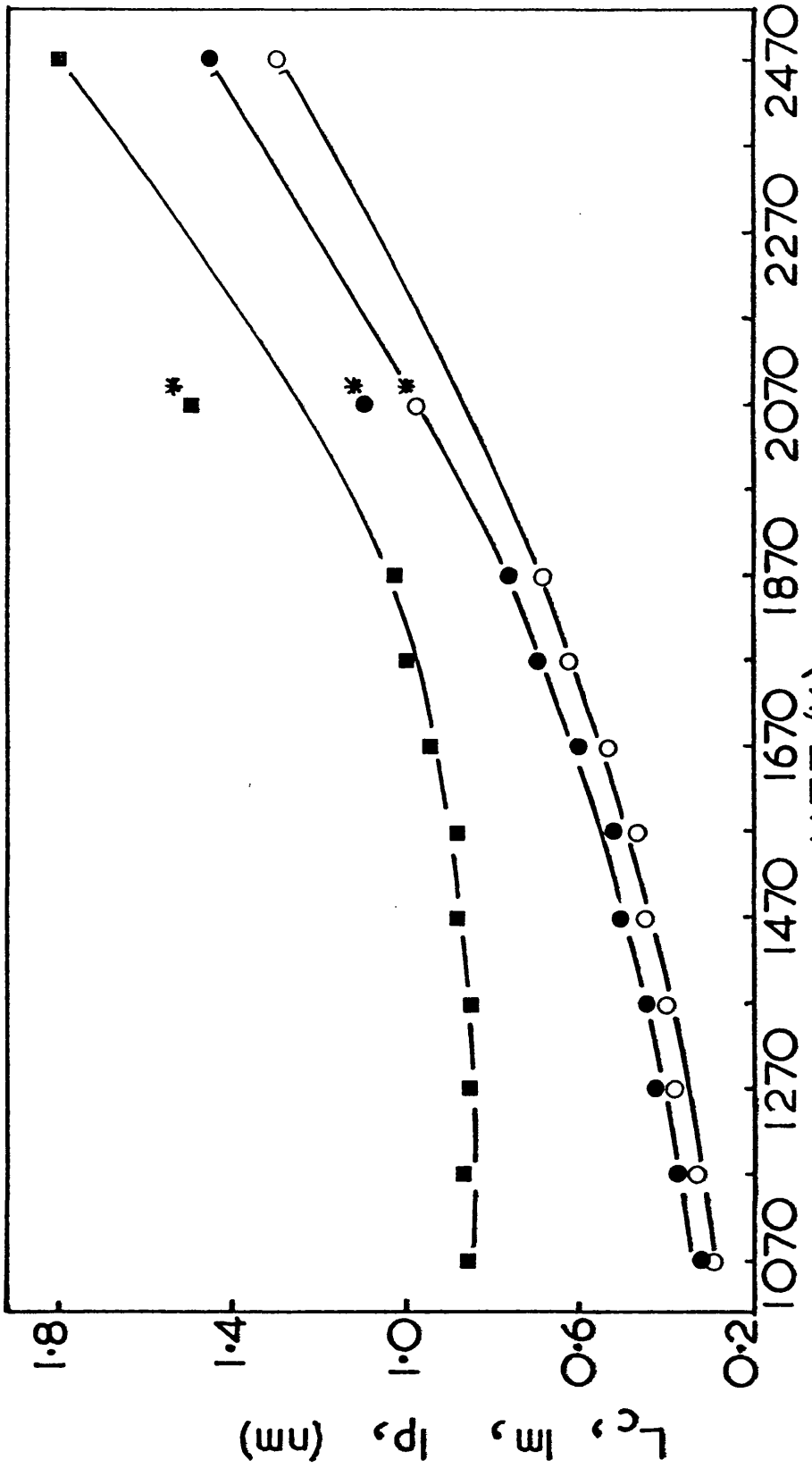

Fig. 7.3 Linear Parameters from SAXS. & X.R.D.

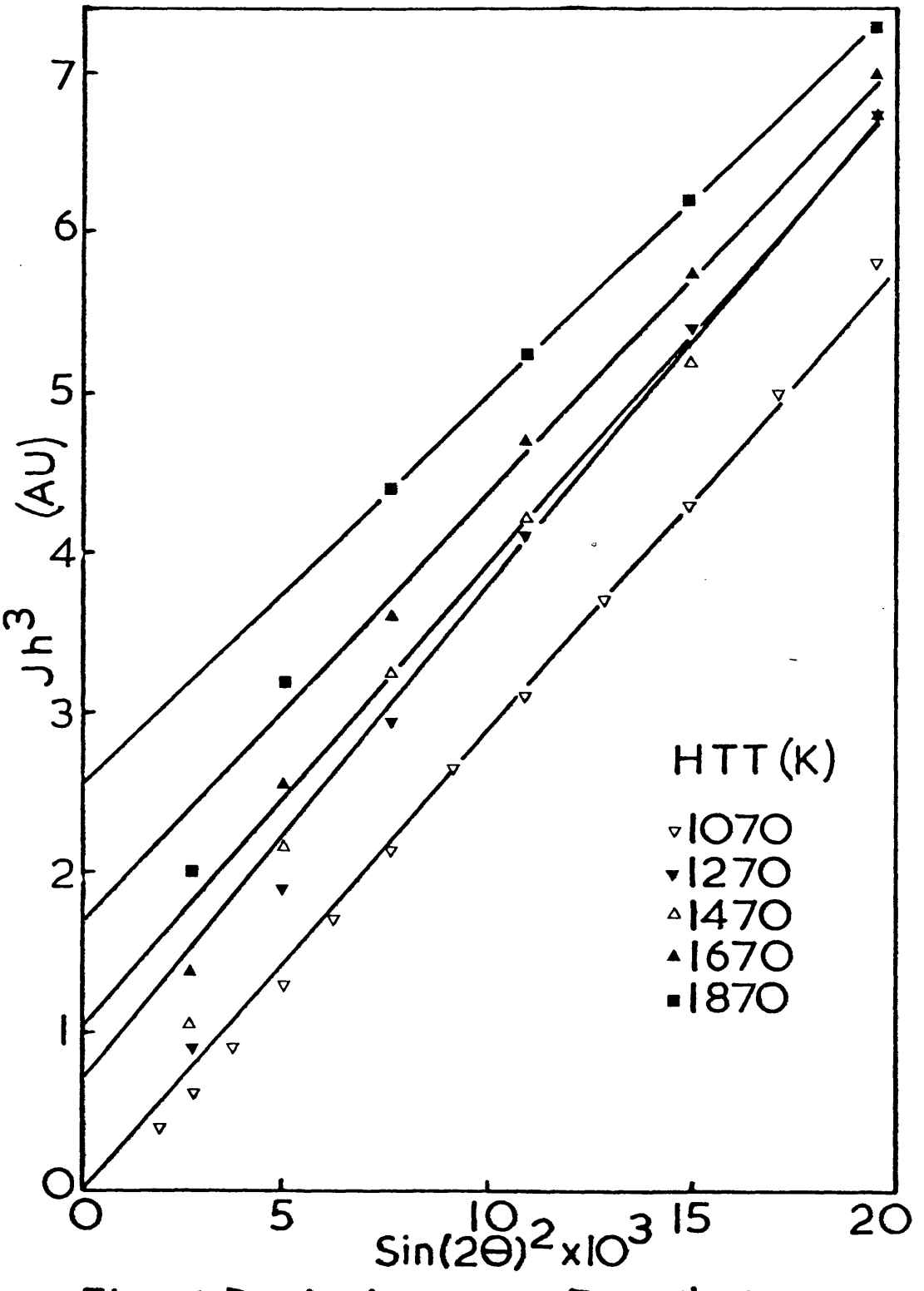

Fig.7.4 Deviation from Porod's Law for Isochronally Heat-treated Carbons

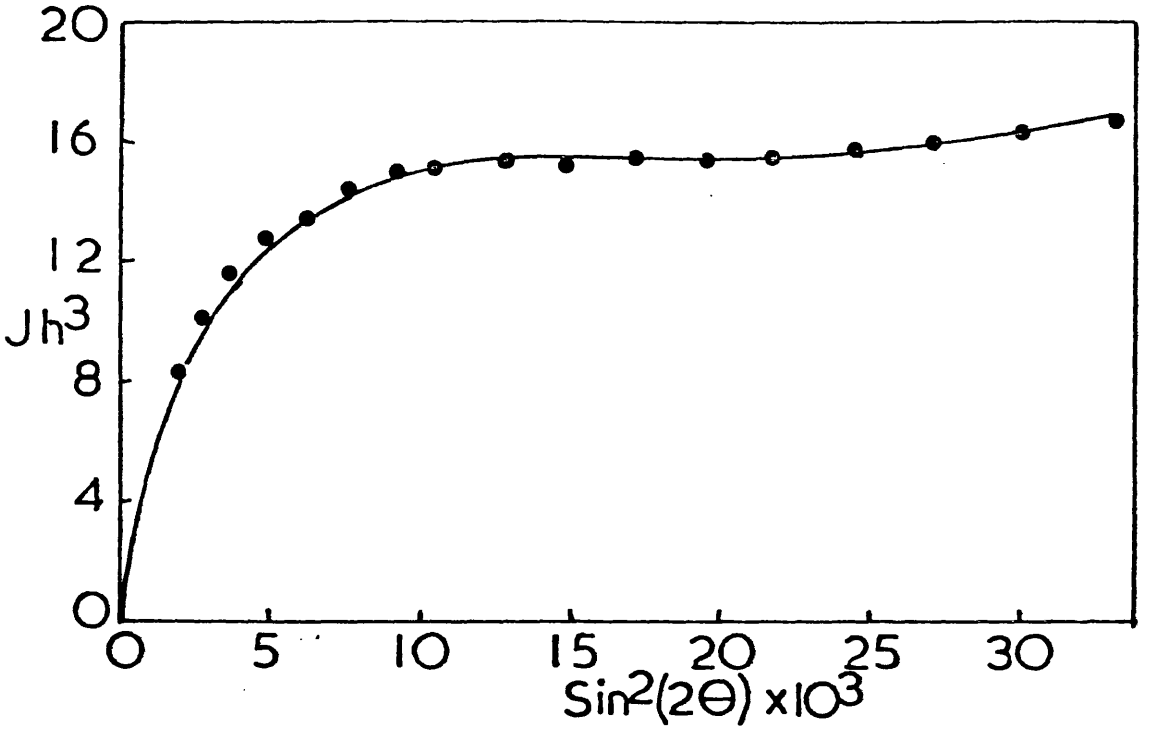

Fig. 7.5

2500 K Sigri glassy carbon.

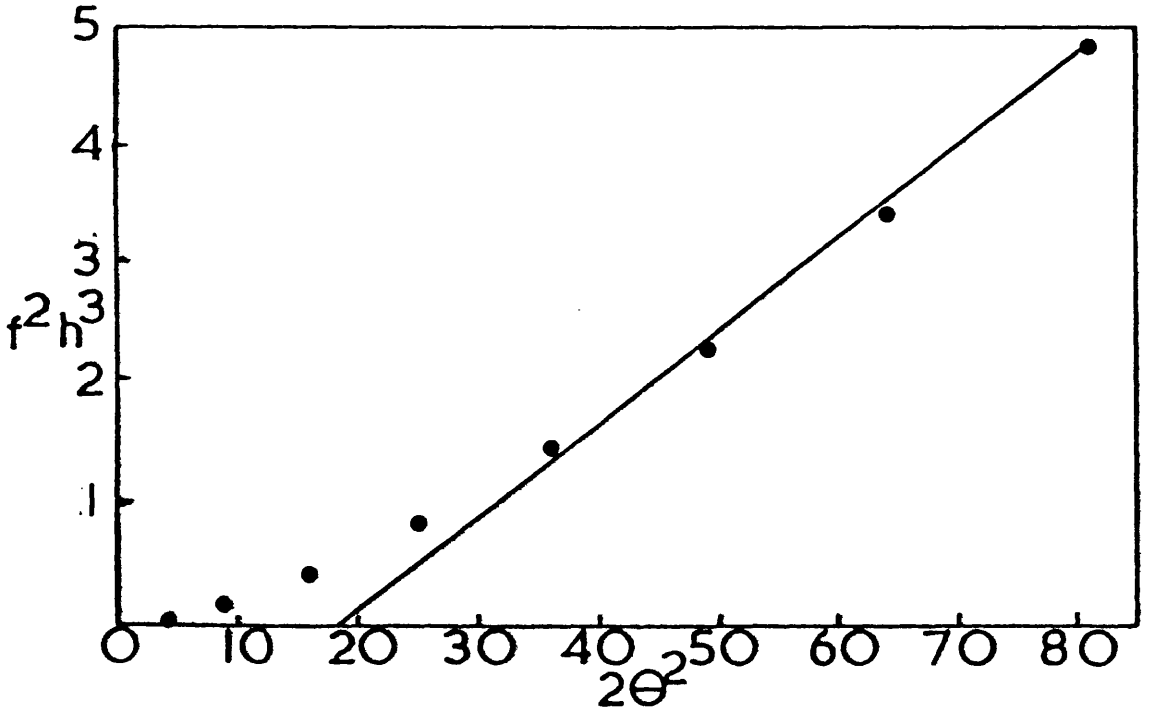

Fig. 7.6 Amorphous scattering.

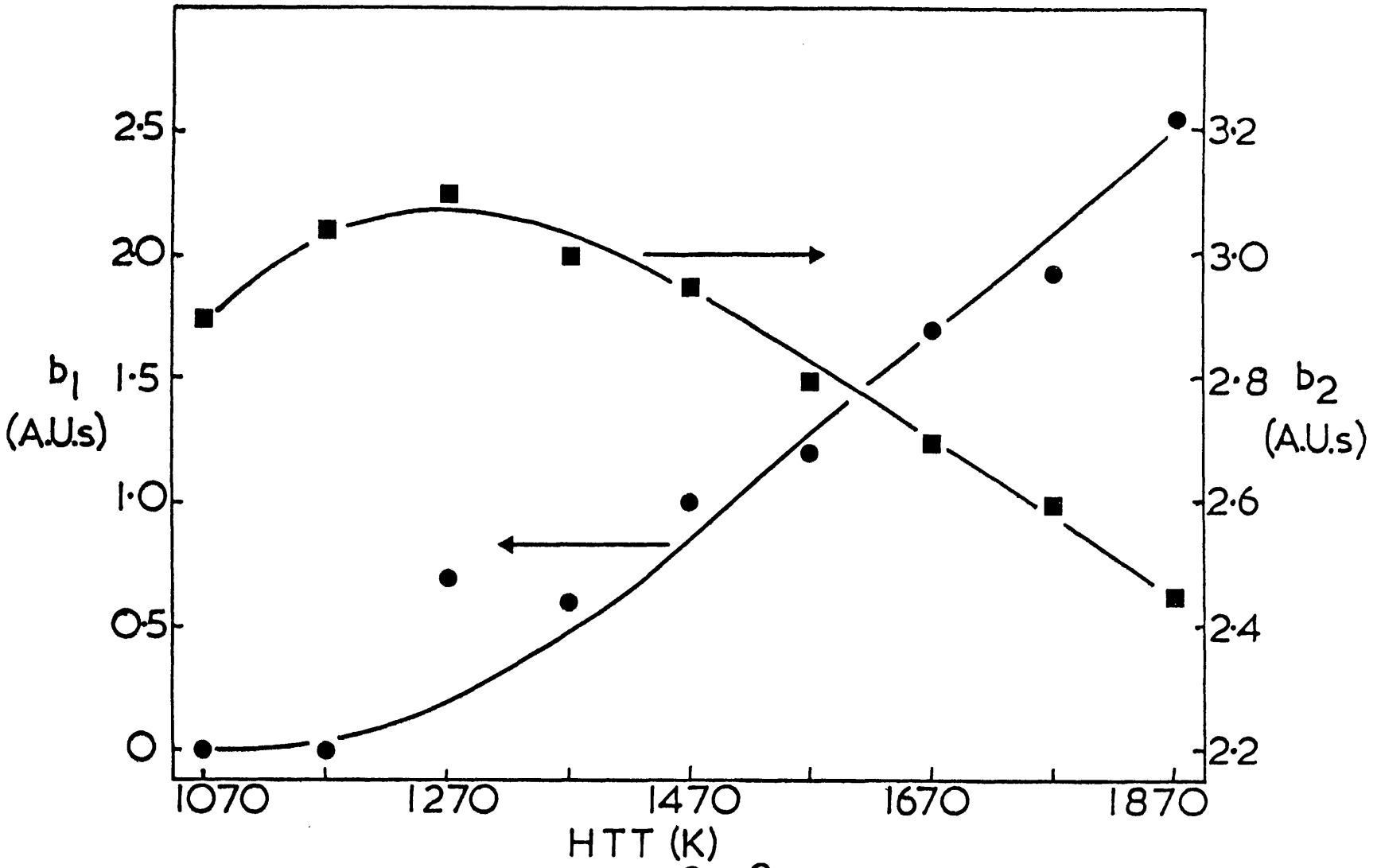

Fig.7.7 Values from Jh^3-h^2 plots

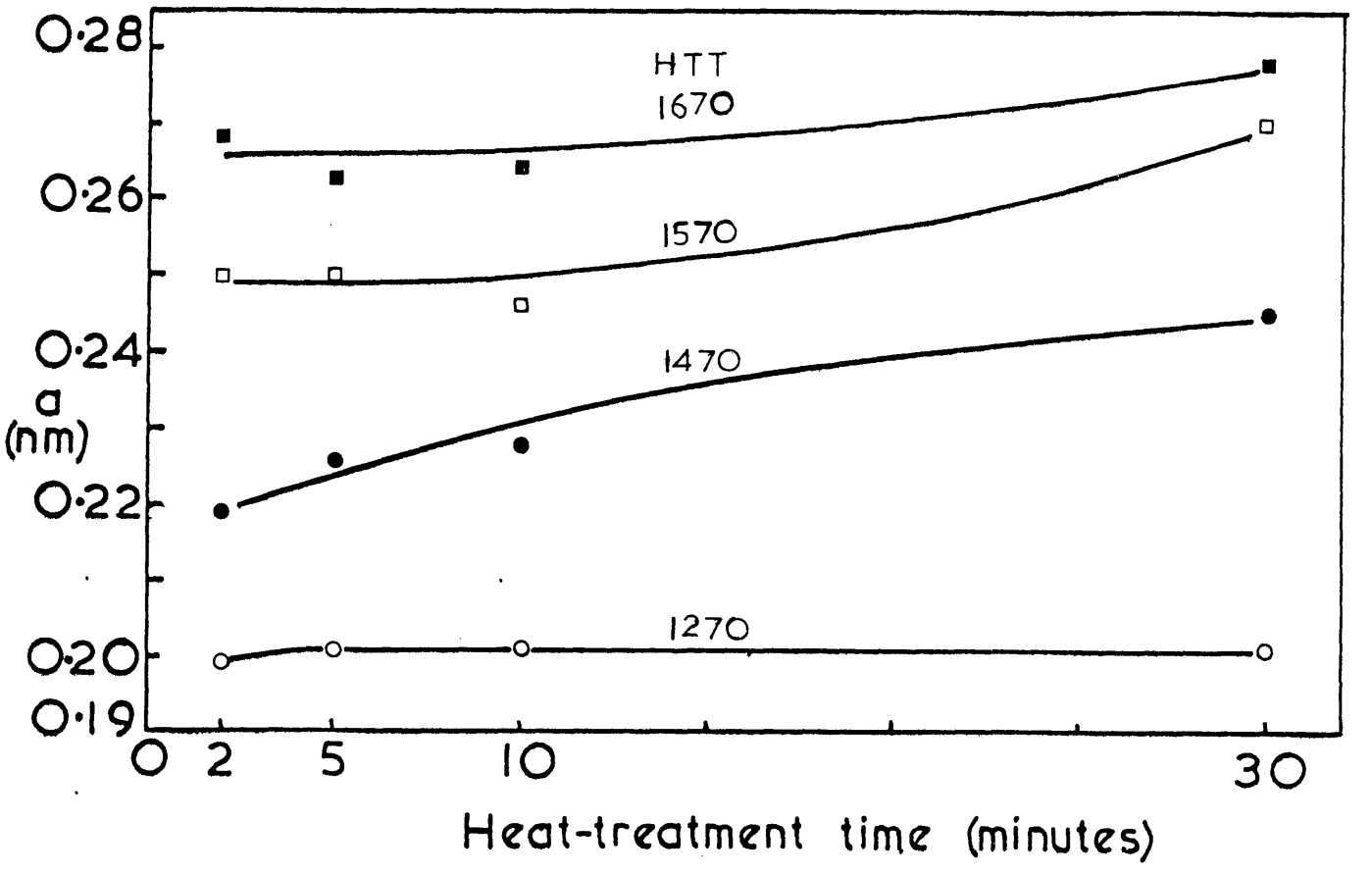

Fig.7.8 Effect of Isothermal heat-treatment on Debye correlation distance, 'a'.

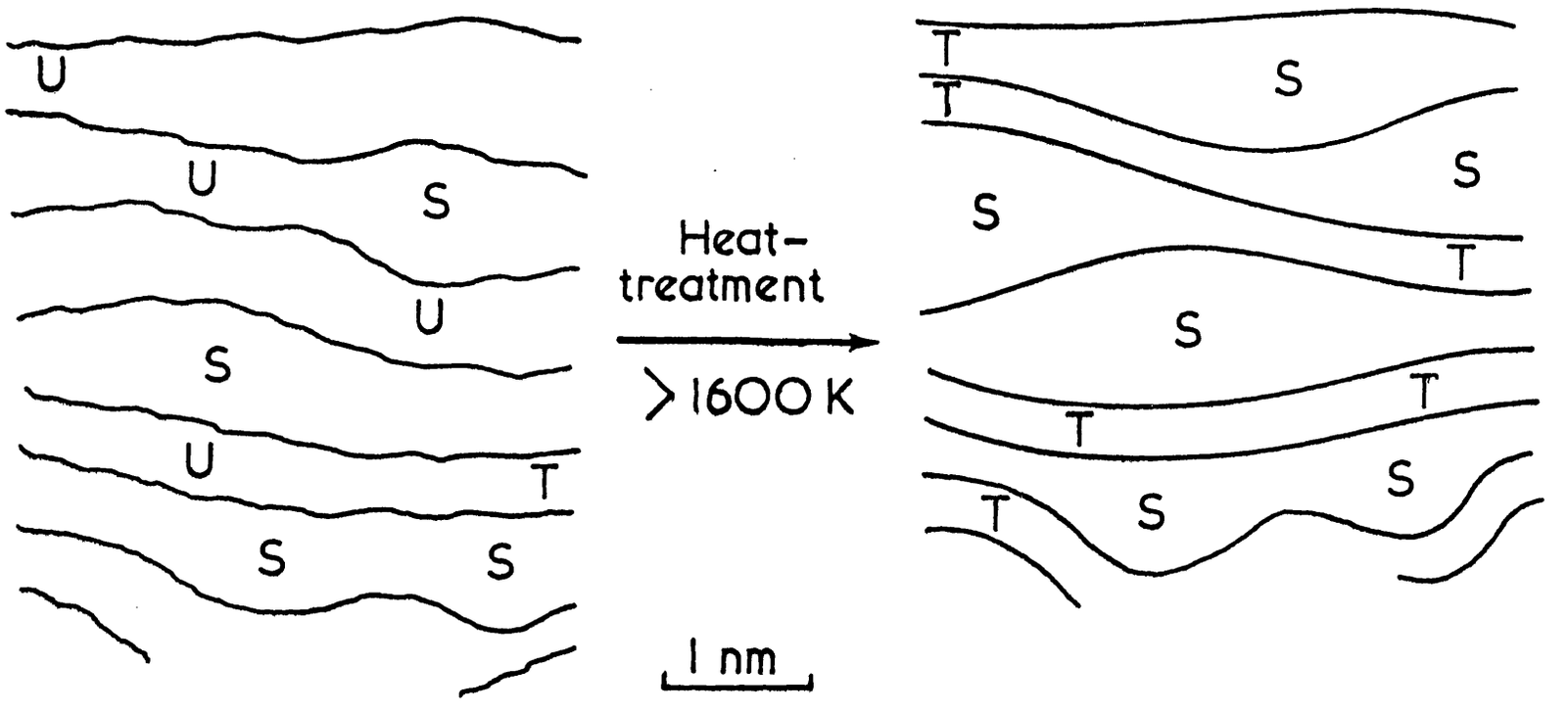

Fig.7.9 Schematic representation of pore coarsening and closure upon heat-treatment. S=Super-micropore, U=Ultra-micropore, T=Turbostratic spacing.

7.4 Adsorption Study of Isochronally Heat-treated Carbons

7.4.1. Introduction

Cellulose carbons of HTT 770 to 1870 K (HTt = 10 mins.) were examined by adsorption of CO_2 at 295 K. Dubinin-Radushkevich (D-R) plots were constructed (figure 7.10) and micropore volumes, V_o, were obtained from the y-axis intercept. Characteristic energies, E and ε_{max}, were obtained from the gradients, m, by : -

$$E = \frac{RT}{\sqrt{-m}} = \frac{2.454}{\sqrt{-m}} \quad \text{kJ mol}^{-1} \text{ at 295 K} \qquad 7.10$$

$$\varepsilon_{max} = \frac{E}{\sqrt{2}} = \frac{1.735}{\sqrt{-m}} \quad \text{kJ mol}^{-1} \text{ at 295 K} \qquad 7.11$$

All gradients were taken from the linear sections at highest pressure, since deviations were found at lower pressures.

7.4.2. Results

Figure 7.11 shows the variation of V_o with HTT and clearly shows a maximum at ~1270 K. A dramatic reduction in V_o is seen after 1570 K. Activated diffusion effects, after 1470 K, were suggested by a lengthening of equilibration times. The 1470 K carbons reached equilibrium in ~3 hours, 1570 K carbons required about 12 hours whilst adsorption could still be detected on 1670 K carbons after one week. Adsorption on 1770 and 1870 K carbons was too small to be detected. The modal value of the free energy distribution,

ε_{max}, can be seen (figure 7.12) to increase with HTT then fall off in the same fashion as the variation of V_o.

Discussion

7.4.3 Pore development stage

The gradual increase in V_o, up to 1270 K, is probably due to structural evolution from secondary carbonisation, since the greatest increases are at low temperature where considerable weight loss and shrinkage occur. ε_{max} is inversely related to the size of the most frequent pore size, because small pores tend to have large ε values. The increase in ε_{max} up to 1270 K must signify the creation of small micropores. There may also be some effect due to the change in adsorption forces, as one changes from a carbon of high oxygen and hydrogen content to one of almost exclusively carbon.

Distributions of volume with potential (figure 7.13) were constructed by inserting V_o and E values into equation 4.14 . Heat-treatment seems to affect small pores (high ε) more than large ones and it must be the pre-eminent increase in small micropores ($\varepsilon > \varepsilon_{max}$) which causes the shift in ε_{max} with HTT.

7.4.4 Pore closure stage

The dramatic reduction in V_o after 1570 K is common feature to many studies of this type [4-9,182] and appears to be due to a closing of pore entrances, as opposed to pore elmination, since this effect is accompanied by a decrease in helium density [4,7,170].

The decrease in ε_{max} values in this region must be due to a closure of small pores to leave larger ones. The small pores (ultramicropores) must play a leading rôle in the transport of adsorbate to larger pores since the loss in V_o is too much to be accounted for solely by ultramicropore loss. One would also expect to find a reduction in adsorption at low pressure with little effect at high pressure, but the volume-potential distributions show a reduction in adsorption over the whole pressure range (figure 7.14). This must mean that closure of ultramicropores effectively closes off larger domains of the total structure. The remaining structure would be depleted in ultramicropores and so exhibit a lower ε_{max} value. The onset of activated diffusion prior to pore closure suggests the general process is one of pore narrowing with certain fine pores closing completely. Although pore-closure is most favoured for fine pores, a narrowing may well occur in larger ones but may not be detected because of a simultaneous enlarging of other pores. This point will be discussed further in Chapter 10.

7.4.5. Negative Deviations from D-R Linearity

When equilibration times of 3 hours were used the D-R plot for the 1570 K carbon exhibited a negative deviation at $\ln^2 P_o/P \simeq 28$, see Figure 7.15. The isotherm was repeated with a minimum of 10 hours between points and is shown in Figs. 7.10 and 7.15. The longer time intervals have resulted in the magnitude of deviation decreasing and its point of deviation moving to lower pressure ($\ln^2 P_o/P \simeq 37$).

This effect illustrates how ultramicropores narrow and so restrict adsorbate access since, if long equilibration times are used, all pores would eventually be filled. For shorter times the pore size which appears closed is apparently larger (hence the deviation point is at lower ε) and more pore volume is involved. The effect of this deviation on the potential distribution is seen in figure 7.14 where it appears as a reduction in frequency of high ε micropores.

These findings support the view that Marsh and Rand type A D-R plots are due to a variation in distribution from the Rayleigh form. The observation of such deviations are, however, very dependent upon adsorbate/temperature/time conditions.

7.4.6. ε_{max} - V_o Correlation - The Pivot Point for Heat-treated Carbons

The similarity of shape for both ε_{max} and V_o plots results in an approximately linear relationship between ε_{max} and V_o (Figure 7.16c). The significance of this relationship is that all the D-R plots intersect at the same point. This point, to be called a "pivot point", can be located as shown in Appendix C, and is found to be $\varepsilon^2 = -270\ (\text{kJ mol}^{-1})^2$ and $\ln V = 1.09$. The plots, therefore, never actually intersect, but only if extrapolated beyond the $\ln V$ axis. One can see that a general correlation will exist because any change in V_o is accompanied by a similar change in ε_{max}, but to see if the linearity of the correlation signified a particular mode of variation, a number of idealized models were considered (Figure 7.16).

If model A were appropriate, a plot of V_o against $\varepsilon_{max}(\varepsilon_{max} - \varepsilon_o)$ would be linear, whereas model B would be correct if V_o against $(\varepsilon_{max} - \varepsilon_o)$ were linear. Model C might be thought appropriate since it predicts linearity between V_o and ε_{max} - which is the experimentally found correlation. Model C is, however, far from the actual distribution shapes (figures 7.13 and 7.14).

In practice the data give straight lines for all three models, and all have sufficient scatter to prevent one being claimed most appropriate. The observed $V_o - \varepsilon_{max}$ correlation is therefore sufficiently insensitive to model as to prevent generalised deductions to be made.

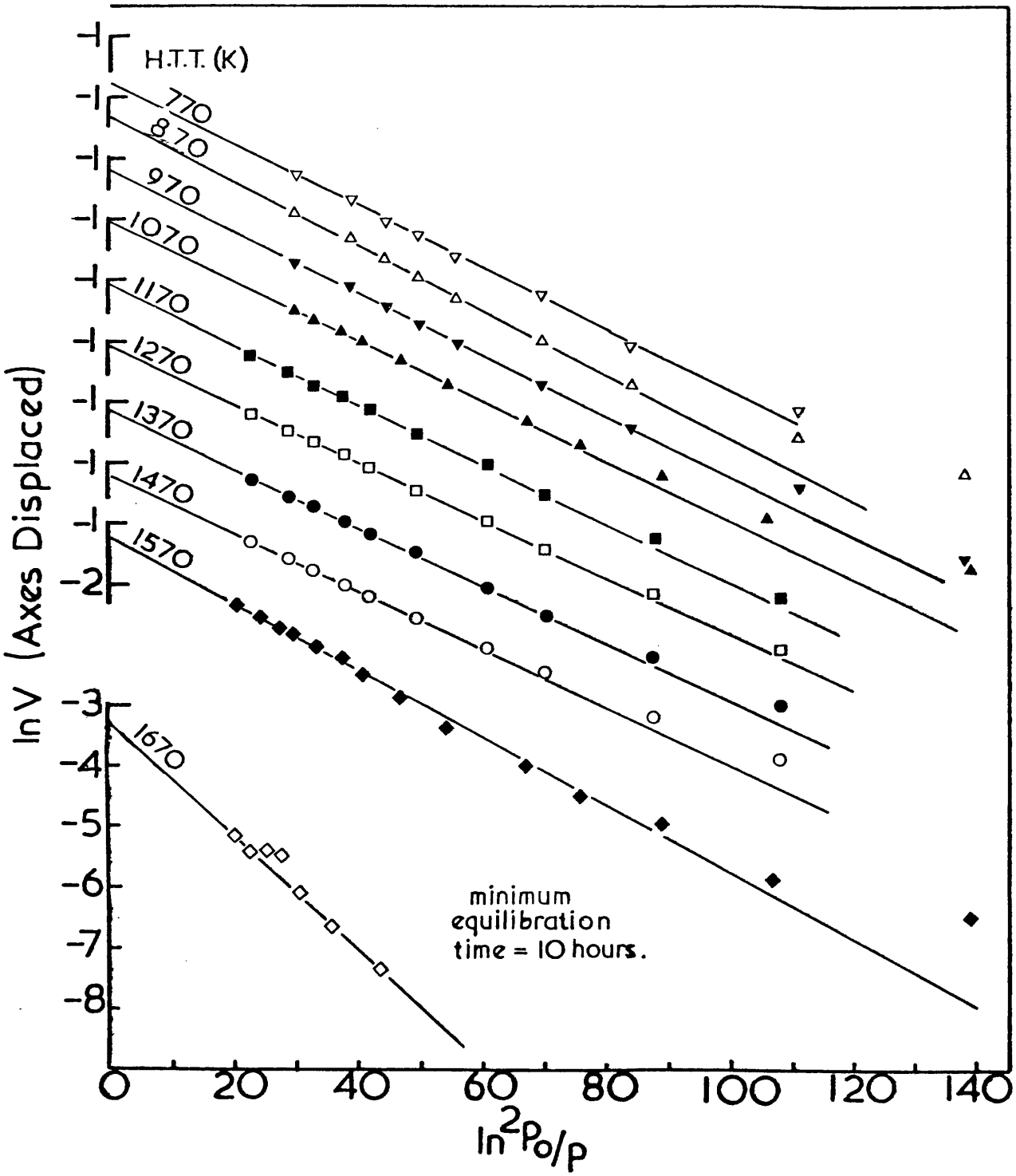

Fig. 7.10 D-R Plots for Adsorption of CO_2 at 295 K on Isochronally Heat-treated Cellulose Carbons.

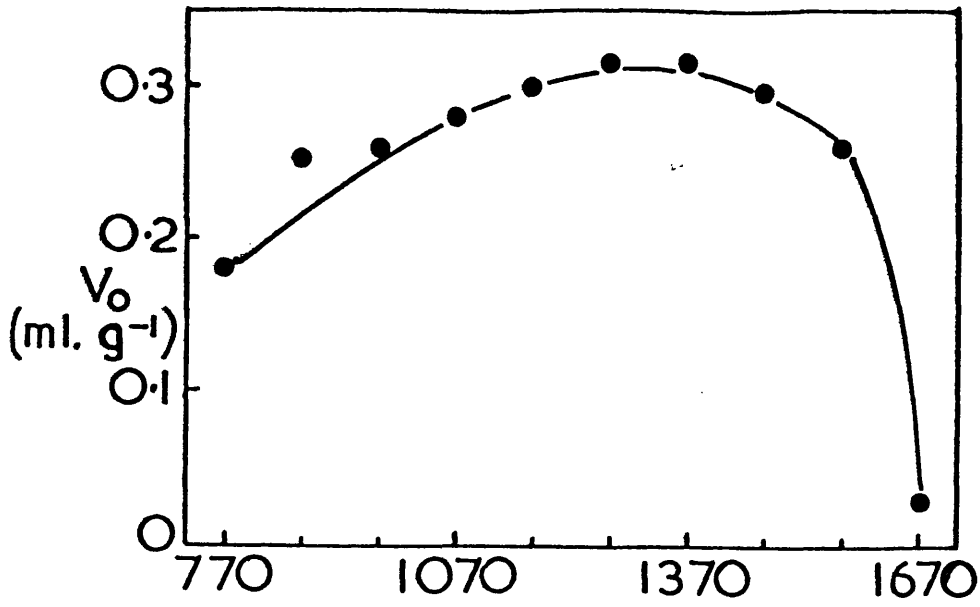

Fig. 7.11 Open Micropore Volume

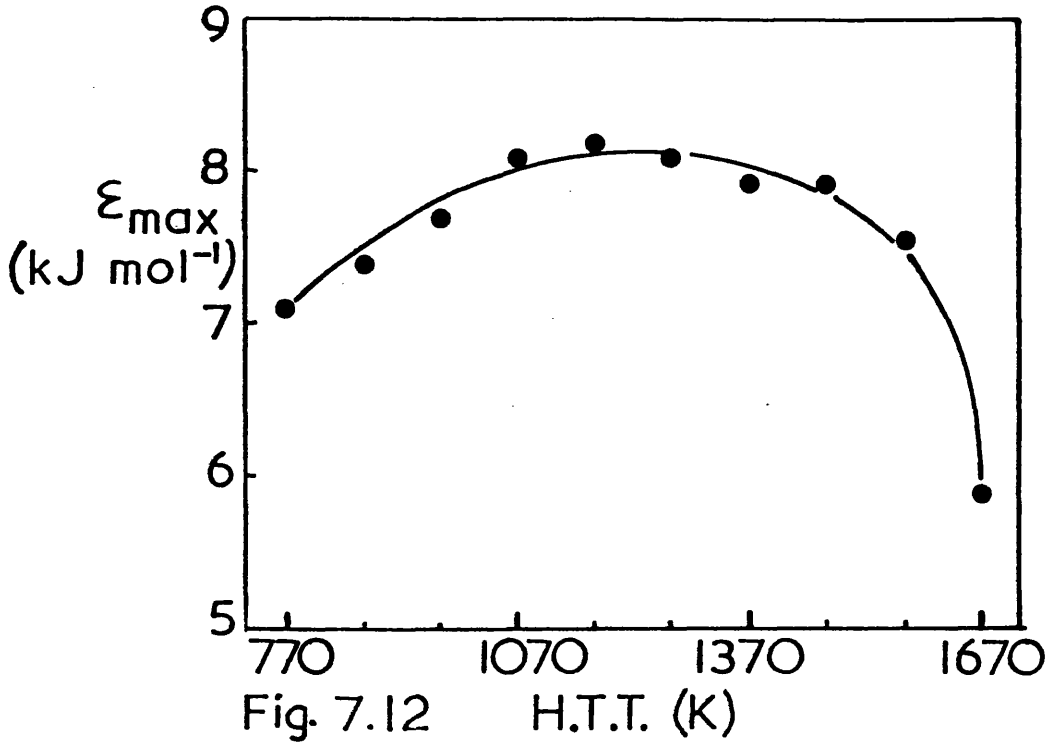

Fig. 7.12 Effect of Isochronal Heat-treatment on D-R Parameters V_o (open micropore volume) & ε_{max} (maximum in the potential distribution).

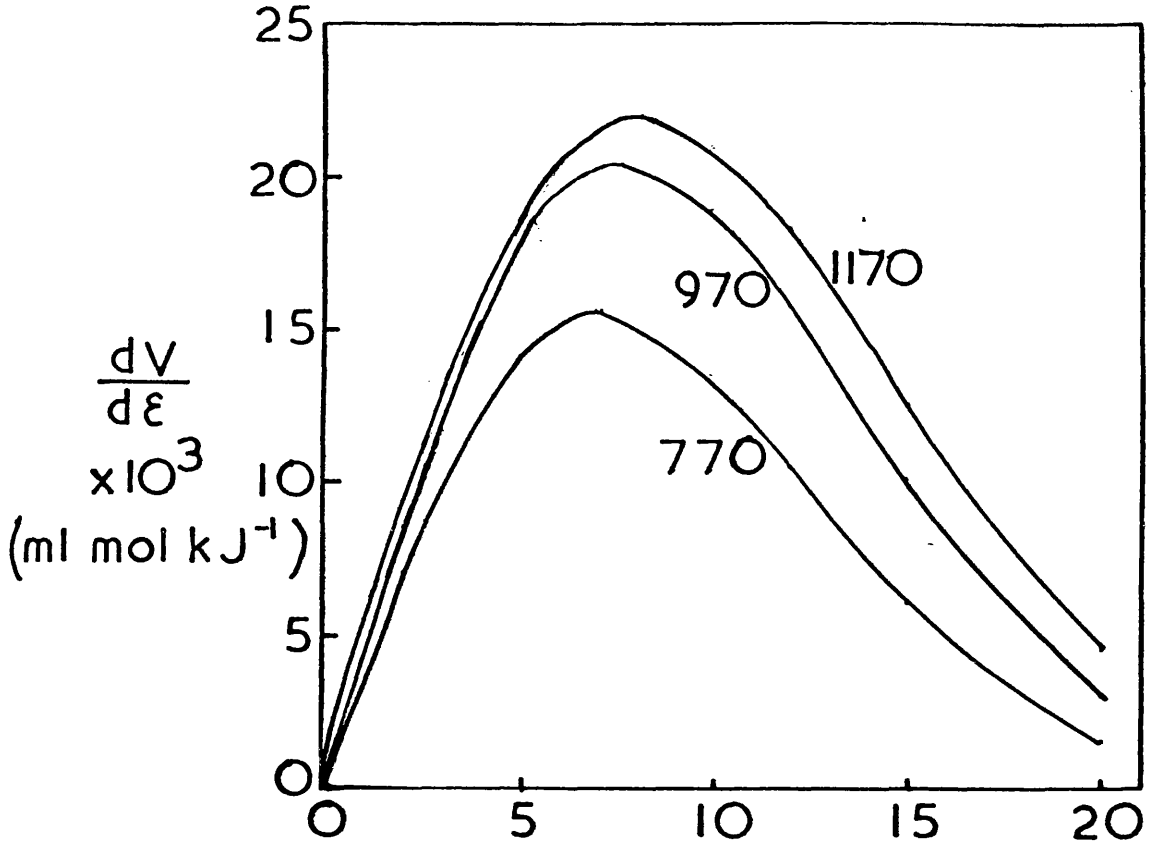

Fig. 7.13

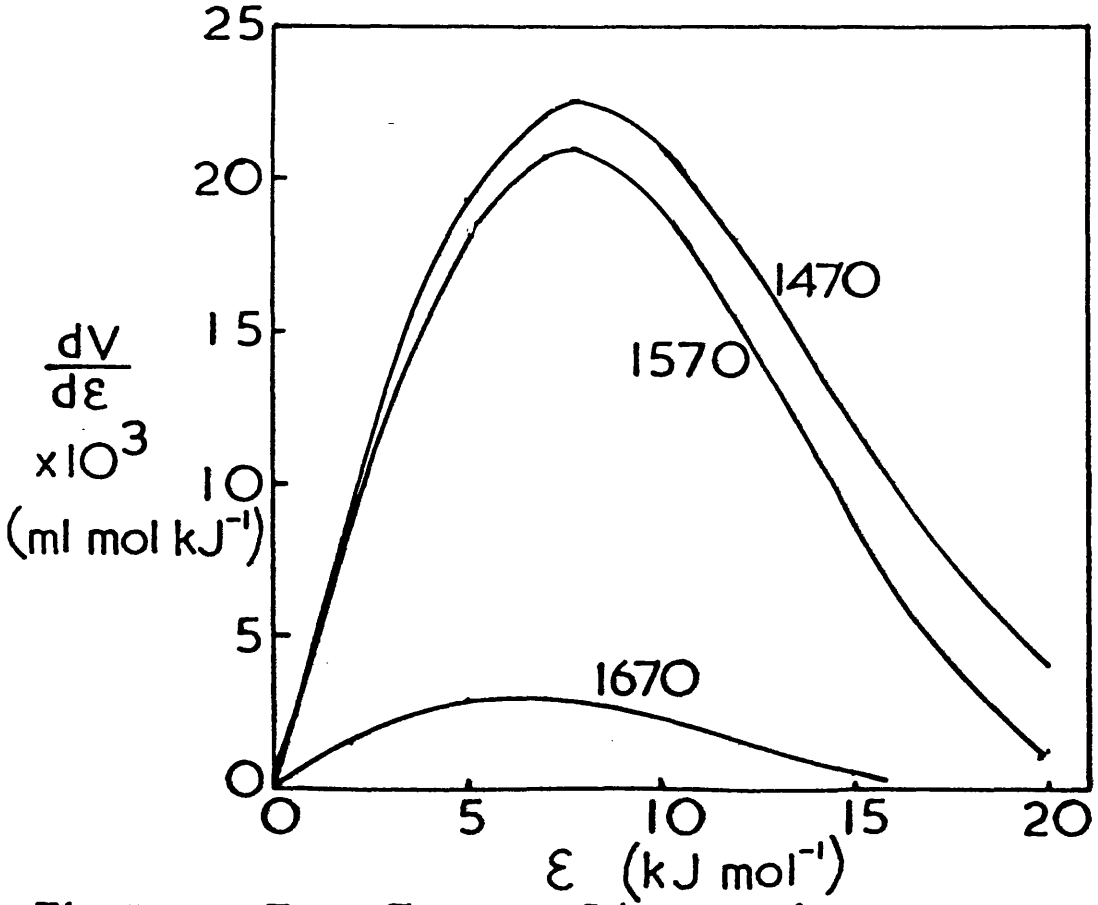

Fig. 7.14 Free Energy Distributions for Isochronal Heat-treated Carbons.

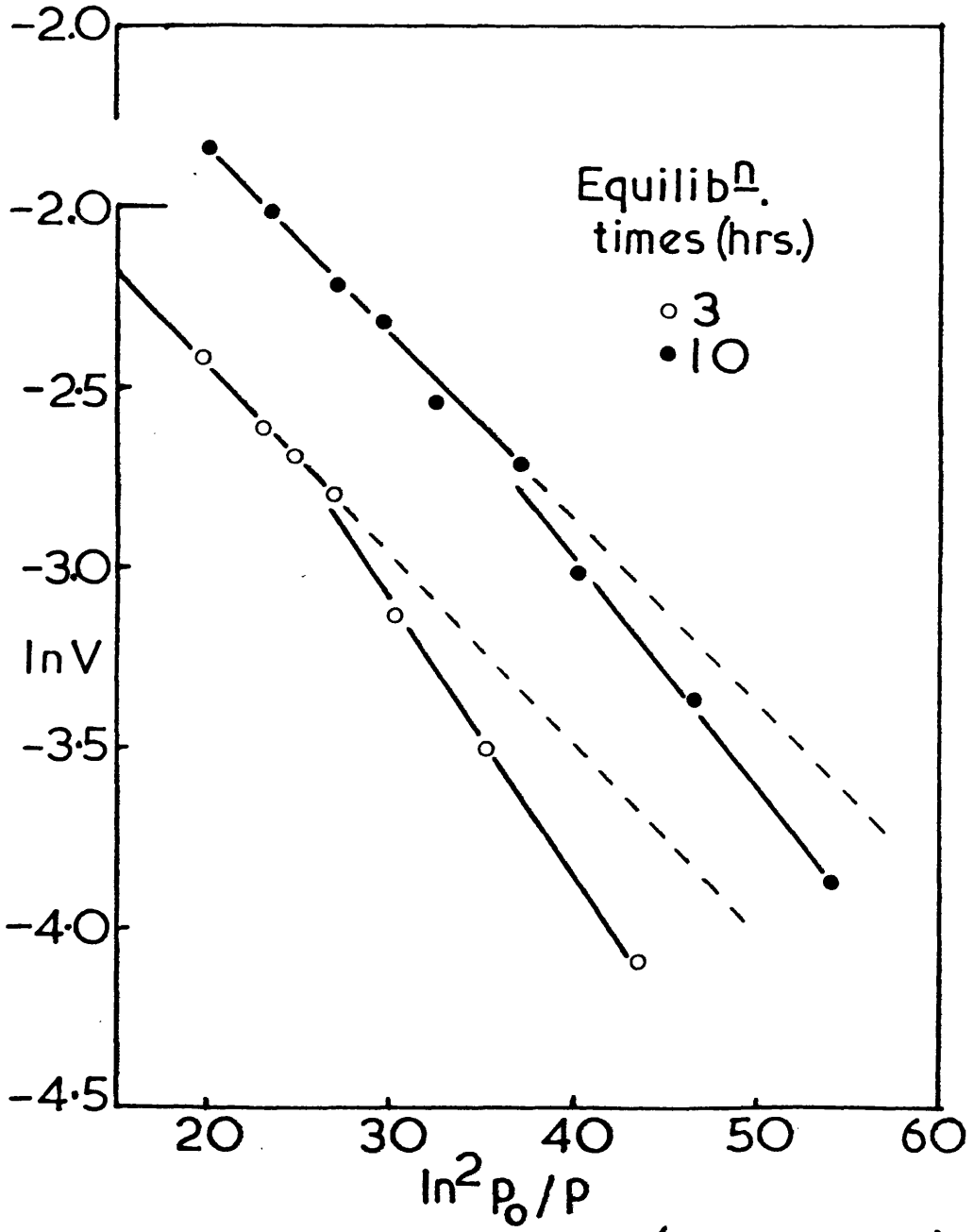

Fig.7.15,Type A D-R Plots (1570 K H.T.T.)

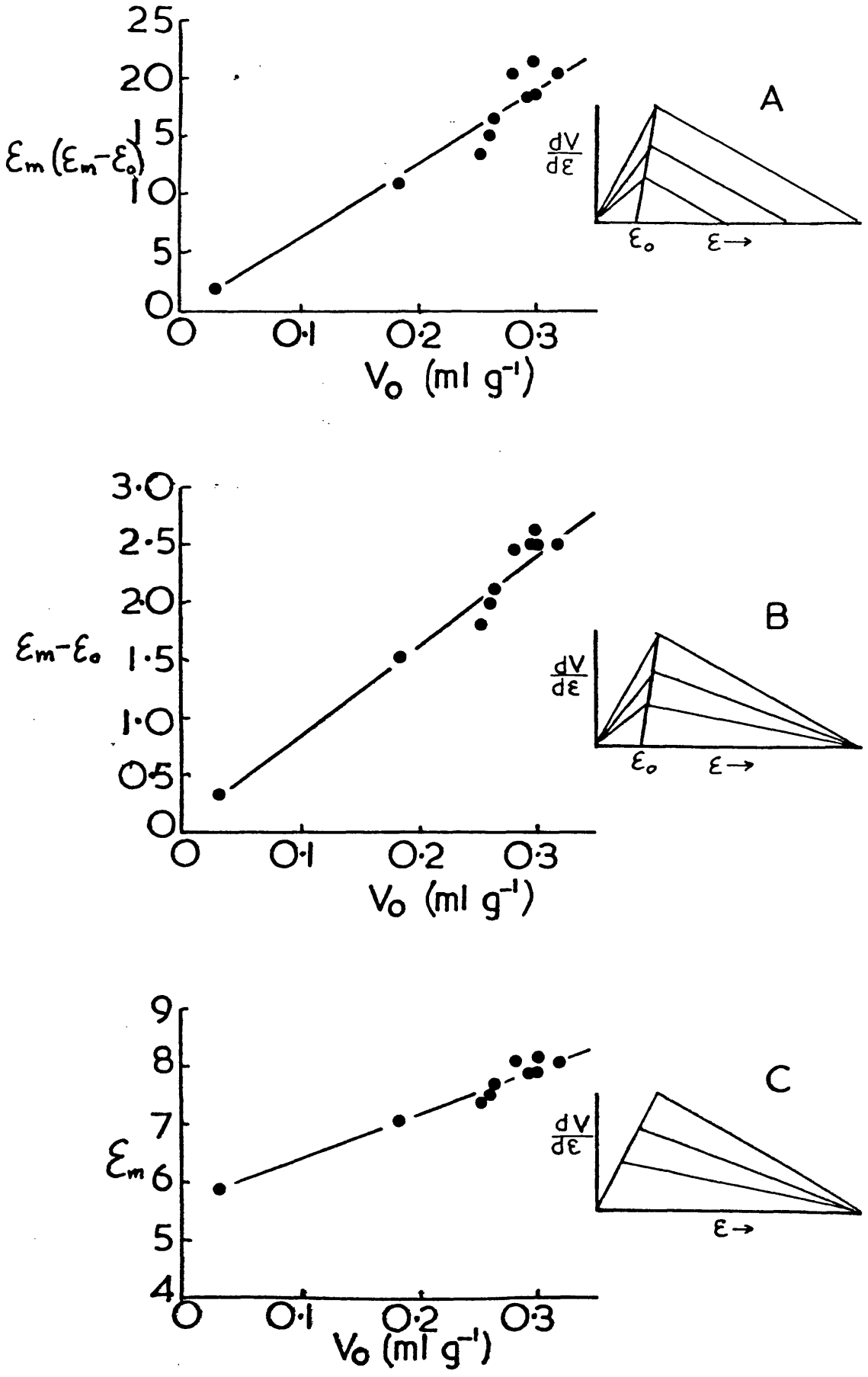

Fig. 7.16 $V_o-\varepsilon_{max}$ correlations predicted for various idealised distributions.

7.5 Adsorption Study of Isothermally Heat-treated Carbons

7.5.1. Introduction

To give some idea of the rate at which structural changes occur, at different temperatures, a set of cellulose carbons were heat-treated for different times at 1270, 1470, 1570 and 1670 K. Times selected were 2, 5, 10 and 30 mins. (the heating programme is given in Appendix A(5)). The nomenclature used is such that a carbon heated at 1470 K for 5 mins is 1470 (5).

7.5.2. Results and discussion

Adsorption data of CO_2 at 295 K were plotted in D-R coordinates, as shown in figures 7.17 to 7.21 . The open micropore volumes, V_o, are shown in figure 7.22 as a function of HTt. The 1270 K carbons are largely unaffected by the time of heat-treatment whilst the 1470 K carbons only show a slight reduction. The variation of ε_{max} for these carbons (figure 7.23) is also uneventful. This suggests that the porous structure is fairly stable at these temperatures and that if an activation energy is required for pore closure it is not attainable at these temperatures.

The gradual loss of V_o at 1570 K suggests pores are closing over the whole time range but this effect is accelerated at 1670 K, where the reduction in V_o is quite rapid and probably continuing after 30 mins. The absolute values of V_o for the 1670 K carbons have little meaning since activated diffusion was pronounced (equilibration times of $\sim$12 hours were

used). This effect not only reduces "true" adsorption at a given pressure but also distorts the isotherm because the samples are closer to equilibrium at high pressure than low pressure. This is a result of the narrow pores having had more time to fill, as well as the higher pressure resulting in more frequent collisons between pore entrances and adsorbate molecules. The V_o value of 0.37 ml g^{-1} for the 1670 (2) carbon should be seen in this light. The relative values are of significance since all 1670 K samples were measured under identical conditions.

7.5.3. The Development of Negative Deviations from D-R Linearity

The onset of pore closure is again evidenced by a type A downward deviation of D-R plots. For equilibration times of ~2 hours the deviation for the 1470 (10) sample occurred at $\ln^2 P_o/P \simeq 50$, but it becomes more pronounced for the 1470 (30) sample, which also deviates at a higher pressure ($\ln^2 P_o/P \simeq 40$) - see figure 7.21. When repeated with 19 hour equilibration times these deviations disappeared (figure 7.18). Type A deviations occurred with all 1570 K carbons, the extent of deviation increasing and its position moving to lower $\ln^2 P_o/P$ values, with increasing HTt. The steep gradients found for the 1670 K samples suggest that the "deviation" has moved to such high pressures as to encompass the whole pressure range. The adsorption at higher ε values, for the 1670 K carbons, is no longer characteristic of micropore filling but probably represents localised adsorption on wide pore surface. This point is discussed in relation to all carbons in chapter 9.

7.6 General Discussion

In the study of isochronally heat-treated carbons it was seen that a loss of V_o was related to a coarsening of pores (i.e. a decrease of ε_{max}). The isothermally heat-treated carbons allow a clearer view of this relationship. Heat-treatment causes a general coarsening of pores so that many fine pores are eliminated. As small pore entrances close, the access for adsorbate molecules to micropores becomes more difficult (hence longer equilibration times are needed). However, in the initial stages, coarsening will occur and many fine pore entrances may close but access will still be retained because other pore entrances exist, which remain open. In this case ε_{max} will decrease but V_o will remain relatively unaffected. During the latter stages of coarsening many of the remaining small pore entrances will be eliminated and the loss of V_o will be more dramatic for a comparatively small reduction in ε_{max}. These effects are shown by the 1670 K carbons where the coarsening (indicated by ε_{max}) has occurred rapidly but V_o continues to gradually decrease whilst ε_{max} is nearly constant.

Because the changes in ε_{max} and V_o have a different time dependence, carbons in the pore closure stage will only exhibit a $V_o - \varepsilon_{max}$ correlation if they have been heat-treated for identical times. This, however, is not necessarily the case for the pore development stage (i.e. up to 1270 K), as is suggested by the less precise carbonisation schedules.

The "before and after heat-treatment" situation is represented schematically in figure 7.9. This shows how the ultramicro-

porous structure coarsens to one of supermicropores, which are closed off by turbostratic spacings.

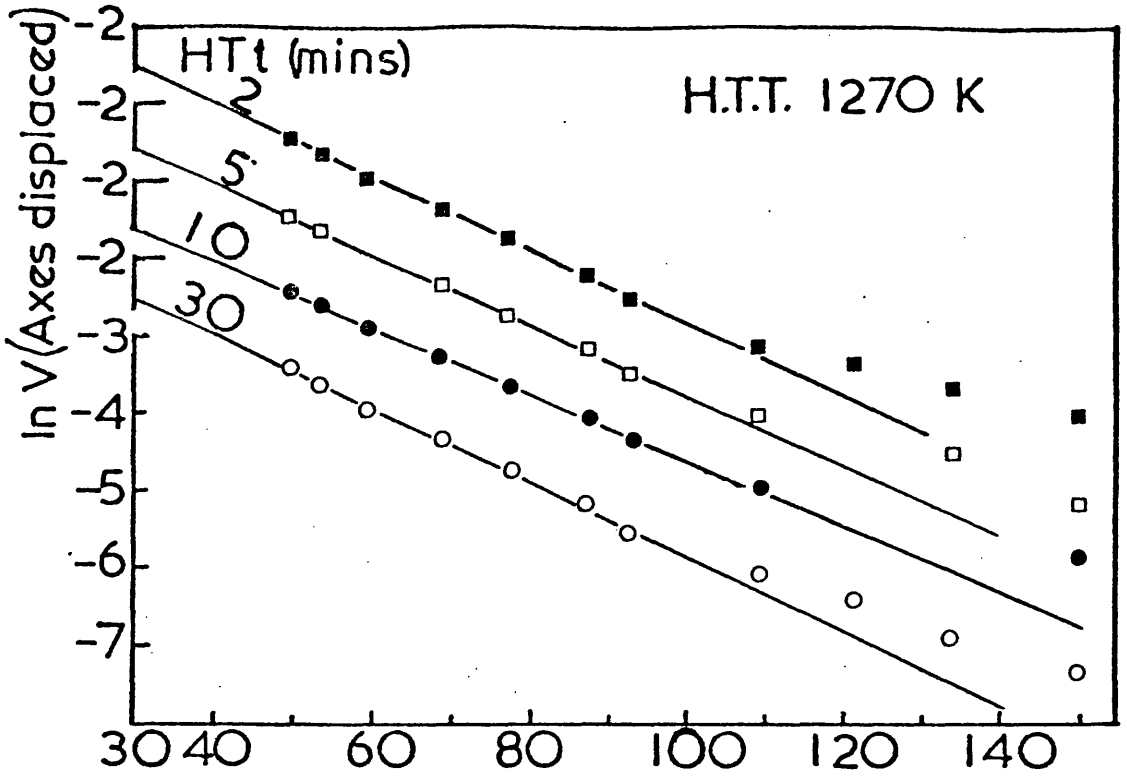

Fig. 7.17

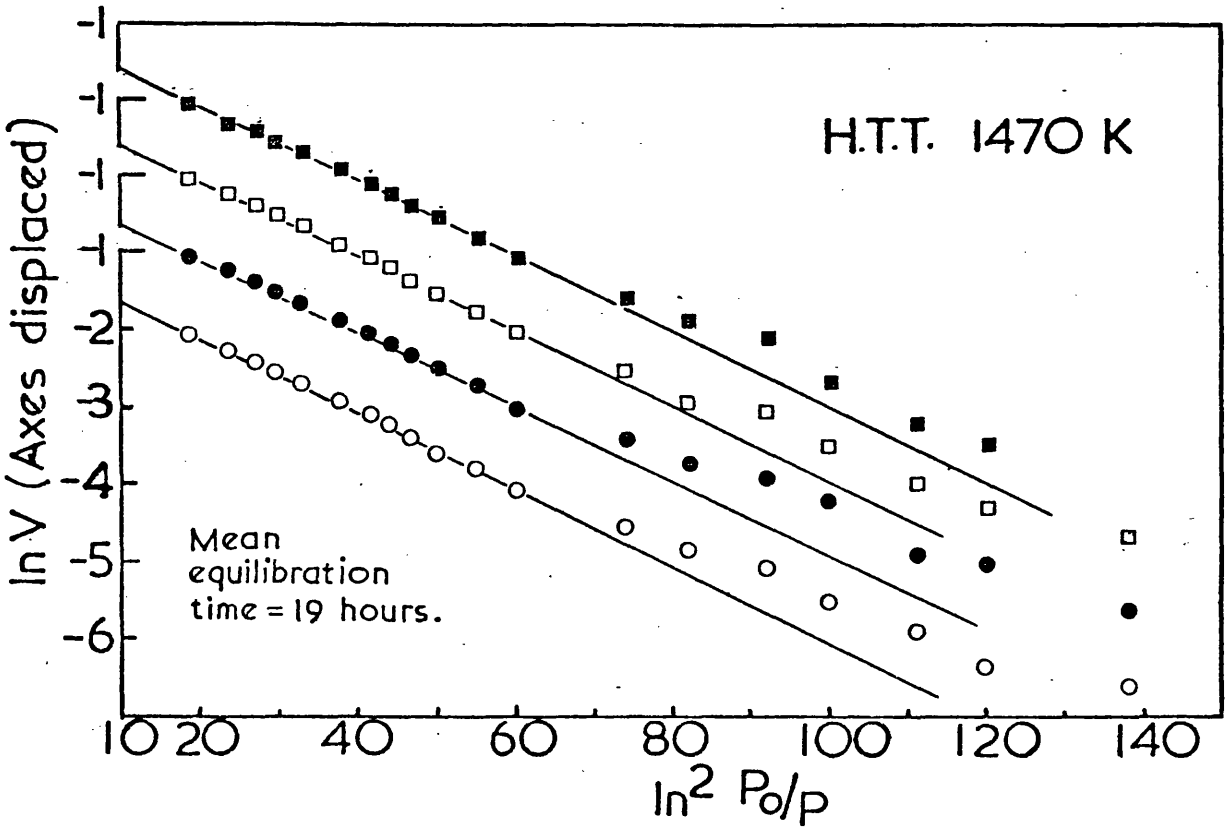

Fig.7.18 ▪2, □5, •10, ○30 mins H.T.t.

D-R Plots for CO_2 at 295 K on Isothermally Heat treated Cellulose Carbons.

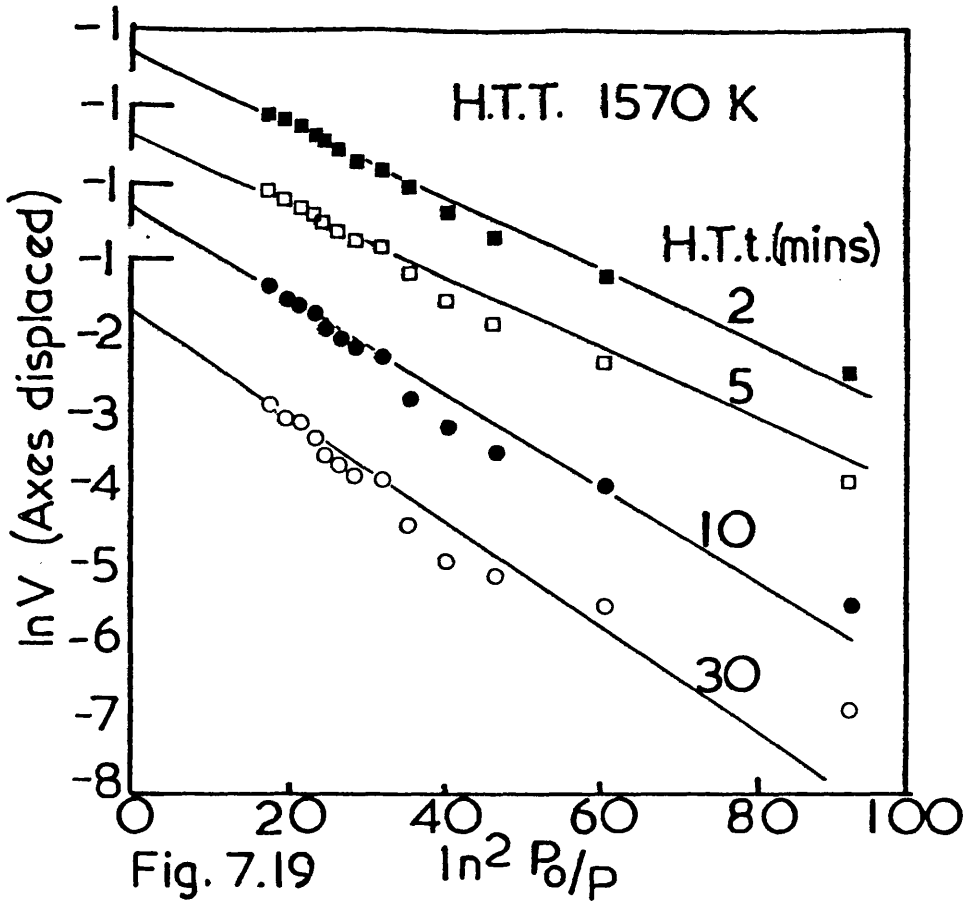

Fig. 7.19

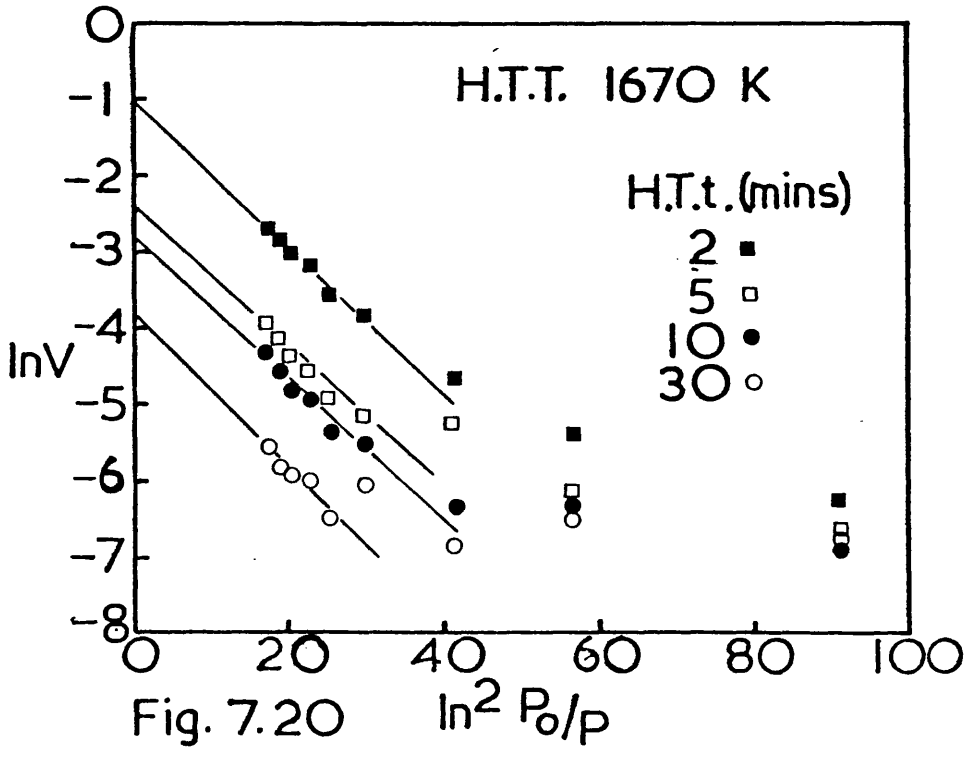

Fig. 7.20

D-R Plots for CO_2 at 295 K on Isothermally Heat treated Carbons.

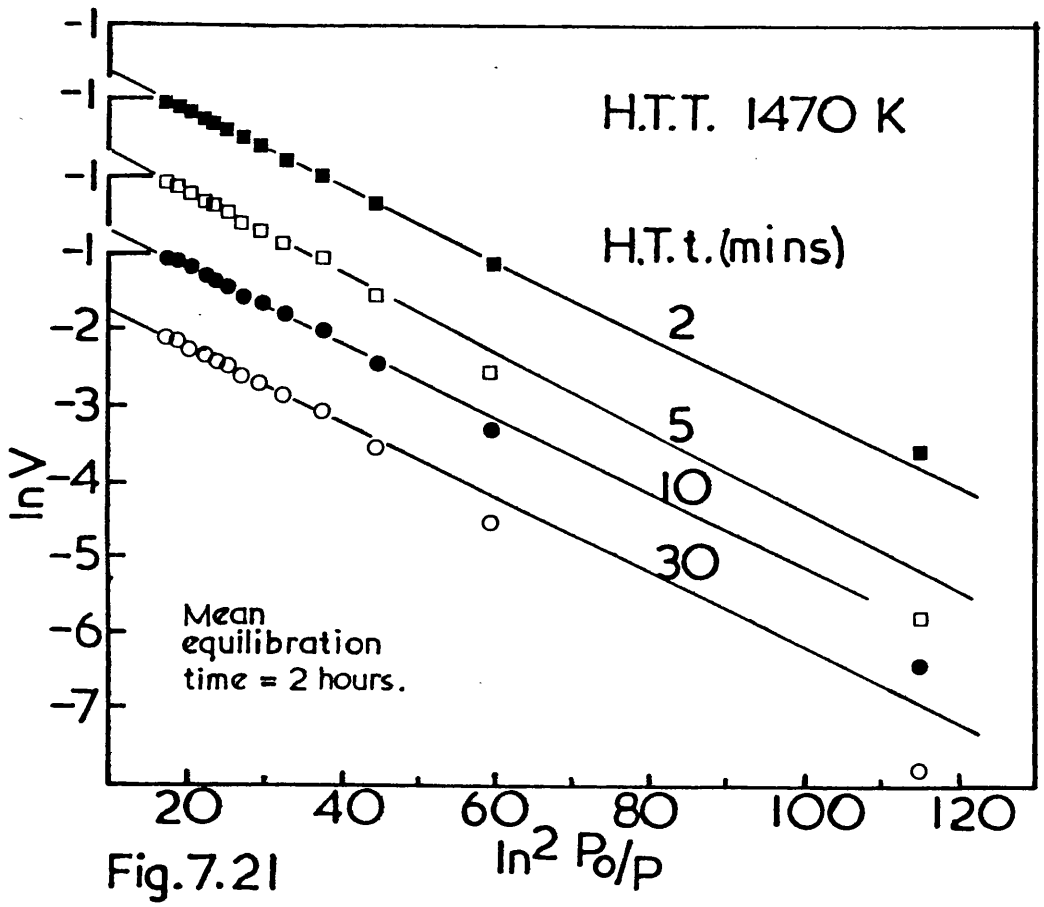
H.T.T. 1470 K
H.T.t.(mins)
2
5
10
30
Mean
equilibration
time = 2 hours.
ln V
-1
-1
-1
-1
-2
-3
-4
-5
-6
-7
20
40
60
80
100
120
ln² Po/P

Fig. 7.21

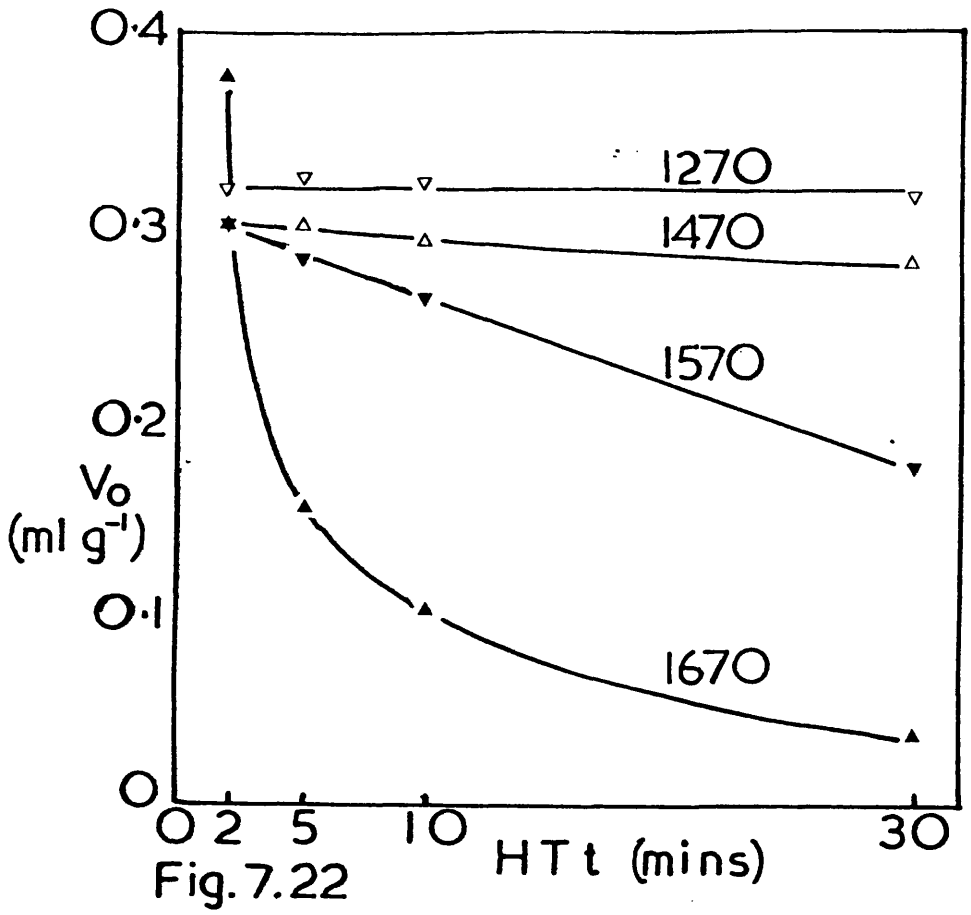

Fig. 7.22

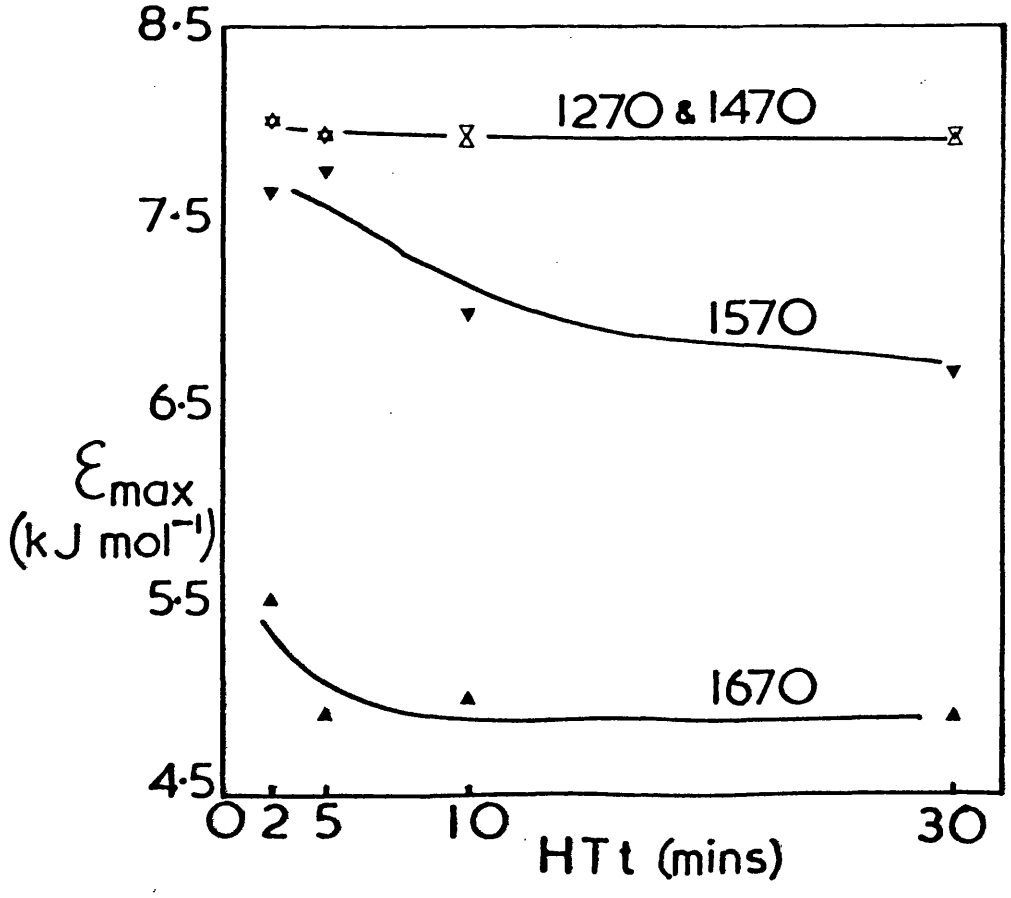

Figs. 7.23 D-R Parameters for Isothermally Heat treated Carbons.

HTT(K) 1270 ▽ , 1470 △ , 1570 ▼ , 1670 ▲ .

7.7. High Resolution Electron Microscopy

7.7.1. Introduction

Any investigation into microstructural changes would be aided considerably by the opportunity to directly observe the structure on a scale commensurate with the pore size. Conventional transmission electron microscopy, operating with diffraction contrast, has a maximum resolution limit of ca. 1 nm [183]. To resolve points below this figure requires the use of phase contrast.

High resolution, phase contrast, transmission electron microscopy (HREM) began with the now classical work of Menter[184] who directly observed the 1.195 nm ($20\bar{1}$) lattice planes of platinum phthalocyanine. Its application to graphitized carbons was initiated by Heidenreich et al[185] who recorded micrographs with fringes which appeared to correspond to the 0.34 nm spacings of the (002) planes. The technique as applied to carbons in general is now well established[186-188].

The theory of HREM is adequately covered in many reviews[189-193] and will not be treated here, except to say that to observe phase contrast one must underfocus the microscope. The degree of underfocus is important since all microscopes exhibit spherical aberration and this results in some spacings being imaged with more contrast than others. The variation of contrast intensity with spacing (known as the "transfer function")

is heavily dependent upon the degree of defocus, hence spurious fringes and a distortion of the true structure can be obtained if the correct degree of defocus is not used.

7.7.2 Experimental

Two microscopes were used-a Philips EM 300 fitted with an image intensifier and a JEOL JEM 100 C. The Philips had a spherical aberration coefficient (C_s) of 1.6 mm and required an optimum defocus of 92.5 nm to image 0.34 nm spacings truthfully. The JEM was fitted with a special high resolution objective lens which gave a C_s of 0.67 mm. This considerably extends the region of defocus over which faithful images are obtained. A defocus of 55 nm was best for this microscope. The defocus is achieved by obtaining zero contrast (i.e. no image) which corresponds to the focal position, then turning the calibrated focus knobs the required amounts. Samples were prepared by dusting dry carbon powder onto holey carbon support films. Only the edges of particles which bridge film holes were looked at. Only if the area is less than the maximum of 10 nm thick will the zero contrast condition arise. Dispersion of powder in solvents is unnecessary and to be avoided due to outgassing effects, which can degrade images[194].

7.7.3. Results - Heat-treated series

Micrographs of carbons heat-treated to 1170, 1470 and 1870 K are shown in figures 7.24 to 7.26 .

The 1170 K carbon has a typically "amorphous" structure which is a result of layer-planes being short and highly

defective. Heat-treatment to 1470 K shows a slight development of structure but the emergent layer-planes are still short. By a HTT of 1870 K the layer-plane structure is well developed and is similar to that found for glassy carbons (the origins of the Jenkins model[82] shown in figure 2.6 should be obvious). A remarkable development of structure occurs over a relatively small HTT range of 1600 - 1800 K and coincides with the completion of secondary carbonisation, total micropore closure, increased growth rate of L_c and a, and reduction of d_{002}.

If we equate light areas with pores and dark areas with matrix, the pores in low HTT carbons appear to be the space between disordered groupings of short layer-planes. For very low HTT carbons (<1100 K), where very little layer stacking occurs, the term "short layer-planes" might legitimately be replaced by "condensed polynuclear aromatic groupings". With this change of sense, the Riley tetraphenylene model (figure2.4)can again be seen as a suitable precursor from which these structures might develop. The pores in these carbons appear to be small and finely dispersed. For the 1870 carbon the pores are much larger, fewer, and are now the voids between reasonably well formed layer-planes. The micropore coarsening effect is, therefore, well illustrated by high resolution microscopy.

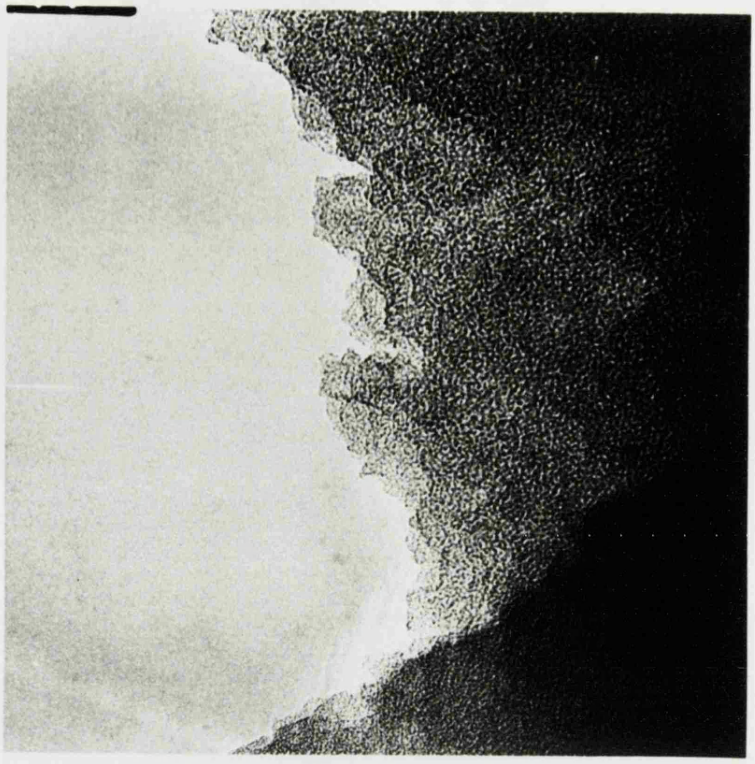

Fig. 7.24 HTT 1170 K 20 nm

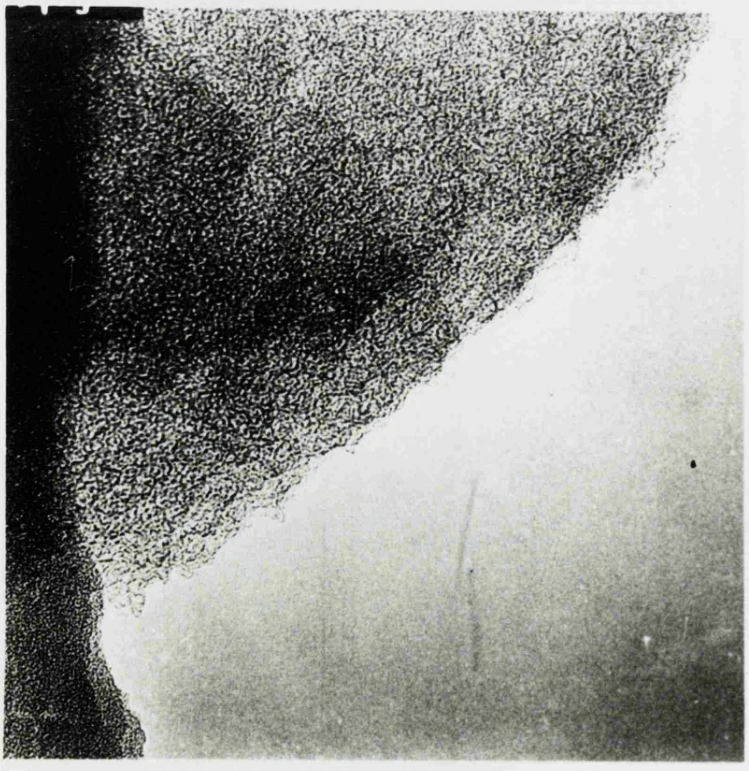

Fig. 7.25 HTT 1470 K 20 nm

High Resolution Electron Micrographs of Cellulose Carbons.

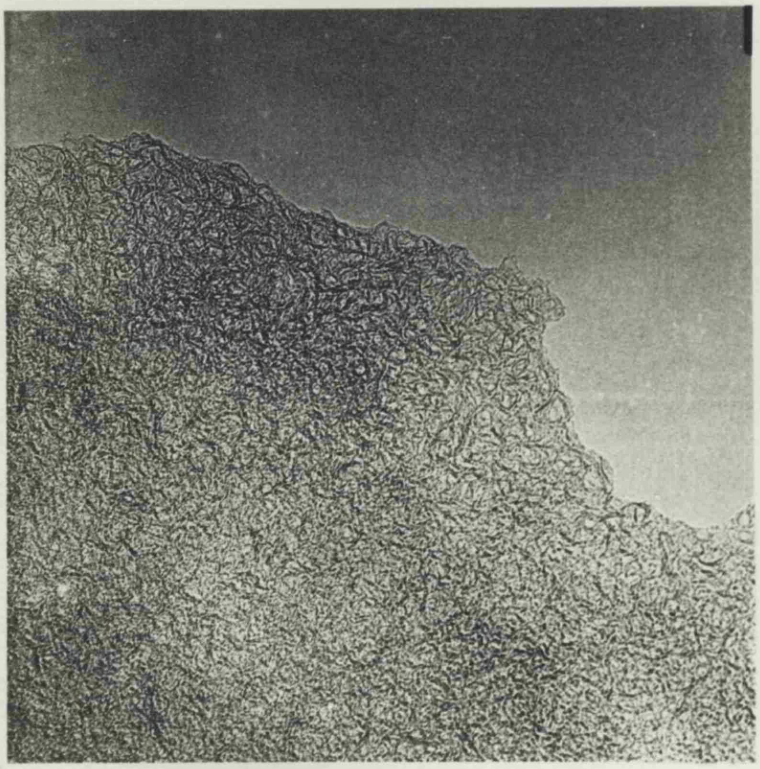

HTT 1870K 20nm

Fig.7.26 HREM of Cellulose Carbon.

CHAPTER 8

THE EFFECTS OF ACTIVATION

CHAPTER 8

8.1 The Effect of Activation on Structure

Introduction

Because the structural changes occurring with heat-treatment appear to be closely linked with the heteroelement and disordered material content, it was decided to partially gasify (activate) carbons, then heat-treat them. If disordered material was preferentially attacked then one would expect activated carbons to be affected differently by heat-treatment. Kotlensky and Walker[195] found that activation of a carbon black caused a larger decrease in helium density, on heating to 1870 K, than for the unactivated carbons. This could either be due to activation increasing the ease with which pores are closed off or it could be a result of the creation of new, small, micropores which subsequently closed off on heating. These possibilities ought to be resolvable by adsorption measurements.

The concept of selective structural gasification has been adopted by a number of workers[196-198] but has only really been demonstrated for carbon blacks[199,200]. Marsh et al[201] examined oxidised carbon blacks by HREM and found no change in their interlayer spacing distributions, but the layers appeared to have increased in alignment and area. This was ascribed to the removal of less organised constituents, leaving the remaining fractions with a more crystalline appearance. HREM was also used by Robins[202] to find where activation was removing carbon from a charcoal

cloth, but he could not detect any changes in the microstructure. Because of the disharmony of the above views, samples were also studied by x-ray diffraction to try and understand the changes induced by activation.

8.2 Adsorption Study of the Effects of Activation

8.2.1. Results

A series of 1170 K carbons were activated in flowing, atmospheric pressure, CO_2 at 1120 - 1170 K (see Appendix A(2) for details). Adsorption data for CO_2 at 293 or 295 K, were plotted in D - R coordinates. Typical plots are shown in figure 8.1 and shows activation to increase both the gradients and intercepts. Carbons of high burn off (B.O.) show a slight curvature over the whole pressure range.

The open micropore volumes, figure 8.2 , increase over the whole range of B.O., but at a decreasing rate. The modal values for the free energy distributions, ε_{max}, were calculated from D-R gradients by equation 7.11. These values, figure 8.3, show a steady decrease with B.O. - implying an increasing mean pore size.

Discussion

8.2.2. ε_{max} - V_o Correlation - The Pivot Point for Activated Carbons

As with the isochronally heat-treated carbons (section 7.4.6) there is a correlation between V_o and ε_{max} but in this case it is an inverse one. The plot of ε_{max} against V_o (fig.8.4) shows an approximately straight line, which becomes more curved at higher V_o (and hence B.O.). The linear part means that for activation up to about 30% B.O. ($V_o \simeq 0.5$ ml g^{-1}) the D-R plots intersect at a common centre - a "pivot point". Application of the equations given in Appendix C to the linear part of figure 8.4 gives the location of the pivot point as ε = 16.4 kJ mol^{-1}, $\ln V = -3.2$, i.e. within the measured range

of adsorption. Inspection of figure 4.4 shows that for distributions of decreasing E to adsorb the same volume by a given point (the pivot point) the total adsorption volume must increase. This is well illustrated by the effect of activation on the change in characteristic curves, figure 8.5 . For carbons activated to less than 30% B.O. the curves are virtually coincident for $\varepsilon > 16.4$. At lower ε values the amount of adsorption increases in order of activation. Activation greater than 30% causes a decrease in adsorption at low pressure so that the curves are no longer coincident up to the pivot point. In the high pressure (low ε) section, activation always, eventually, causes an increase in adsorption but the point at which this occurs shifts to lower ε values as the activation increases.

These results suggest that activation, up to 30% B.O., creates new, fairly large, pores, but leaves the very small ones relatively unaffected. This could involve a complete burn out of groups, or domains, of micropore structure, with the actual micropores remaining less affected because of the difficulty of oxidant to diffuse in, or CO to diffuse out - both of which inhibit the gasification reactions. At higher activations a process of enlargement of existing pores seems to occur, with much of the large pore volume being gained at the expense of small pores. This changeover from essentially external to internal gasification must be due to the initially formed large pores constituting a connecting mesopore network, which allows transport of oxidant to the micropores - so causing their attack.

Although the precise relationship between ε and pore size is unknown, we may expect (from Morse type potential curves) that, for a given increase in size, the change in ε for a small pore will be greater than for the same increase in a large pore. This being so, the decrease in ε_{max} for a given increase in V_o will be largest when activation occurs in small micropores, i.e. at high B.O. The deviation from linearity of the $\varepsilon_{max} - V_o$ correlation, at high B.O., suggests this to be the case.

8.2.3. Positive Deviations from D-R linearity

If the porous structure does not gasify uniformly, activation will cause an initially Rayleigh distribution of potential to develop an excessive tail at high ε - due to increased retention of fine pores. The resultant concave D-R plots are indeed found for high B.O. carbons. This lends evidence to Marsh and Rand type B plots being due to a structural artefact.

Whilst the curvature found at high pressure is believed to be due to a change in distribution, the low pressure deviations are probably due to localised adsorption. This effect is revealed most clearly for highly activated carbons because of the high gradient of the plot at high pressure. These points are discussed further in Chapter 9.

8.3 X-Ray Study of Activation

8.3.1 Introduction

The most obvious effect of activation is to considerably increase the intensity of SAXS over its whole range. This can result in a complete overshadowing of the (002) reflection (see figures 8.6 and 8.7), not only because of the increased relative intensity of the SAXS but also because the scattering reduces the effective intensity of the incident beam, as seen by the crystallites.

To avoid the problems of variation within a range of virgin samples two separate carbon pellets (both carbonised to 1170 K) were activated to different degrees of burn off (B.O.), in stages. Activation was carried out with CO_2, under atmospheric pressure, at 1170 K (details in Appendix A(2)).

8.3.2 Small Angle X-ray Scattering

The correlation distances, a, obtained from Debye plots (fig.8.8) are shown in figure 8.9. Activation clearly increases a, apparently at a linear rate up to ca. 25% B.O. then at a decreasing rate. Unlike with the heat-treated series one cannot make assumptions about constancy of the volume fraction of pores, since activation will remove carbon from within the porous structure.

Fortunately, the structure is sufficiently open for adsorption at 295 K to yield the total micropore volume. Micropore volumes were therefore taken from D-R plots for an activated

series (see figure 8.2). The density of the carbon phase was taken as 2.8 g ml^{-1}, for the reasons given in section 7.1.1. The values of ℓ_p and ℓ_m are shown in figure 8.10.

8.3.3. Effect of Activation on ℓ_p

The mean intercept length of pores, ℓ_p, is seen to increase, almost linearly, with B.O. This suggests pore widening, or the creation of large pores, which occurs even at low B.O. The creation of small micropores does not seem to be very noticeable since this would cause a constant, or decreasing, value of ℓ_p with B.O.

8.3.4. Effect of Activation on ℓ_m

The slow, but definite, increase in ℓ_m with B.O. suggests that, where micropores are affected, it is the thin-walled ones which are preferentially burnt out - so leaving a matrix of statistically thicker walls. This process might be envisaged as a burn out of defective single layer-planes to leave the more stable stacks, or well formed planes. Even at 60% B.O., ℓ_m is only 0.49 nm - which is somewhat less than L_c for an unactivated carbon (0.88 nm). This suggests that many of the defective stacks and layer-planes are not removed by gasification. This must reflect the difficulty of oxidant gas to reach within the microporous structure, and so selectively gasify the defective material.

8.3.5. The Need for Jh^3-h^2 plots

Thus far, there is a similarity between activation and heat-treatment, since both cause a coarsening of both pores and matrix. This is not the full story since a cursory glance

at the experimental diffraction patterns shows activation to increase the intensity of SAXS at large angles, so as to overshadow the (002) peak. Heat-treatment only causes an increase in scattering at low angles and, in fact, causes a reduction in SAXS at high angles. These differences are well illustrated by $Jh^3 - h^2$ plots (see section 7.1.2) for some activated carbons, figures 8.11 and 8.12 .

8.3.6. Effect of Activation on b_1

The intercepts from such plots, b_1, are given in figure 8.13 and show an increase over the whole range of activation. This must result from the production of well defined pores. These could either be mesopores created by burn-out of domains of micropores, or large supermicropores which have been widened from ultramicropores - the latter process probably being favoured at high activation. The increase in b_1 is considerably greater than that caused by heat-treatment, for instance, the increase caused by heating an 1170 K carbon to 1870 is the same as obtained by activating the carbon to 20% B.O. This is to be expected since removal of carbon by gasification creates large voids easier than by a packing together of widely spaced layer-planes

8.3.7. Effect of Activation on b_2

The major difference between heat-treatment and activation is seen from the b_2 values (Figure 8.14). Whilst heating causes an overall reduction in b_2 (neglecting a small maximum at low HTT), activation causes it to increase up to 35% B.O., level off, then apparently decrease after ~60% B.O. The

following explanations were considered for the initial increase in electron density fluctuations with activation : -

1, Activation could be producing vacancies and vacancy loops within layer-planes - the increased defect concentration would increase scatter which has a h^{-1} dependence.

2, Hydrogen rich material could be preferentially removed from micropore surfaces. This material would cause a blurring of the solid/void interface so that its removal would sharpen the boundary. Such an effect would result in the removal of a negative, h^{-1} dependent, contribution to the scattering (see section 7.1.2).

3, From the adsorption section (8.2) it seems that, due to transport difficulties, very little attack of fine micropores occurs, up to 30% B.O. - yet this is the region where b_2 increases most. Explanations 1, and 2, both require an intimate attack of micropore structure such that specific parts of layer-planes are gasified, but with retention of the network. It seems more likely that a complete burn out of supermicropores (i.e. those easily accessible) occurs - to leave the narrower ultramicropores. Now, so far we have assumed that very small voids - density fluctuations - scatter according to a $J \propto h^{-1}$ dependence. This division must be arbitrary since small pores must exist which scatter x-rays with an intermediate angular dependence, i.e. a combination of h^{-1} and h^{-3}. Supermicropores will, therefore, have a smaller h^{-1} component that ultramicropores, so that their preferential burn-out will cause the resultant matrix to scatter with a more intense h^{-1}

component.

The reduction in b_2 at high B.O. may reflect the increasing attack of defective layer-plane stacks - which constitute the non-uniform density matrix - to leave the well formed stacks, which contain less fluctuation of interlayer spacing. The need for activations over 60% again emphasises the over-riding effect of oxidant transport into the structure, before selective oxidation of defective material can occur.

8.3.8. Wide Angle X-ray Diffraction

The results of the wide angle (002) profile analysis is given in Figures 8.15 and 8.16 but must be treated with caution.

L_c is found to decrease significantly over 20% B.O. which might be attributed to a reduction in size of layer stacks except that one would expect the less ordered stacks to be preferentially removed, leaving the relatively perfect ones (that diffract x-rays) less affected. This is the picture given by SAXS (ℓ_m increases) and would result in an *increase* in the statistical value of L_c.

Casting further doubt on these results is the increase of interlayer spacing with B.O., suggesting less perfect crystallites are remaining - again at variance with expectation.

The anomalies are believed to be experimental rather than real since the carbon pellets become so porous after about 20% B.O. that, in the reflection mode, the x-ray beam penetrates further

into the sample before being diffracted. This would result in a deviation from the correct diffraction geometry viz. diffraction no longer occurs at the centre of the goniometer circle. Small displacements (ca. 1 mm) of a specimen from its axial position shown the result to be a broadened peak with a small displacement to lower angles - apparently confirming the above doubts. This aberration is of negligible effect at small angles but clouds any changes in crystallite parameters at wide angles (which are very small).

It is suggested that further work to resolve the question of the effects of activation on crystallite structure should be carried out in transmission geometry. If corrections for absorption effects are made (advisable in this case) account should also be made for the effect of porosity on the effective sample thickness. Powder samples with an internal standard would be a viable alternative since absorption corrections could be made by the method of Jones[203].

8.4 Electron Microscopic Study of Activation

Samples of partially gasified cellulose triacetate (C.T.A.) carbon were examined in high resolution transmission, and scanning, electron microscopes. The samples for TEM were ground and dusted onto the microgrids, therefore any particle edges observed are likely to be representative of the inner parts of the carbon granules rather than the outer surface.

Figure 8.17 shows a high resolution TEM of 1230 K, 30% B.O., CTA carbon. The structure is quite typical of many activated carbons examined and shows no sign of burnt-out layer-planes. This suggests that these pores are relatively unaffected by gasification - at this degree of activation. Unfortunately, more highly activated carbons were not examined but figure 8.19 shows a lattice fringe image from a highly activated anthracite char [193,204] which shows a very open structure - suggesting considerable burn-out of individual layer-planes.

It may be noticed that figure 8.17 shows patches of light (A) and dark (B). These were not generally found in unactivated carbons and are indicative of considerable variations of sample thickness - probably due to mesopores[205]. The complete burn-out of domains of structure is shown by the S.E.M. of a 1230 K, 46% B.O. CTA carbon (figure 8.18). The pores seen in this micrograph equate with macropores but these may have resulted from burn-through of mesopores.

To conclude, it seems likely that large domains of structure are removed in the early stages of activation. The remaining structure is unaffected until a sufficiently high mesopore volume is obtained, which enables a more intimate attack of the microporous structure.

8.5 Effect of Heat-treatment to 1470 K on Activated Carbons

Adsorption Study

8.5.1. Results

1170 K carbons which had been activated were subsequently heat-treated to 1470 K for 10 mins and isotherms measured for CO_2 at 295 K.

Figure 8.2 shows that heat-treatment causes a reduction in V_o which increases in magnitude up to 20 - 30% B.O. then remains approximately constant. ε_{max} values are shown in figure 8.3 . At low B.O. heat-treatment causes a decrease in ε_{max}, but very little effect is seen for pre-activations of 30 - 40% B.O. At higher B.O. the heat-treatment apparently causes ε_{max} to increase.

Discussion

8.5.2 The Effect of Heat-treatment on V_o

The increasing amount of pore closure, upon heat-treatment, seen at low B.O. may be due to a number of effects :-

A, Heat-treatment may cause an increase in pore volume by completing secondary carbonisation; it can also result in a closing of pores. There will be a certain amount of competition between these two factors so that if activation removes material (which would be expelled on heating to cause an increase in pore volume) there will be less compensation for the pore volume lost by pore closure.

B, It is possible that oxidation of heteroelements removes restrictive (sterically hindering) material from layer-planes and so allows them to collapse together more easily.

C, Activation could be opening some closed pores, or creating new narrow pores, which become closed upon heating to 1470 K.

D. Activation could preferentially remove carbon from wide pores - which would not close on heating to 1470 K. The remaining structure will have a higher concentration of very narrow pores - which close upon heat-treatment, to cause a greater loss in V_o.

As far as adsorption is concerned it is not possible to distinguish between the above without recourse to further work - such as activating a heat-treated series, or using a higher subsequent HTT. The SAXS study, however, suggests D to be the most likely (see section 8.6.2.)

At larger degrees of pre-activation, the most noticeable effect is that the amount of volume lost on heat-treatment is virtually constant - despite a considerable increase in the total pore volume. This suggests that the pore entrances which close are relatively unaffected by gasification - even up to $\sim$50% B.O., where fine micropores are known to be opened out. These pore entrances must be very narrow and well disposed to assuming a turbostratic spacing, since they close upon the mild heating to 1470 K.

Since the pore entrances which close upon heating appear to be

unaffected by gasification one would not expect them to be re-opened by activation after the heat-treatment. The results of McEnaney and Dovaston[4] support this view. They found that heating an unactivated cellulose triacetate (CTA) carbon from 1230 to 1475 K caused V_o to decrease from 0.21 to 0.17 ml g^{-1}, i.e. a loss of 0.04 ml g^{-1}. Activation of both 1230 and 1475 K carbons to 30% B.O. increased V_o to 0.37 and 0.33 ml g^{-1}, respectively. It would appear that the loss in V_o of 0.04 ml g^{-1}, due to heat-treatment, was not recovered, even after activation to 30% B.O. It seems likely that the effect of activation was, in both cases, to create mesopores. Activation of a 1675 K CTA carbon, to 30%, was found to increase V_o from 0.03 to 0.10 ml g^{-1} which, again, suggests that the volume lost by heat-treatment is not recovered. The authors also found that the pores created by activation tended to be larger for higher HTTs. It would seem that, as micropores progressively close off, the domains of structure which are inaccessible to oxidant gas become larger. Activation is restricted to burning between, and on the surface of, these domains, but not within them. As HTT increases, fewer, and therefore larger, pores will be created for a given burn off.

8.5.3. The Effect of Subsequent Heat-treatment on ε_{max}

Figure 8.3 shows that at low B.O. heat-treatment causes a decrease in ε_{max}, which must be a result of the closure of small pores to leave larger ones. At ~ 30 - 40% B.O. ε_{max} is hardly affected by the heat-treatment and it appears that at higher B.O. heat-treatment may actually cause ε_{max} to increase. To understand this we must remember that at 30% B.O. much of the

pore volume exists in large pores, which are apparently unaffected by heat-treatment. The loss of a fixed volume of small micropores will have a much smaller effect in these carbons than in carbons where the pore volume is less, and is solely contained in micropores. The apparent increase in ϵ_{max} for heat-treatment of high B.O. carbons must reflect a general narrowing of micropores which have become widened by activation. Being wider, they may not actually close off but simply narrow. Although shrinkage was not looked for, some might be expected for these carbons. The general narrowing of all pores, with shrinkage, is known to occur for carbons heat-treated up to 1300 K and the above effect may be similar to this, but accentuated by the loss of sterically hindering layer-planes and heteroelement material (such as non-aromatic side groupings).

As previously mentioned, the HTT of 1470 K causes a relatively mild pore closure effect and probably only affects micropores which are small enough to remain unaffected by pre-activation. If a HTT of, say, 1800 K were used, the closing of larger pores would probably result. Such a HTT might close many of the pores created by activation so that pre-activation, followed by heat-treatment, would create more closed porosity than with no pre-activation. This may be the explanation for the results of Kotlensky and Walker (see section 8.1). These authors also used carbon blacks, which are of very fine particle size - this may cause the porosity to have a higher supermicropore to mesopore ratio, due to the easier access for oxidant to the micropores.

8.6 SAXS Study of the effect of Heat-treatment to 1470 K on Activated Carbons

Activated carbons (HTT 1170 K) were subsequently heated at 1470 K for 10 mins. (full details are given in Appendices A(2) and A(4)).

8.6.1. Results

The correlation distances, a, as a function of degree of pre-activation, are shown, together with those for un-heat-treated carbons, in Figure 8.9. Pre-activation up to 10% has a constant effect on the final correlation distance, even though the 1170 K carbons show an increase. From 10 - 30% B.O. an increase in a is seen, which then levels off. The variation of b_1 (Figure 8.13) is very similar to that of a, but an actual crossover is found at high activations. The decrease in b_2, found on heating, figure 8.14, is seen to increase with degree of pre-activation.

8.6.2. Discussion

From the isochronally heated carbons (section 7.1.1.) we can see that pore coarsening is not restricted to the elimination of ultramicropores but occurs in all pore sizes. Much of the coarsening seen for unactivated carbons must involve the collapse together of widely spaced layer-planes to create larger pores. These same layer-planes will also tend to be accessible to oxidant gas and so be easily removed in the initial stages of activation. The apparent insensitivity of a and b_1 to heat-treatment, after pre-activation of less than 10% B.O., must be due to both heat-treatment and activation creating similar pore space from

the space occupied by the widely spaced layer-planes.

A preferential burn-out of supermicropores, up to 30%, is also suggested because b_2 (Figure 8.14) experiences an increasing loss, upon heat-treatment, with activation. Ultramicropores are of small enough size as to be classified as density fluctuations in the carbon matrix, so will therefore make a large contribution to the b_2 scattering component. A preferential removal of supermicropores will leave a matrix with a higher proportion of ultramicropores. The closure, and loss, of these will therefore cause a larger reduction in b_2 for activated than unactivated carbons.

Beyond 30% B.O. the main effect is a creation of supermicropores by widening ultramicropores. It is possible that the layer-planes which border these pores are relatively unrestrained due to removal of sterically hindering groups. The supermicropores, so created by gasification, are therefore prone to collapse on heat-treatment, possibly causing some overall shrinkage, or creating large meso or macropores. These very large pores scatter x-rays at very low angles and their production would not be detected by the SAXS analyses used (which concentrate on high angles). This would explain why b_1 apparently decreases and a levels off.

8.7.1. Summary of the Effects of Activation on Structure

Low activations (up to ~30% B.O.) seem to be restricted to gasification of supermicropore walls with the creation of mesopore channels. The matrix which surrounds these pores appears to have a higher concentration of ultramicropores - either by virtue of a higher stability or lower accessibility to oxidant. This view is demonstrated by both the concentration of density fluctuations and pore closure increasing up to 30% B.O.

Higher activations increase the accessibility of the structure and enable gasification to occur on the larger surface area of ultramicropores. In this region there is a simultaneous widening of ultramicropores to supermicropores, and burn-out of the supermicroporous structure. These two effects cause the concentration of ultramicropores to hardly change - as evidenced by the constant loss of V_o on heat-treating and levelling of b_2. The layer-planes at this activation are sufficiently unrestrained and widely separated (see figure 8.19) for heat-treatment to cause them to generally narrow and collapse together. This results in ε_{max} increasing with heat-treatment whilst both the correlation distance and b_1 level off. The overall shrinkage expected for this heating may make some contribution to the loss in V_o. No production of narrow spacings seems to occur since b_2 is not particularly affected - it may be that the approaching layer-planes are incorrectly oriented to form turbostratic crystallites.

It appears that selective structural attack of faulty layer-plane stacks probably only occurs after ~60% B.O. since this is when b_2 decreases. However, selective structural attack on widely spaced, and perhaps single layer-planes occurs at low B.O. since ℓ_m increases and supermicropores are removed. The criterion for attack appears to be accessibility rather than disorder. To stretch a definition, it could be argued that the widely separated and disorientated layer-planes that constitute supermicropore walls are more disordered than the closer packed ones which constitute the walls of ultramicropores.

8.7.2. Amorphous Carbon

In section 7.1.3 it was shown that the b_2 component could result from amorphous carbon, *inter alia*. From the arguments presented in this section this seems rather unlikely. Not only would such a phase need to be extremely inaccessible to resist 60% B.O. but it would also need to be created by activation, up to 30% B.O. Both suggestions seem untenable. Whilst truly amorphous carbon may not exist, disordered or *paracrystalline*[206] carbon is possible, and indeed, to be expected. This carbon will exist at defects and regions of distortion within layer-planes (including edges). The atoms are still bonded to neighbours but are sufficiently displaced from the regular lattice positions to prevent their adding to the Bragg diffraction pattern. This distorted type of lattice has been suggested as existing to HTT > 3000 K[76] and, being intimately within the layerplanes, would be difficult to remove by gasification. The existence of such carbon would support the view of Ruland[181] that the b_2 component is due to fluctuations in interlayer spacings, since these would

be caused by bends, kinks and distorted areas in general. A contribution from defects, notably vacancies, also cannot be discounted.

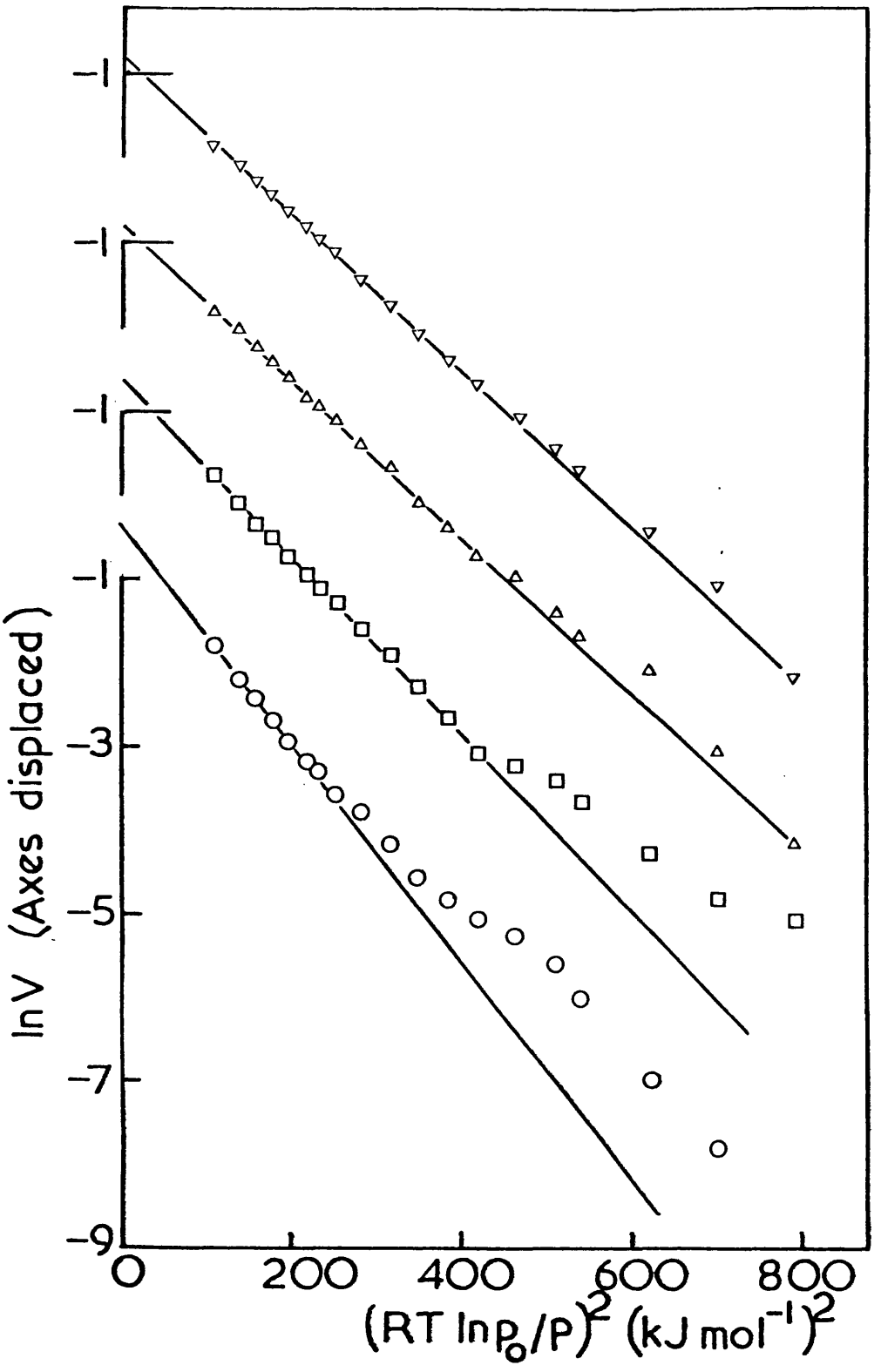

Fig.8.1 D-R Plots for Activated 1170K Cellulose Carbons (CO_2 / 293 K).
% B.O. ▽13, △19, □38, ○58.

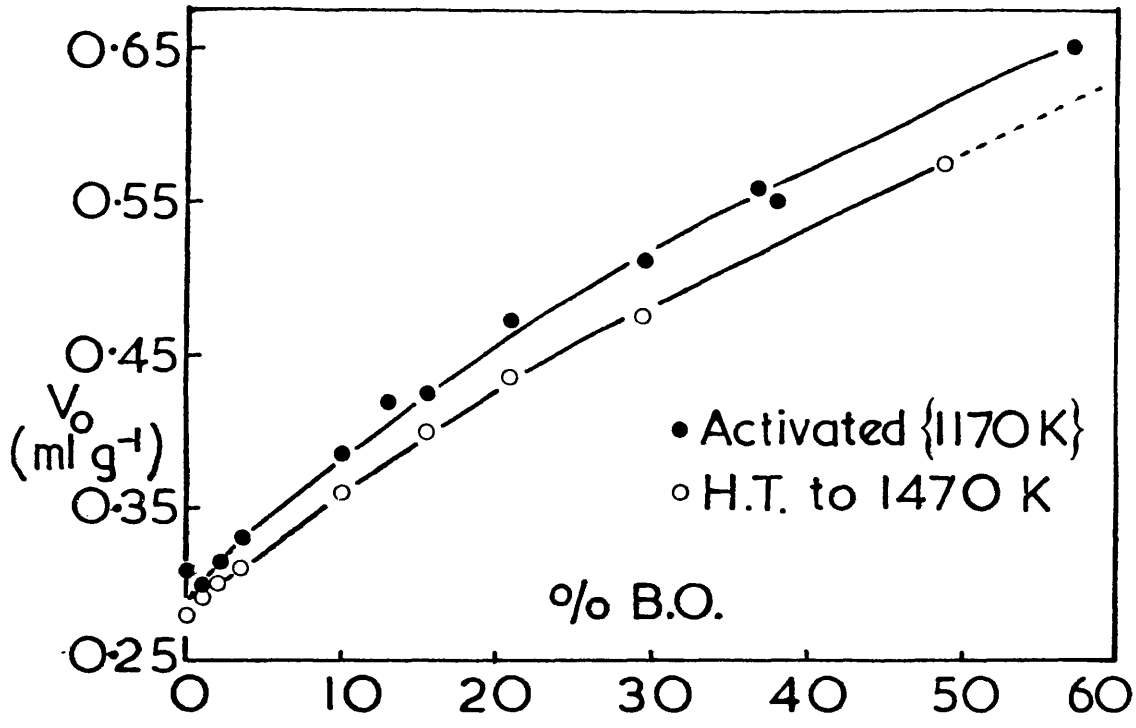

Fig. 8.2 Effect of Activation & Subsequent Heat-treatment to 1470 K on Micropore Volume.

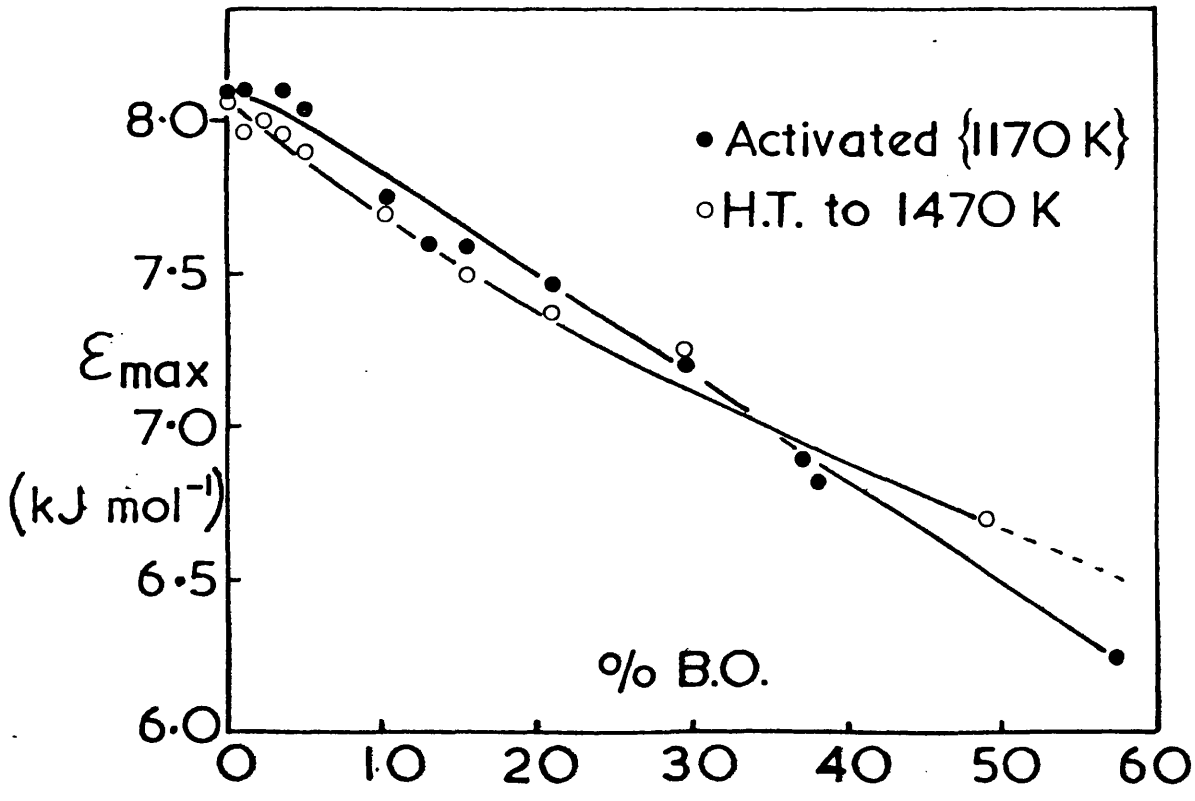

Fig. 8.3 Effect of Activation & Subsequent Heat-treatment to 1470 K on the Modal Value of Adsorption Potential.

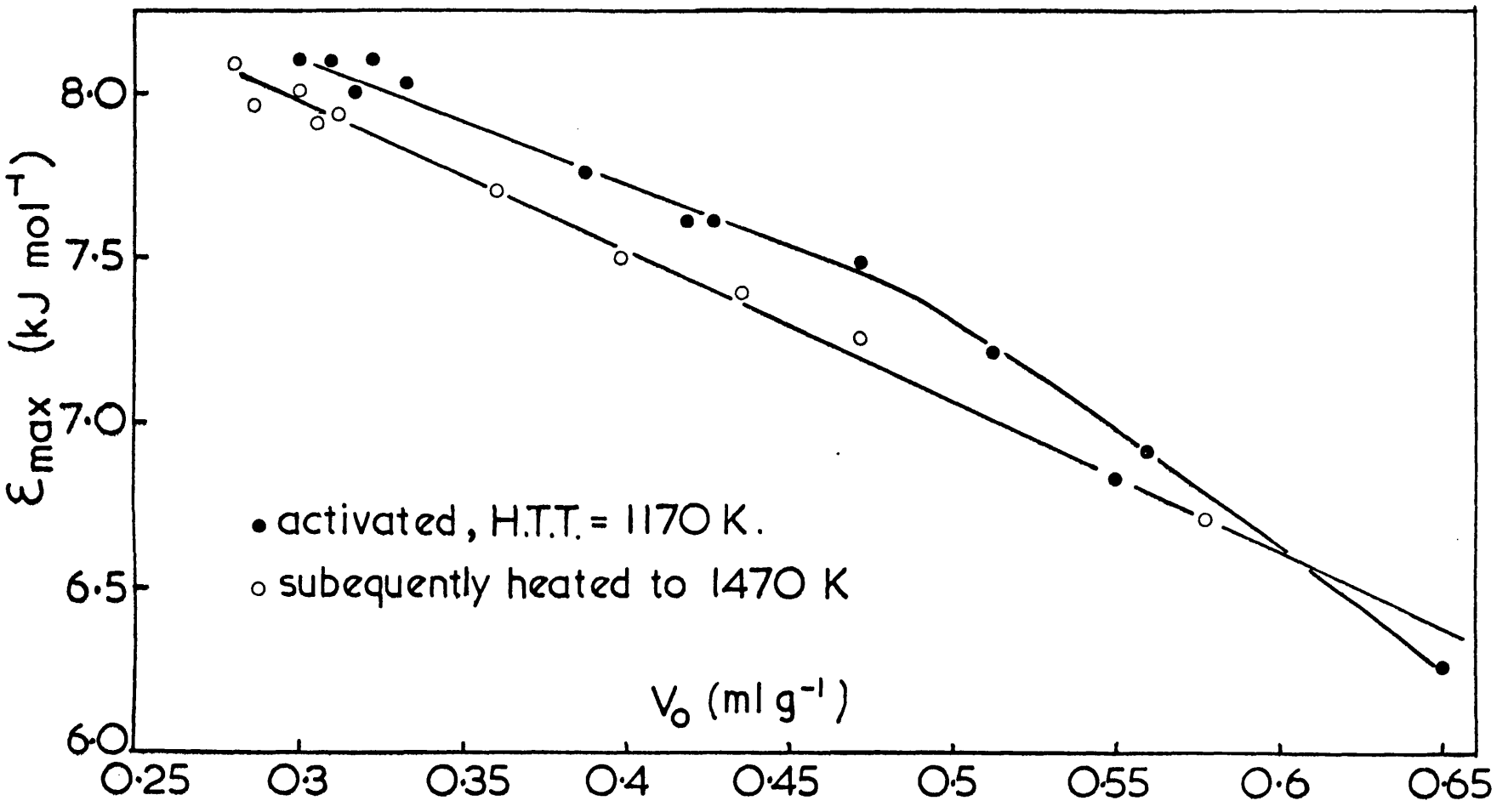

Fig. 8.4 $\varepsilon_{max} - V_o$ Correlation for carbons activated then H.T. to 1470 K.

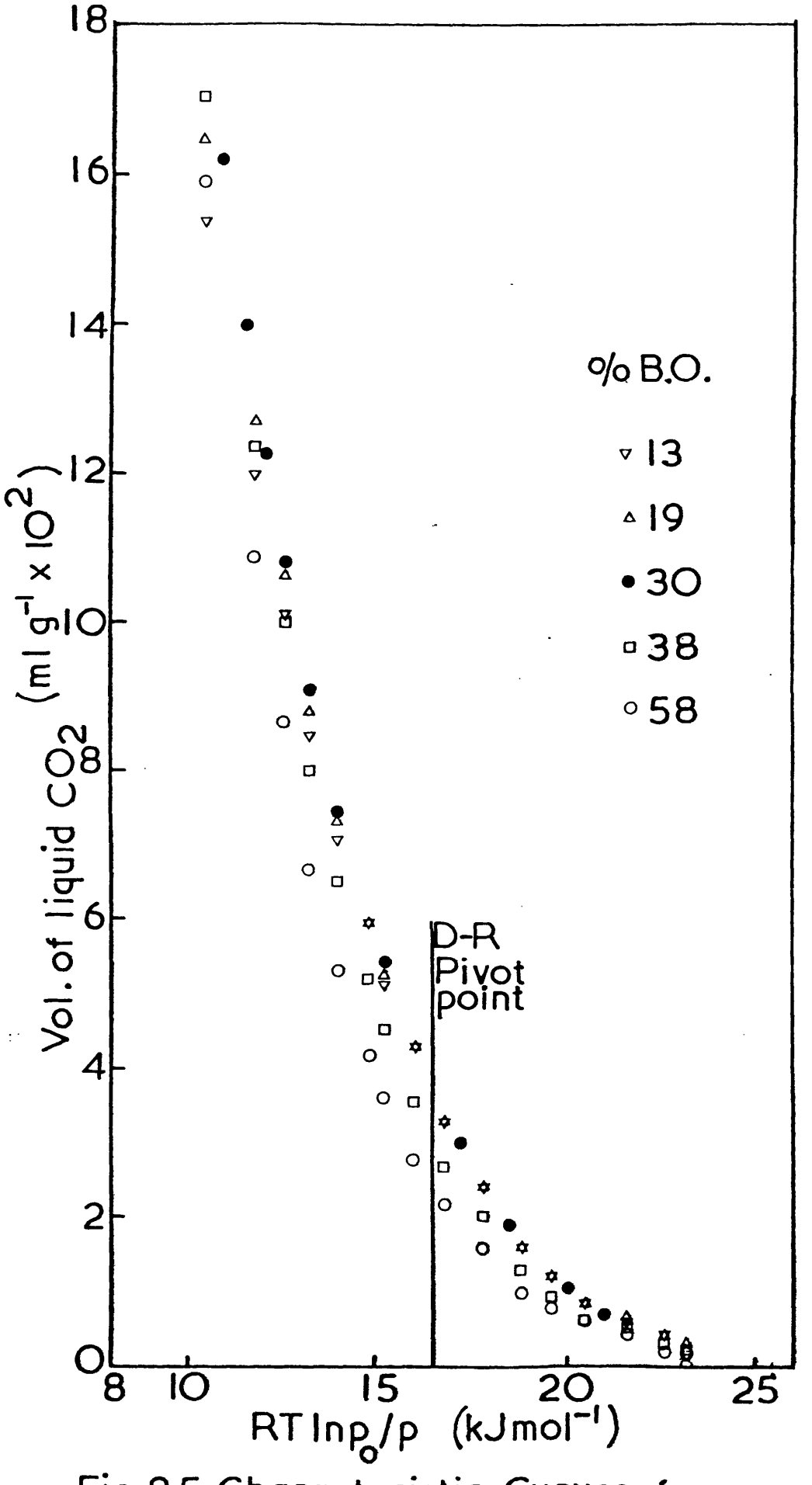

Fig. 8.5 Characteristic Curves for Activated Carbons.

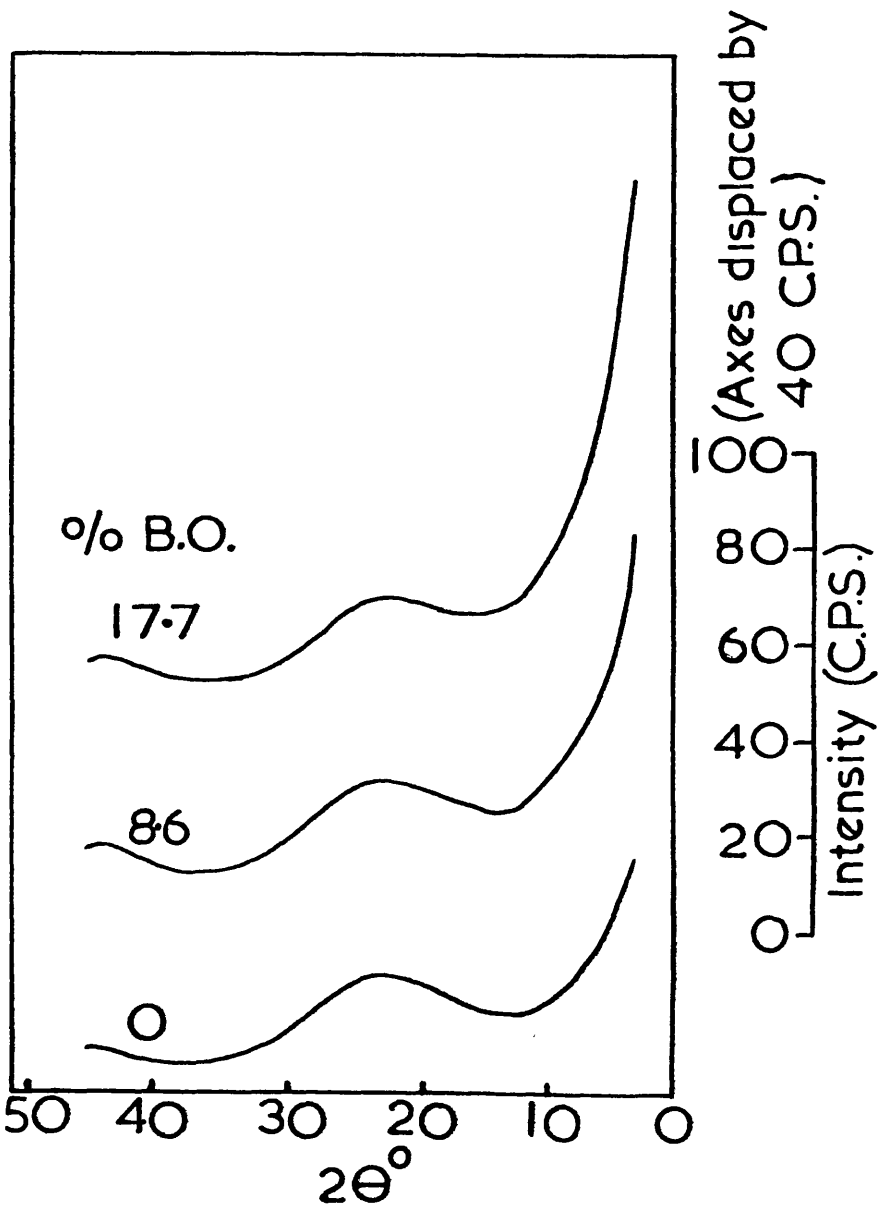

Fig.8.6 Effect of Activation on X.R.D. Patterns.

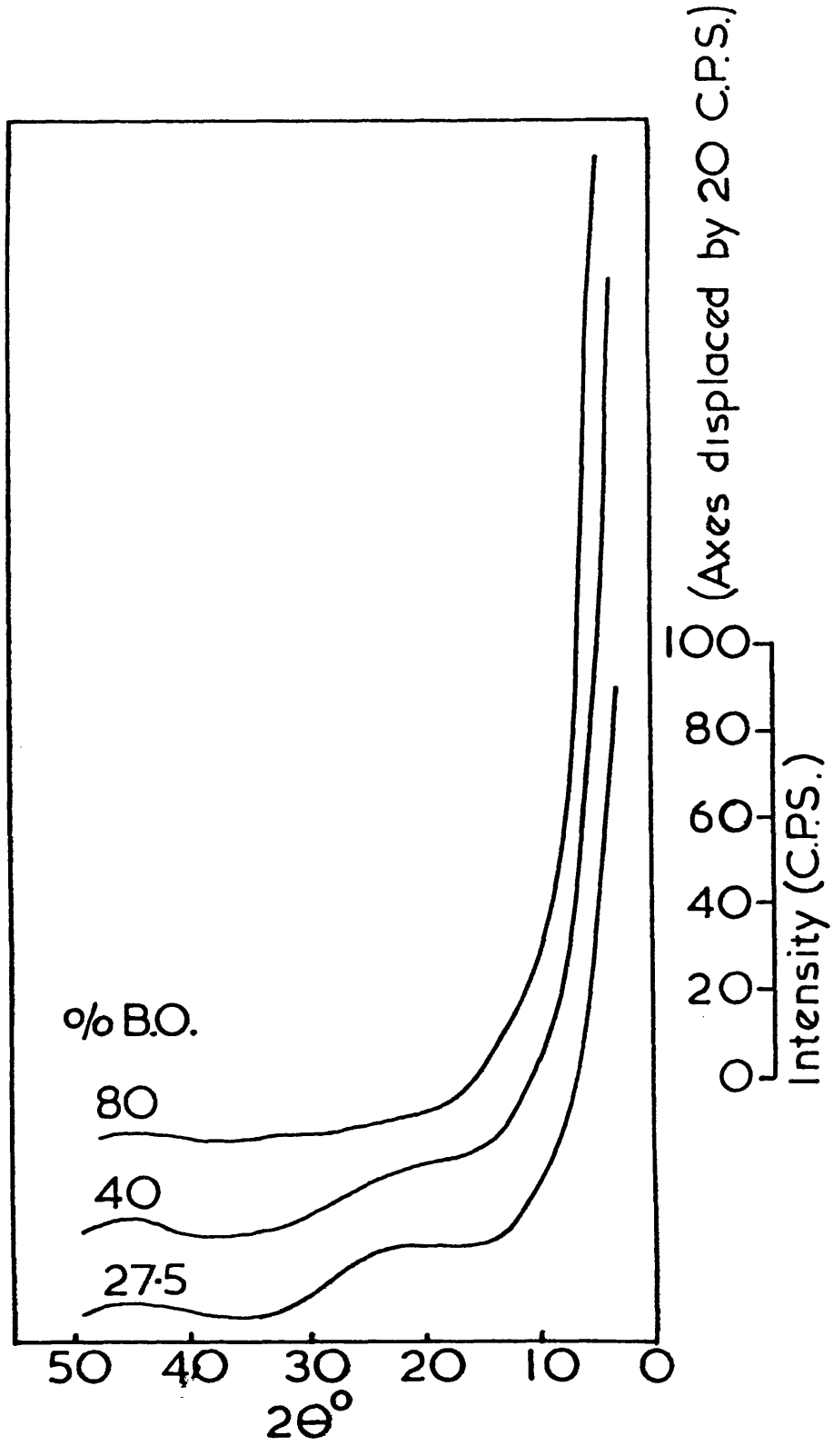

Fig.8.7 Effect of Activation on X.R.D. Patterns

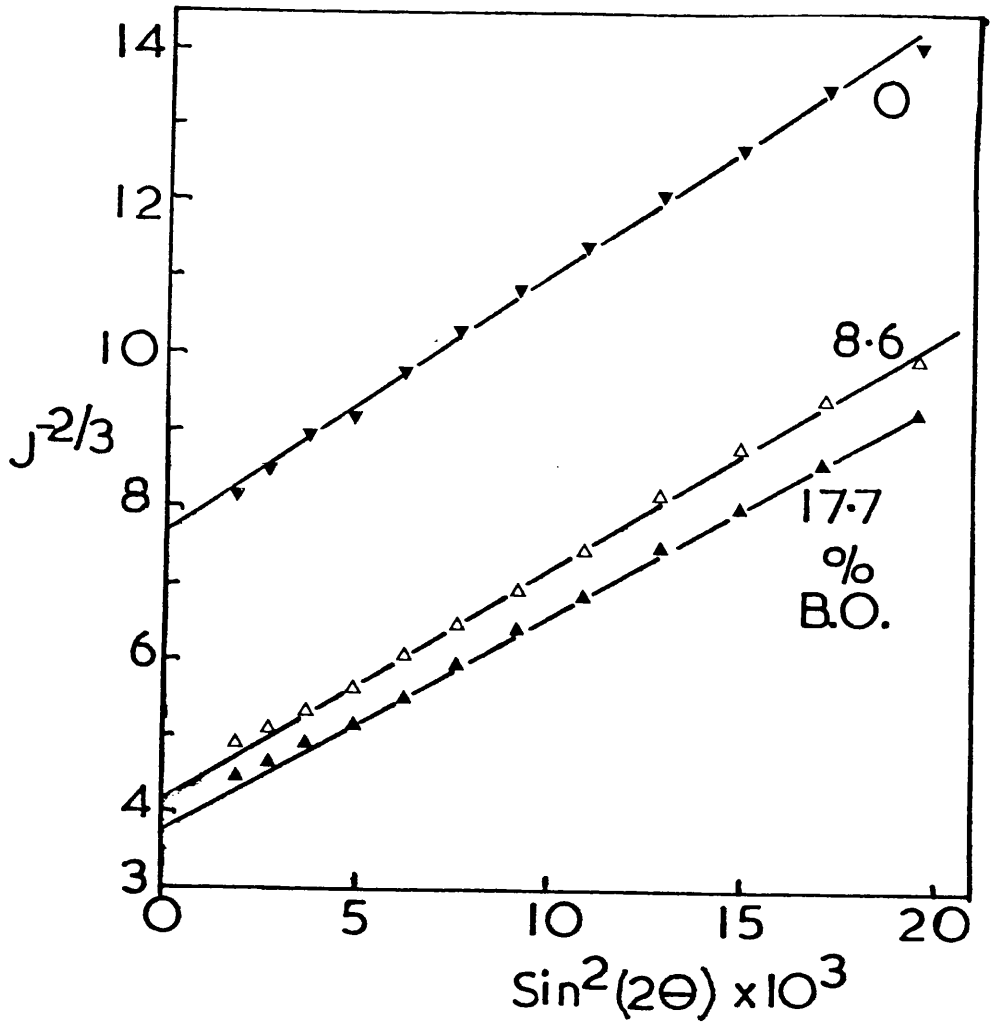

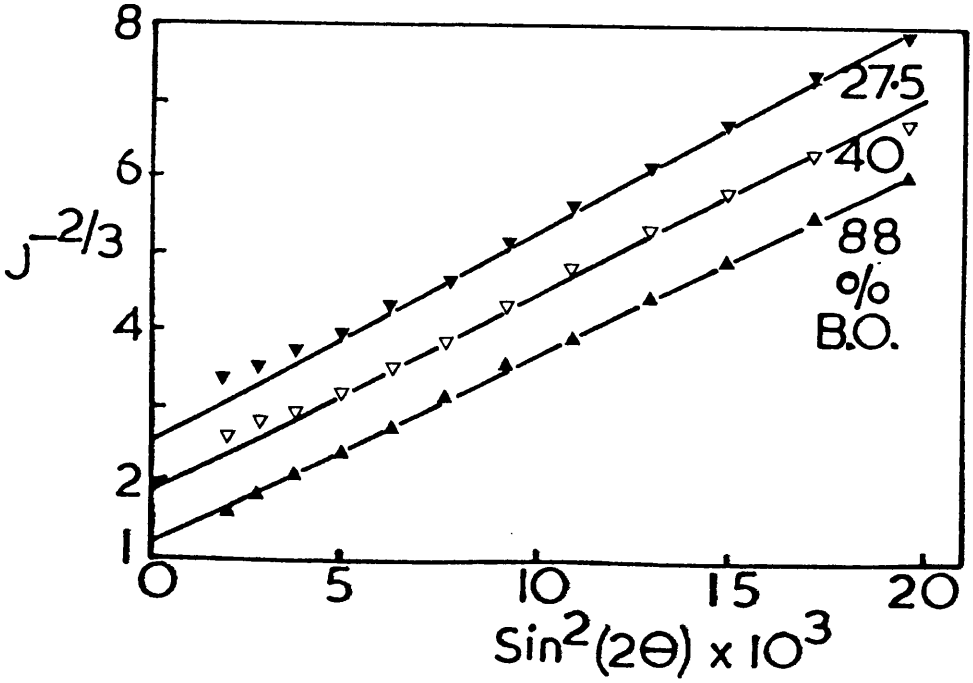

Fig.8.8 Debye plots for activated carbons.

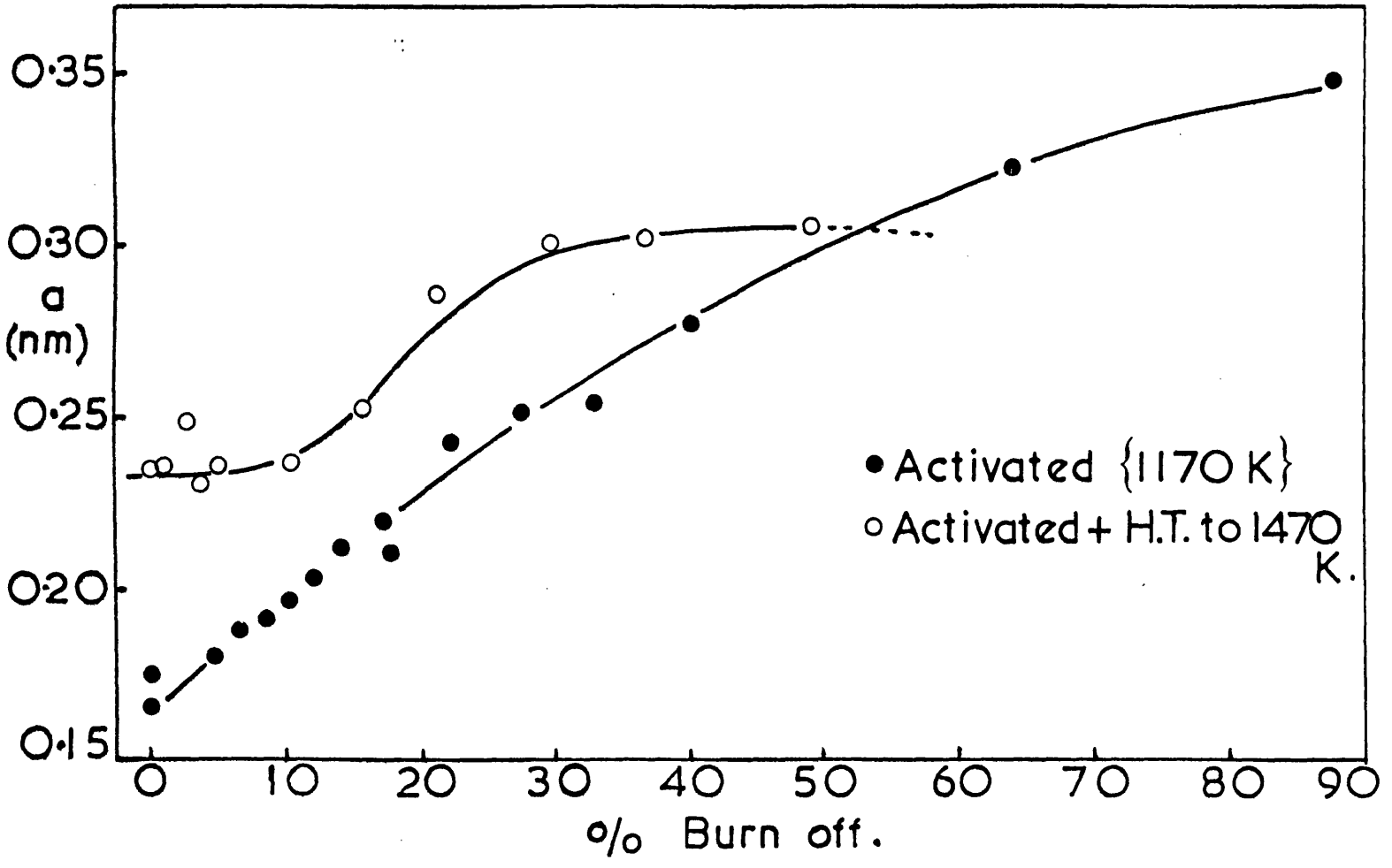

Fig. 8.9 Effect of activation, & subsequent H.T. to 1470 K, on Correlation Distance.

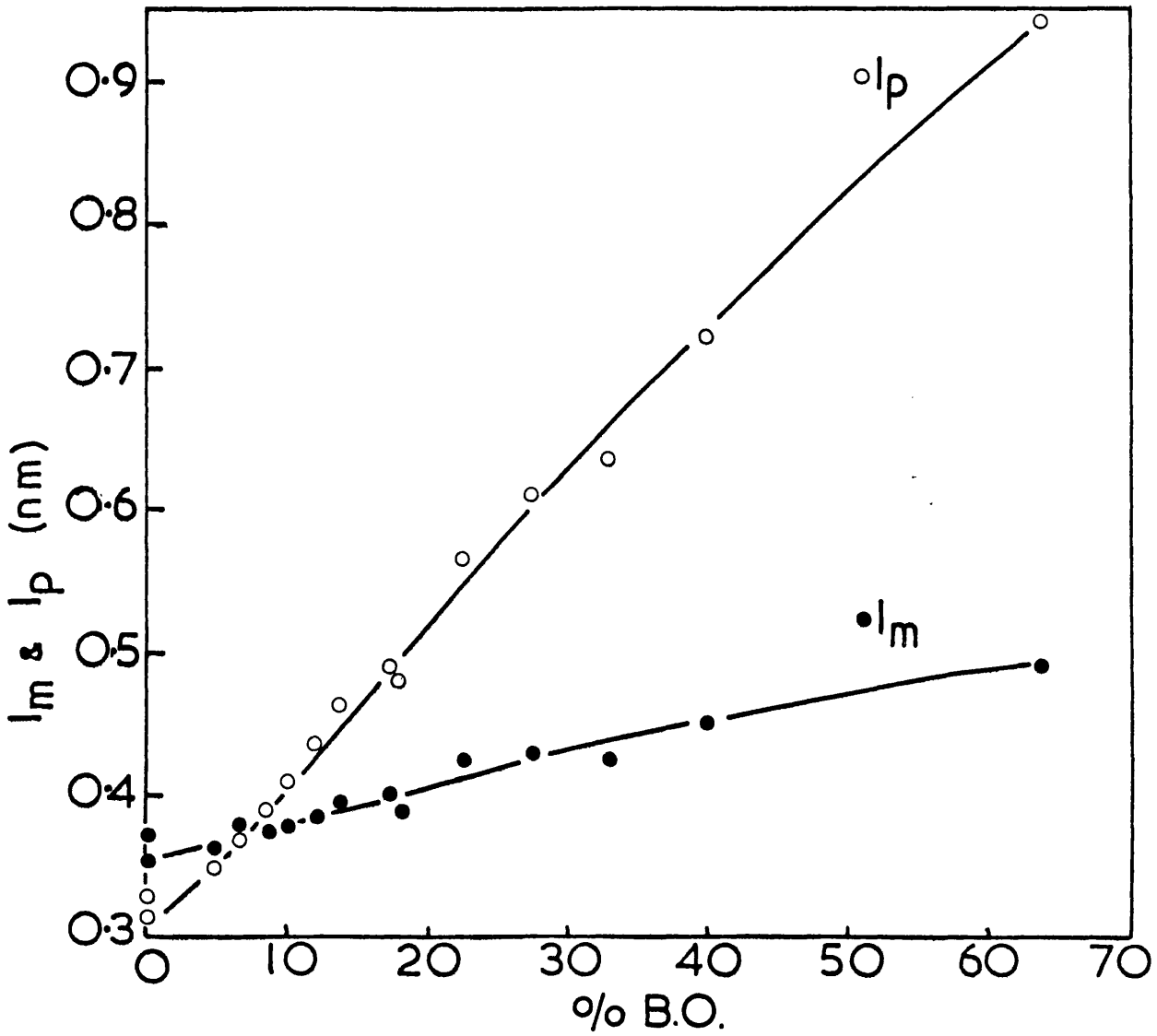

Fig.8.10, Effect of Activation on linear S.A.X.S. parameters.

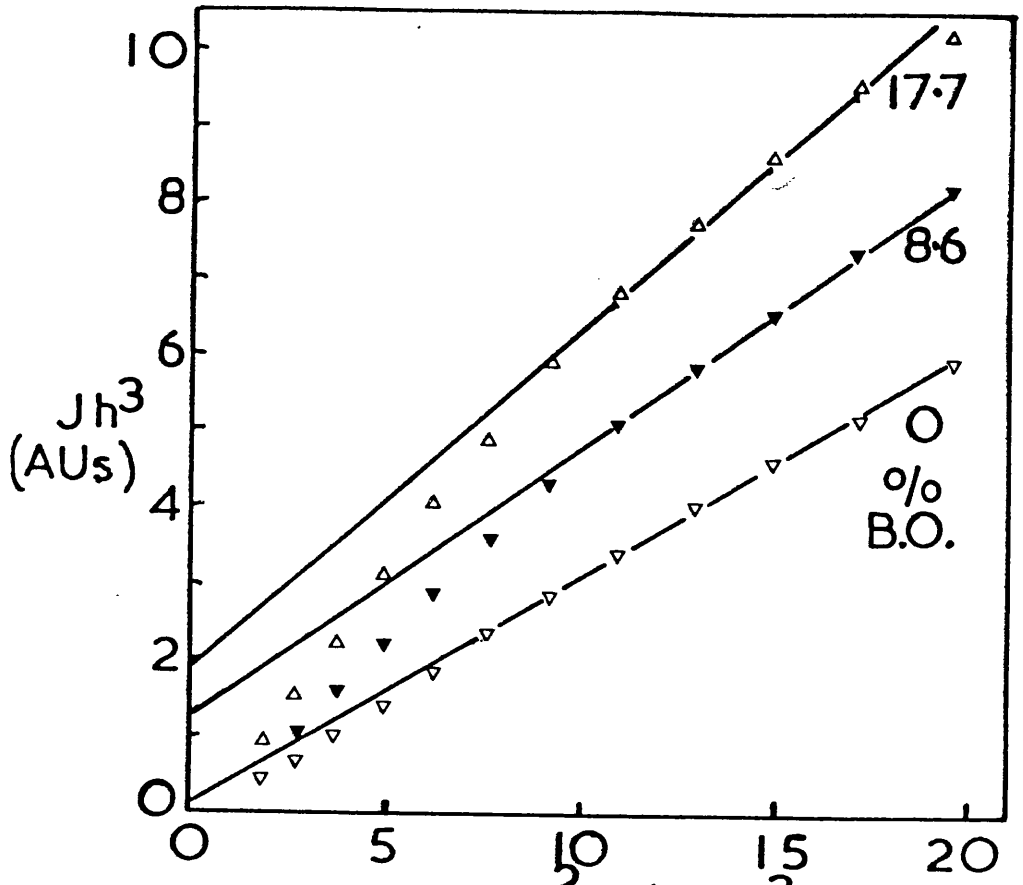

Fig.8.11 $Sin^2(2\theta) \times 10^3$

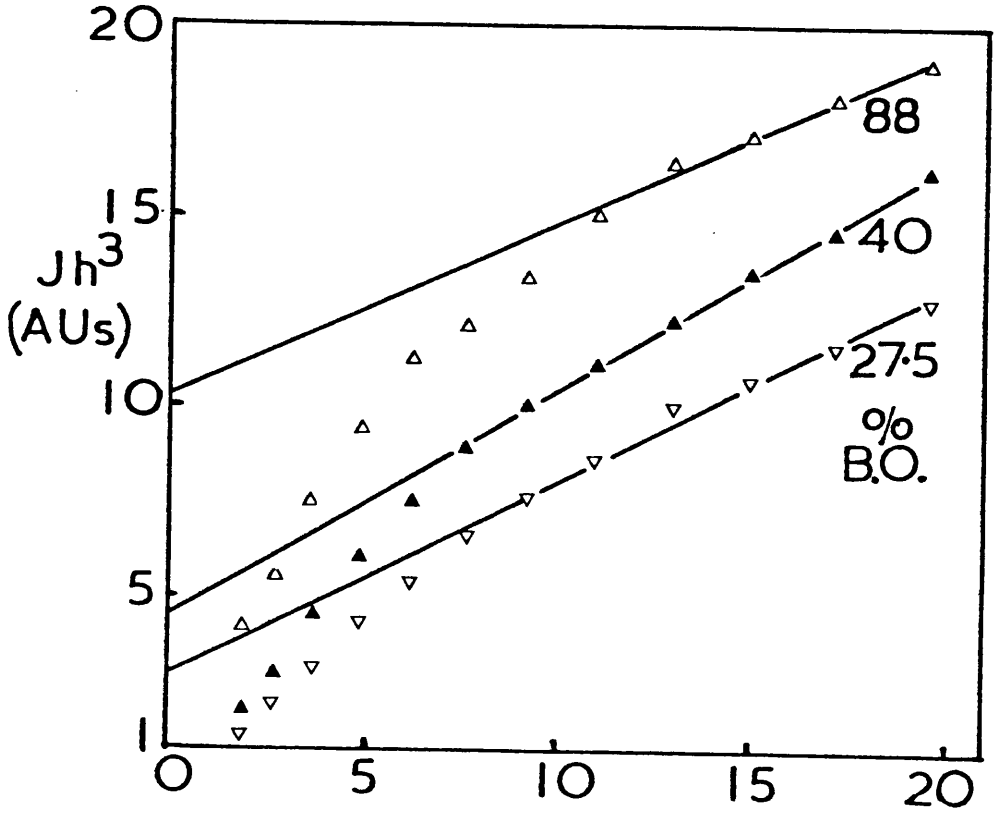

Fig.8.12 $Sin^2(2\theta) \times 10^3$

Deviations from Porod's law.

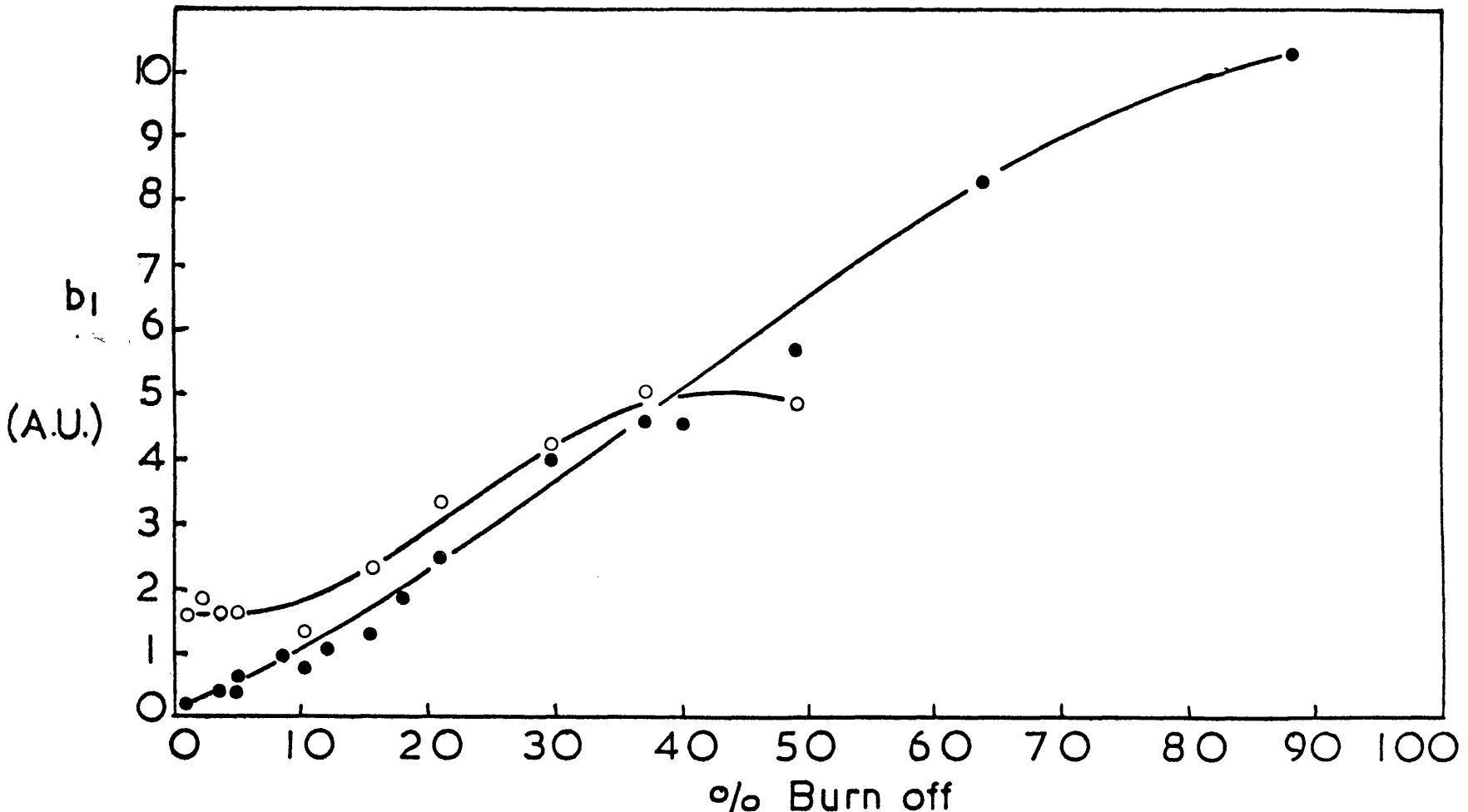

Fig. 8.13 b_1 values from $Jh^3 - h^2$ plots, •1170 K activated.
°H.T. to 1470 K.

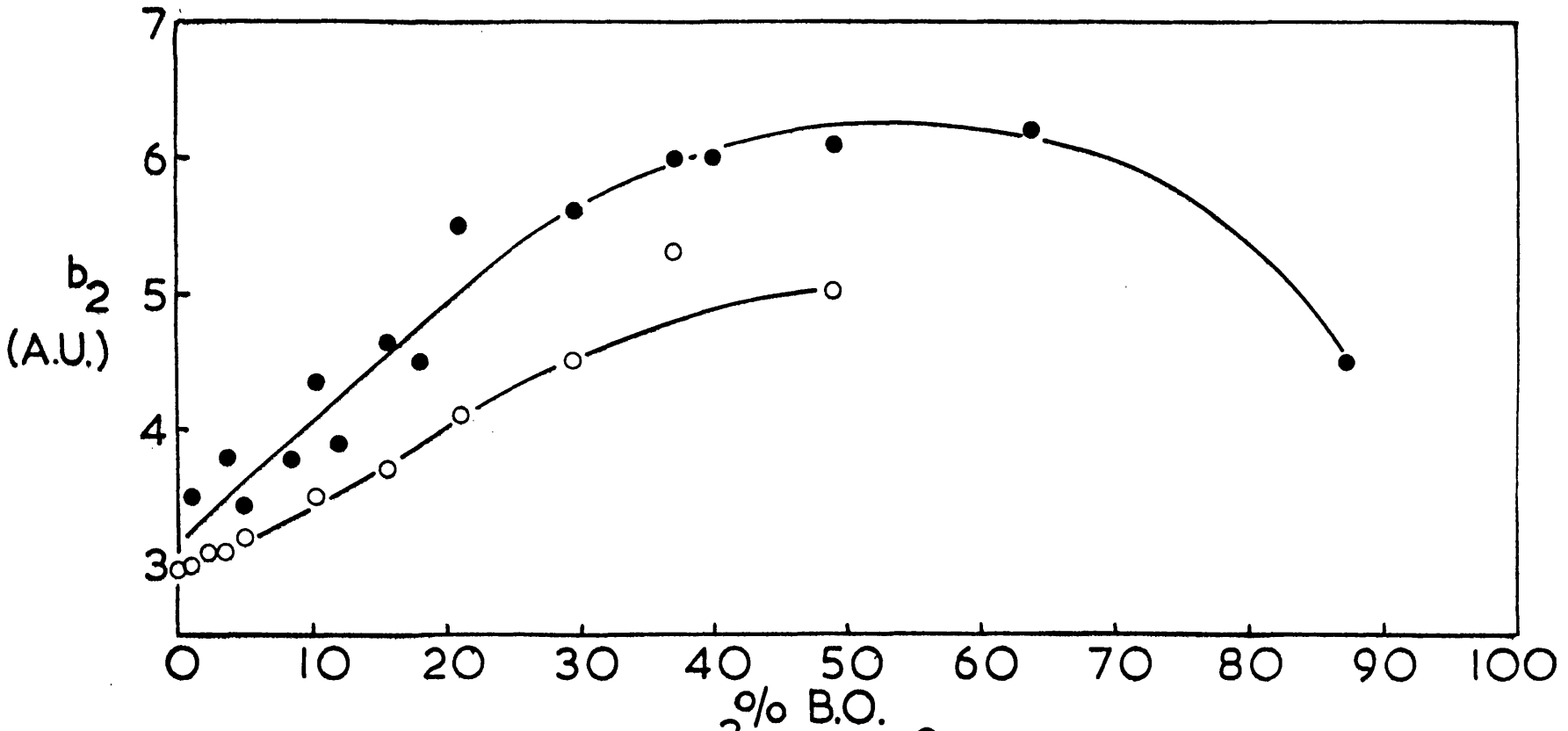

Fig. 8.14 b_2 values from $Jh^3 = b_1 + b_2 h^2$ plots for carbons :-
•Activated, ○Subsequently heated to 1470 K.

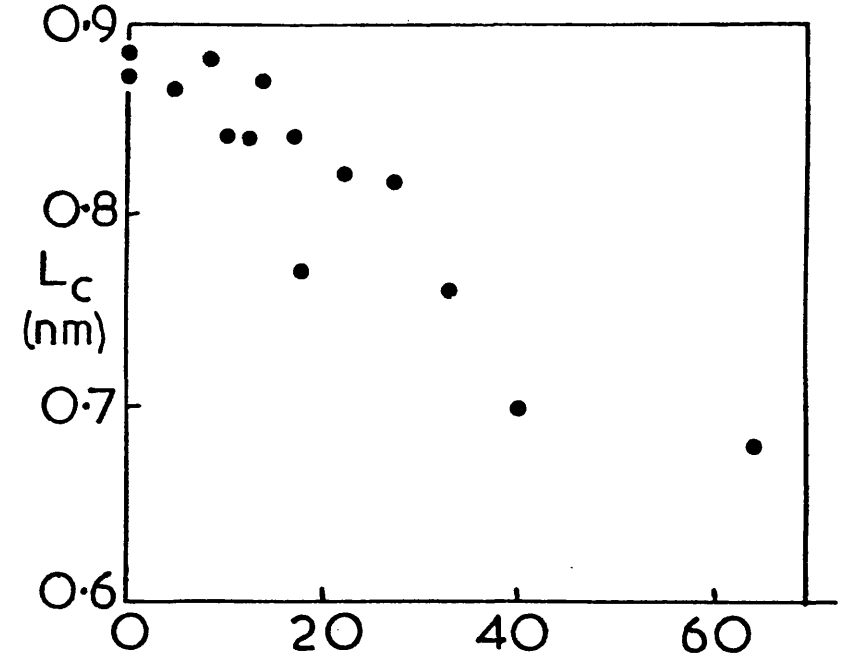

Fig. 8.15

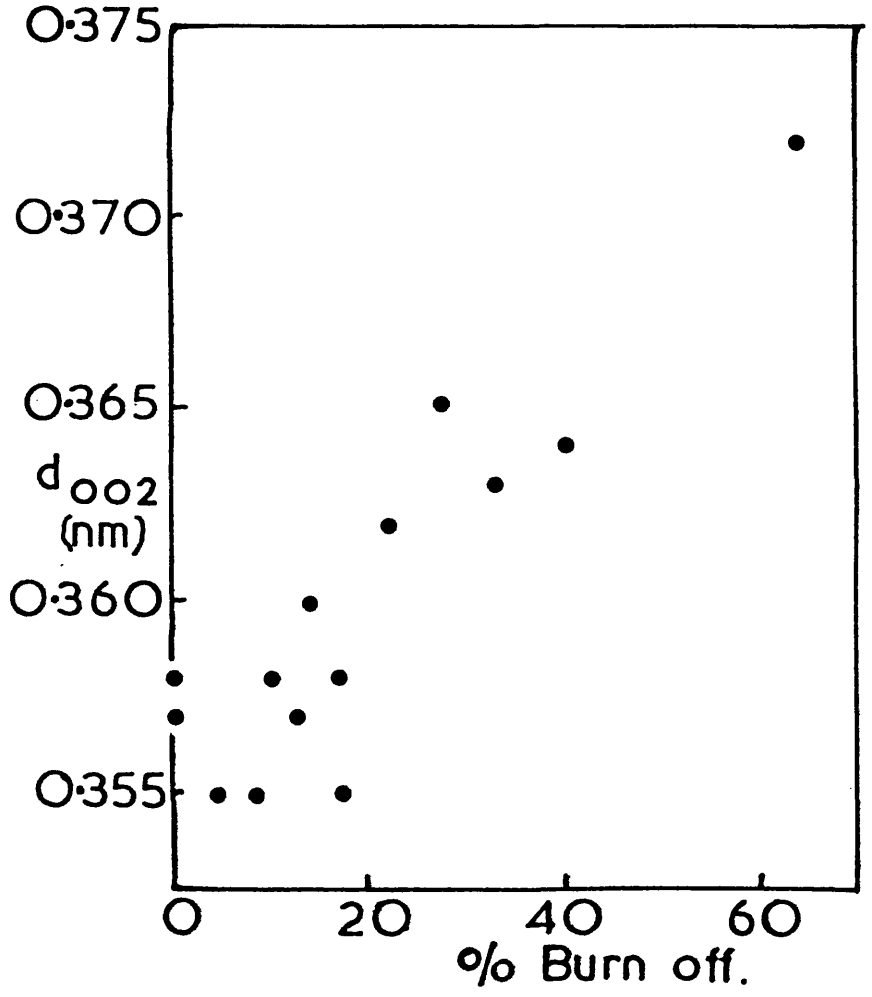

Fig. 8.16 Apparent effect of activation on XRD parameters (N.B. see text)

20nm Fig.8.17 H.R.E.M. of CTA Carbon. H.T.T. 1230K, 30% B.O.

100μm Fig.8.18 S.E.M. of CTA Carbon. H.T.T. 1230 K, 46% B.O.

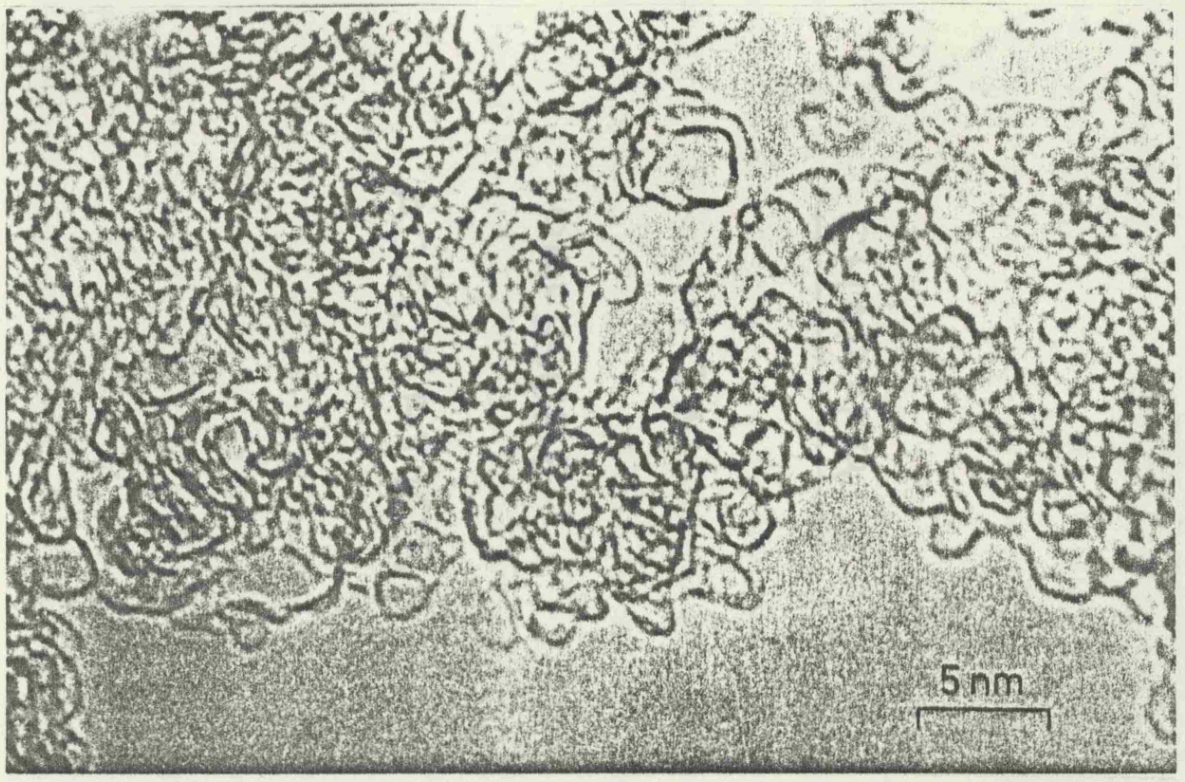

Fig. 8.19 HREM of Strongly Activated Anthracite Char.

CHAPTER 9

LOW

PRESSURE

ADSORPTION

CHAPTER 9

LOW PRESSURE ADSORPTION

9.1 Deviations from D-R Linearity

It can be seen from figures 7.10 & 7.17-7.20 that nearly all D-R plots exhibit positive deviations at low pressure (high ε), which appear to be least pronounced for carbons of HTT $\sim$ 1200 K.

If such deviations were due to a departure from a Rayleigh distribution of ε with V, then from previous arguments, one would expect a negative deviation for low and high HTT carbons, since the micropores filling in this region would either not be fully developed, or have closed off. In fact, the reverse of what would be expected is found.

A closer inspection of the plots shows that the adsorption at low pressure is similar for *all* carbons and that the deviations occur at similar positions (degree of filling $\theta = 0.02 \sim 0.03$) but are more discernable for D-R plots with steep gradients. The apparently wide range of linearity for 1200 K carbons is because the D-R gradient is at a minimum for this HTT, and so blends in with the smaller gradient of the low pressure region. The same can be said for activated carbons where the overall curvature of the plot also blends in with the deviation. Because of its universality this particular type of deviation appears to be independent of micropore structure .

A possible explanation is that the mechanism of adsorption differs from low to high pressure. The adsorption process implicit in the Dubinin theory assumes that micropores are empty until a particular value of

ε is reached, at which point the pores possessing that potential fill completely with liquid-like adsorbate. In reality, though, adsorbate molecules will be distributed amongst the whole adsorption space - albeit concentrated in the smallest pores. At low pressure there may be no pores of potential sufficient to compress the adsorbate to liquid, so that the adsorbate pressure will be somewhat less than P_o. At higher pressures the pores will be capable ofcompressing adsorbate to P_o and, as $\theta \to 1$, the empty adsorption volume will decrease, hence sequential filling of pores with liquid will become the predominant mechanism.

If the above argument is correct, then the adsorption potential at low pressures will be given by

$$\psi = RT \ln \frac{\bar{C}_a}{C_g} \qquad 9.1.$$

where $\bar{C}_a$ is the concentration of adsorbate within the adsorption space V_1 and C_g is the gas phase concentration.

For an ideal gas

$$C_g = P/RT \qquad 9.2$$

If V_1 is a fixed volume, the absorbate pressure will be proportional to the amount adsorbed (Henry's law), hence

$$P_a = P_o \theta \qquad 9.3$$

$$\Rightarrow \quad \bar{C}_a = \frac{P_o \theta}{RT} \qquad 9.4$$

where $\theta = V/V_1$ and is the degree of filling. Equation 9.1 thus becomes :

$$\psi = RT \ln \theta \frac{P_o}{P} = \varepsilon + RT \ln \theta \qquad 9.5$$

where ε is the Polanyi adsorption potential.

The value of V_1 will be less than V_o (the total adsorption space) since many of the larger pores have a negligible effect on low pressure adsorption. It will also be greater than the volume of pores which are first to fill completely, as partial filling of larger pores is inevitable.

Figure 9.1 shows a D-R plot for a 1470 K carbon (HTt = 10 mins., unactivated), where the low pressure region has been plotted against ψ as defined by Equation 9.5. The value of V_1 has been taken as the volume filled by the point of deviation. The fit is good until the very low pressure region is encountered, where over-compensation occurs. The very low pressure points can, in fact, be brought into line if a smaller value of V_1 is used to calculate their values of θ. This may suggest that V_1 is not constant as θ decreases (i.e. Henry's law is not fully obeyed) but that a series of subvolumes are being filled.

An alternative view of low pressure adsorption is that localised, specific site, interaction may be occurring. It was previously mentioned that positive deviations from linear D-R plots (e.g. Marsh and Rand type B deviations) could be corrected by use of the Dubinin-Astakhov equation, where $n < 2$. When $n = 1$ (e.g. for type B structures - equation 4.9) the D-A equation is merely another form of Freundlich's

equation, since

$$V = V_o \exp(-k\varepsilon) = V_o \exp\{-kRT \ln(P_o/P)\}$$
$$= V_o (P/P_o)^{kRT}$$
$$= CP^{1/n} \quad \text{- Freundlich's equation 9.6}$$

n is a constant dependent on temperature.

It can further be shown[207,208] that Freundlich's equation is a special case of Langmuir's equation where a distribution of sites exist such that the heat of adsorption decreases logarithmically with surface coverage. If localised adsorption were to be occurring in the low pressure region, then the data should be linearized by application of the D-A equation with n = 1. Figure 9.2 shows the data from Figure 9.1 plotted in this form. The slight curvature at high pressure is to be expected as n should be 2 for this region. The low pressure data points are, however, linearized to some extent.

If localised adsorption were to be the predominant effect at low pressure then the definition of θ, used to derive equation 9.5, should be changed from "degree of filling of a volume of micropore space" to "fraction of occupation of a given distribution of adsorption sites". The failure of equation 9.5 to linearize low pressure data may then be seen as due to the assumption of a homogeneous range of sites, whereas considerable heterogeneity exists - as implied by the variation of V_1 with θ. The importance of localised adsorption at low pressures has also been stressed by Dovaston et al[209] to explain positive values for the differential entropy of adsorption, at low pressures. The separation of adsorption into specific site interaction + micropore

filling has been proposed as the mechanism for adsorption on some zeolites[210,211]. In this case adsorption in the low filling region occurs on active centres by electrostatic interactions. Once the active centres are blocked the free adsorption space is filled by interaction of dispersion forces. Where forces other than dispersion exist the Polanyi postulates may be expected to fail. The characteristic curves for polar molecules on carbons are frequently found to be temperature dependent[212] which suggests dipole-induced dipole interactions. That a different adsorption mechanism is present for adsorption on planar surfaces has been suggested by Zukal[224] since his characteristic curves for C_6H_6 on graphitized (non-porous) carbon blacks varied with temperature. These deductions must, however, be open to dispute since, when the different adsorption temperatures vary markedly, one is not always sure that the density of the adsorbed phase varies as that for the bulk liquid. This is specially true if the adsorbed phase resembles a two dimensional gas with different partition functions to the liquid. In addition, as one approaches T_c the liquid density changes considerably, which means that the *volume* adsorbed, before complete saturation of adsorption forces occurs, also increases. This is due to the lower "shielding" effect of a less dense adsorbate. For example, the volume of an empty adsorption space encompassed by $\varepsilon = 0$ is greater than the volume occupied by adsorbate at $P/P_o = 1$, because the dispersion forces, emanating from the solid, will be reduced by the presence of adsorbed molecules. This effect will be of most importance for non-porous solids at temperatures close to T_c but is of less importance for microporous solids where most of the adsorption space is contained within micropores - which all fill completely at $P/P_o = 1$.

9.2 Low Pressure Hysteresis

Micropore filling is essentially a reversible process and should not exhibit any hysteresis on desorption. When samples were evacuated from their highest pressure they would lose about 90% of adsorbate within $\sim$ 10 minutes and the majority of the remainder within $\sim$ 4 hours. However, a small amount, corresponding to about 2% of V_o, remained even after pumping at pressures below 10^{-4} Torr for 3 days. If the sample was heated to $\sim$ 470 K, the residue could be removed within 30 minutes. Interestingly, the amount retained was frequently found to correspond to the point of deviation of the D-R plot (see figure9.1).

Adsorption frequently results in dimensional changes[213-215]. It has been suggested that this can result in sufficient stress to cause microfracture[216] or elastic deformation[217], which may close off pores and so trap molecules. Bailey et al[218] consider the phenomenon as due to a perturbation of the adsorbent's chemical potential which results in a stress-strain type of hysteresis.

At low pressures the interaction between adsorbate and adsorbent will predominate since the admolecules are widely spaced. Mutual (or lateral) interactions will only become more important at higher pressures. One may therefore propose that at low pressure adsorption will occur at specific high energy sites, where a considerable relaxation of the solid's surface "tension" will occur. Following the arguments of Bailey et al, such relaxation will perturb the surface so as to cause a further stabilisation of the admolecule/surface complex. This process is shown schematically in figure 9.3 and would effectively trap molecules on the surface since the

potential energy barrier over which admolecules must pass, to be desorbed, is now much greater. Since the adsorption in this region increases progressively with P/P_o there must exist a range of sites (or homotattic areas) which perturb at progressively higher concentrations of adsorbed molecules. These sites may be related to areas of stress, frozen in from the carbonization stage. Thermal annealing will allow the structural perturbation to be relieved, as well as affording the extra kinetic energy necessary for desorption.

The large amount of low pressure hysteresis found by McEnaney[216] for CCl_4 on 3000 K cellulose carbon suggests this mechanism in preference to one of pores being opened and closed by swelling, since this system would be predominantly of monolayer and multilayer adsorption, the CCl_4 molecule generally being inaccessible to micropores. The difference in amount retained by 1170 and 3000 K carbons (the latter being less) may reflect the less stressed structure after heat-treatment to 3000 K.

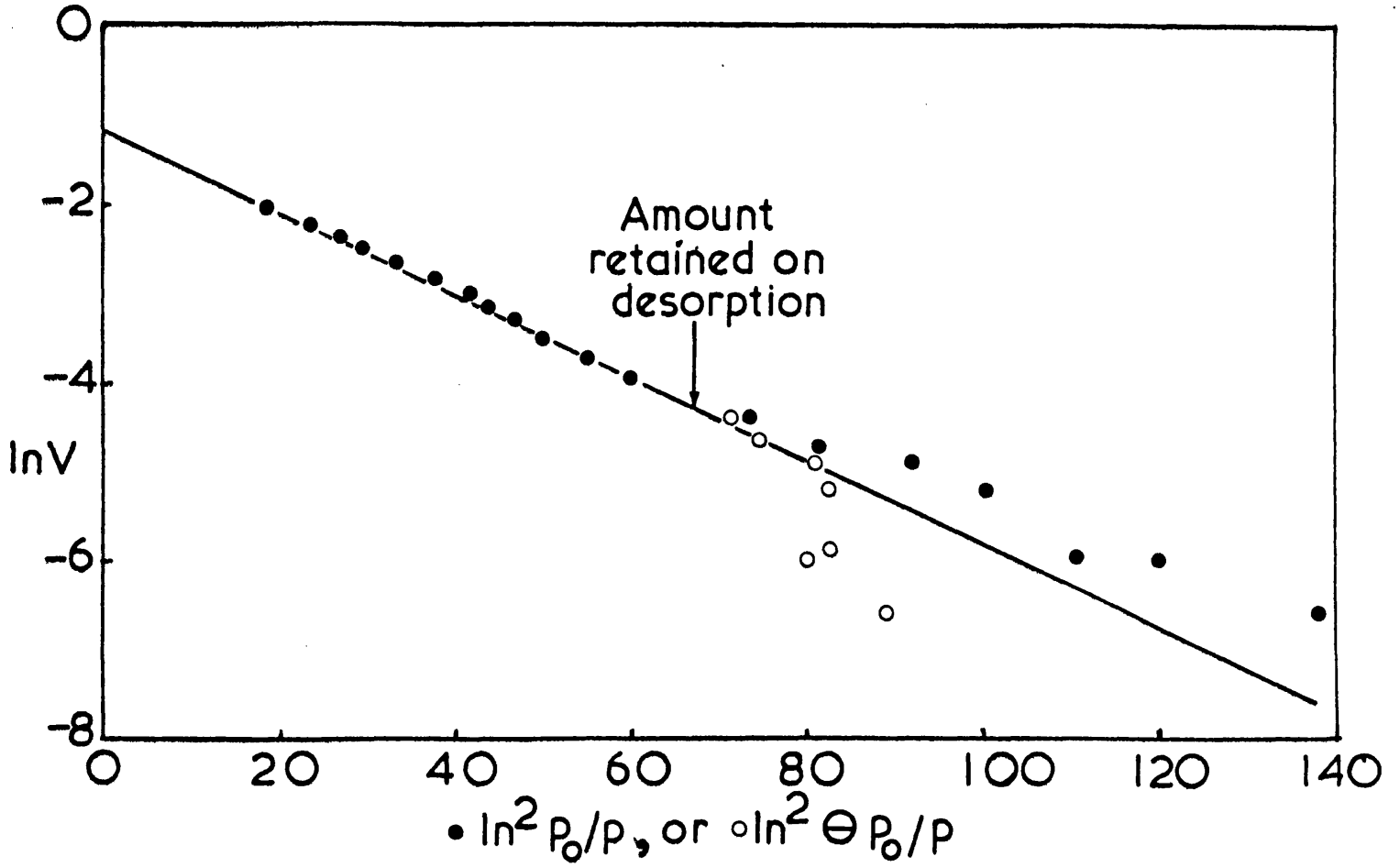

Fig. 9.1 Effect of using ψ to linearize low pressure points.
CO_2 / 295 K, H.T.T. = 1470 K, H.T.t. = 10 mins.

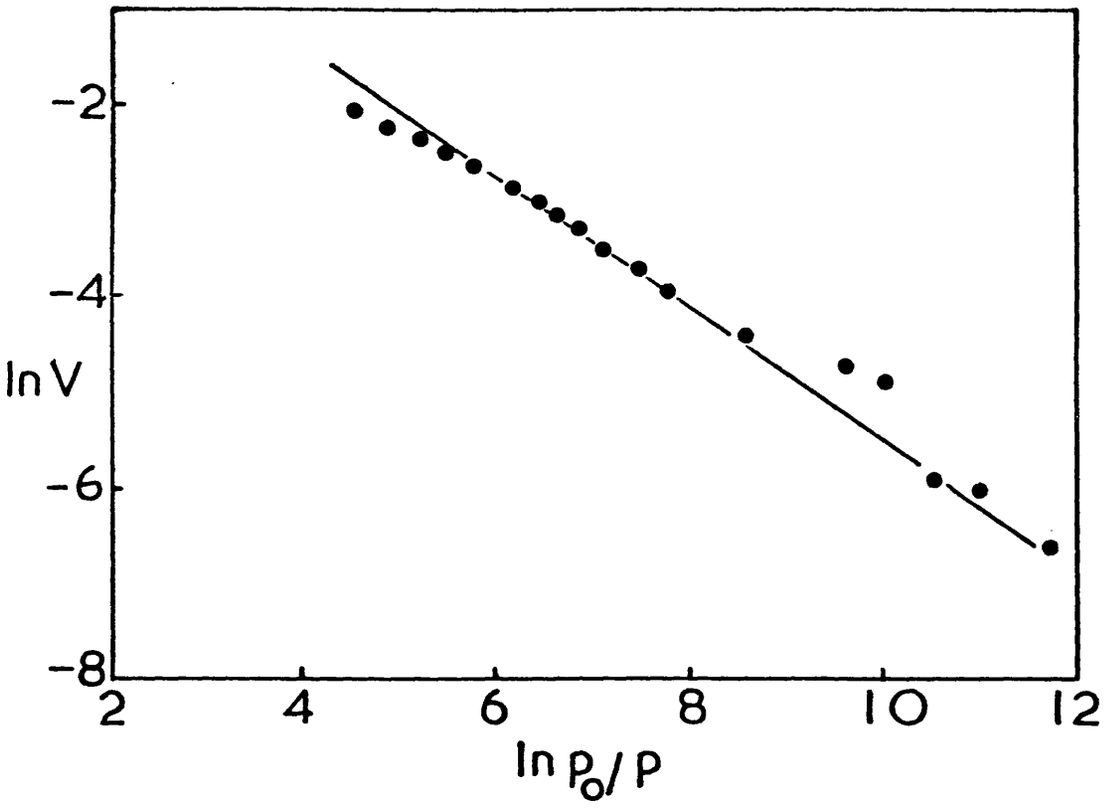

· Fig.9.2 Use of Freundlich type equation to linearize low pressure points. CO_2/295 K, HTT=1470K, HTt=10 mins.

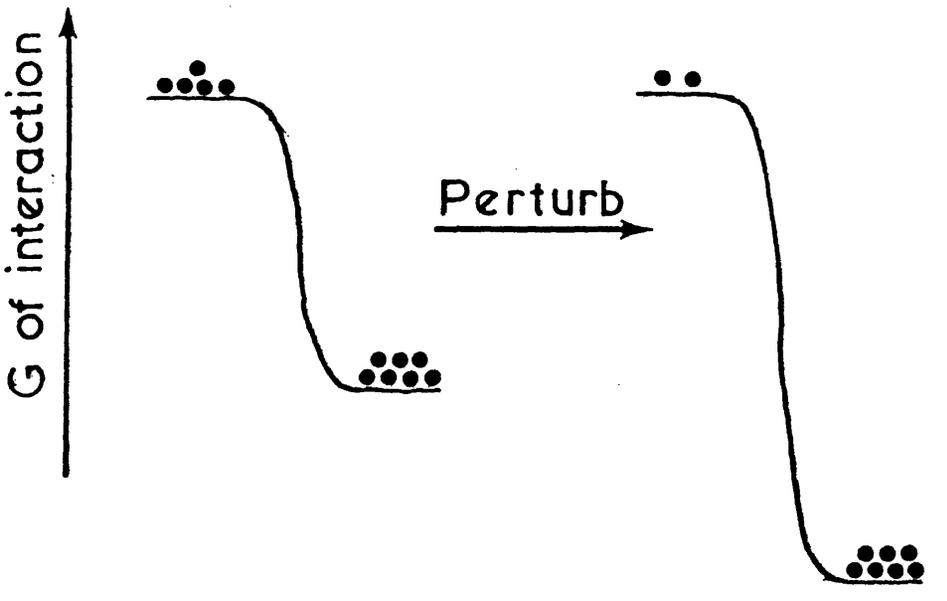

Fig.9.3, Effect of structural perturbation on thermodynamic stability of adsorbate/ adsorbent system.

CHAPTER 10

GENERAL DISCUSSION ON THE EFFECTS OF HEAT-TREATMENT

CHAPTER 10

General Discussion on the Effects of Heat-Treatment

The aim of this discussion is to draw together the findings from the previous sections, so as to understand the structural evolution of hard carbons.

From carbonisation temperatures to ~1470 K the principal effects are due to the loss of considerable amounts of hydrogen and oxygen. This results in the formation of condensed aromatic lamellae*. Although bulk shrinkage occurs (~ 30%), considerable voidage is created within the structure - resulting in an increased micropore volume. The similar increase in ε_{max} suggests these pores are very small, probably because they are the gaps between, and within, small aromatic groupings. The electron density map of this carbon is one of very short range order, hence the correlation distance is short. The x-rays scattered at small angles have a strong component due to density fluctuations within the matrix (i.e. large b_2). The maximum in ε_{max} corresponds to a maximum in b_2, which suggests the pores are little more than density fluctuations within a disordered matrix. In this context the word "matrix" tends to lose its meaning since, below 1270 K, no real distinction can

* A distinction is made between aromatic lamellae and layer-planes so as to emphasise the latter's larger size and disposition to stacking in turbostratic array (see page 139).

be drawn between a pore and its surrounding medium - as borne out by the lack of "ideal" Porod scattering (b_1). This view agrees with the lattice fringe images which show the lamallae to be short with no extensive layer-plane network.

As aromatic lamellae are formed there is a simultaneous coalescence to form crude layer-planes. This ordering is seen to increase the correlation distance by a process of producing regions of uniform electron density i.e. larger volumes of uniform matrix and pore, hence b_1 increases as b_2 decreases. Whilst the layer-planes overlap in certain regions, no change is found in the mean crystallite parameters until >1570 K - which coincides with the cessation of hydrogen evolution. Biscoe and Warren[48] also noted a lack of growth for L_a, before virtually all the hydrogen had gone. They reasoned that hydrogen was concentrated at lamellae edges so that its removal was necessary for contiguous planes to coalesce. A similar process of coalescence was invoked by Berkowitz and Den Hertog[171] to explain the low activation energy for hydrogen evolution (2 - 4 kJ mol^{-1}). Their view was slightly different in that the ordering process was controlled by the mobility of lamellae, and hydrogen could only be evolved as a result of a bimolecular reaction between two favourably oriented lamellae. The structural significance of hydrogen was also implied by the hydrogen evolution study, (Chapter 6), where the carbon atoms, previously attached to hydrogen, seem to undergo re-arrangement upon hydrogen loss. The last remaining hydrogen must be concentrated so as to prevent ordering of layers. It would seem, therefore, that up to ~1570 K, formation and ordering within layer-planes are the principal effects and that the dis-

order is stabilised by hydrogen. The commonly found correlation between large interlayer spacings and small crystallite sizes[44,219,220] (L_a and L_c) must reflect the difficulty of stacking when layer-planes are small, defective, and possessing considerable hydrogen.

For HTT >1570 K the evolution of residual hydrogen causes an increased rate of layer stacking with a consequent increase in L_c and decrease in d_{002}. These changes must result in the collapse together of parallel layer-planes. In the same HTT region the closure of micropores occurs, so it may be proposed that much of the access to the micropore structure is *via* the spaces between parallel layer-planes viz. ultramicropores. Such a view is consistent with the preferred sorption of flat molecules[95-98]. It has been demonstrated, by correlating XRD with direct observation of lattice fringe images[86, 201], that the d_{002} value is only the mean of a distribution of inter-layer spacings, which is heavily biased towards the smaller values (i.e. within crystallites). The reduction in d_{002}, after 1570 K, therefore signifies a reduction in spacing for many parallel regions, which were sufficiently wide to allow passage of adsorbate molecules (albeit by activated diffusion). The general closing together of parallel layer-planes will cause many to assume a turbostratic spacing and so become closed to adsorbate molecules. Such pore closure is irreversible, even if occurring at low HTT, and cannot be reversed by activation (in contrast to other workers' views[4]).

The criterion for collapse of layer-planes is that they are parallel, but as the angle between planes increase, so the energy required to stack them will increase. For acutely curved planes the energy may be prohibitively large so that pores enclosed by these will be retained. Although figure 7.9 shows orientated layer-planes, one may visualise that for an isotropic structure, the collapse of parallel regions (u) will not cause shrinkage, so much as an increase in volume for the misaligned regions (s).

The decrease in ε_{max} during pore closure must be due to a combination of the loss of fine micropores (u) and an increase in size of larger ones (s). The loss of fine pores would be expected to reach completion by ~1800 K but the correlation distance is increasing more rapidly at this temperature and continues, even to 2500 K. The pores in these carbons are predominantly bounded by stacks of layer-planes and so increases in a must be due less to annealing of short range defects and more to an increasing order of stacking. Further evidence comes from the similarity in growth of L_c and a - both accelerate on cessation of hydrogen evolution and have a similar trend beyond 1800 K. Both pore[174] and crystallite sizes[162] are known to increase up to 3000 K so it is plausible that the pore coarsening effect seen in this temperature range is related to a packing together of layer-planes which deviate considerably from parallelism. Lattice fringe images of PVDC carbons[86] in this HTT range show that considerable growth in layer-plane length, stacking and linearity occurs. The two structural models derived by these authors for carbons of HTT 2223 and 2973 K are shown in

Figure 10.1 , and show how the increase in pore size must involve considerable re-arrangement of whole layer-planes. The mechanism of these changes might loosely be termed "graphitization". Such a process would involve migration of residual vacancies, or even atomic diffusion, and may well be the cause of structural perfection *within layers*. However, these processes would not cause the apparent movement of whole layer-planes to form larger stacks. An attractive possibility for this is localised fracture of constricted layer-planes due to their strong anisotropic thermal expansion. Such fracture would afford more mobility to planes - allowing stress concentrations, kinks and bends to become annealed out. The tangled structure would still prevent a complete three dimensional ordering. This effect may be likened to Mrozowski cracking in graphites but whereas Mrozowski cracks are aligned due to the anisotropic nature of graphite, the equivalent fracture in isotropic carbon will only occur at particularly restricted ("knotted") regions - hence the resultant aid to structural perfection. Calculations[221] have shown that sufficient stress is available, from this effect, to cause fracture with Griffith crack lengths of ~1.0 nm i.e. of the order of extent of the micropores. Localised re-arrangement caused by localised stress may be analogous to the larger scale graphitization which occurs at points of contact between particles of hard carbon, when subjected to heat-treatment under pressure[222].

Suggestions for Further Work

Since pore closure seems to be a microstructural effect, caused by a stacking of layer planes, there should be no effect of heat-treatment on mesopores - as appears to be the case. It would be of interest to investigate the means whereby small mesopores could

be introduced into a carbon - which were small enough to exhibit a high adsorbing area but large enough to be free from layer-plane ordering effects. Such work might involve heat-treating an activated series to different temperatures to find the relationship between HTT and size of pore which closes. It would also be advantageous to examine the effect of activating carbons of low carbonisation temperature - or even activating during carbonisation, in an attempt to produce the smallest possible pores, prior to heat-treatment.

The high temperature transformations are also of considerable interest and remain open to speculation. A SAXS analysis of carbons heated to ~3000 K (isochronally and isothermally) would be useful - especially to see what contribution to pore growth is achieved by the annealing of electron density fluctuations. The potentialities of HREM in this type of study cannot be over-emphasised especially when used quantitatively with gold evaporated onto the support film as a lattice standard. The application of HREM to studying the mechanism of stress graphitization of hard carbons might also be a rewarding field.

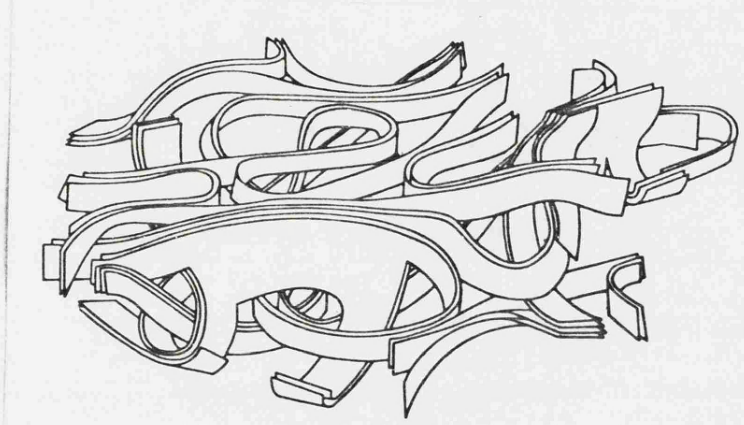

HTT 2223 K

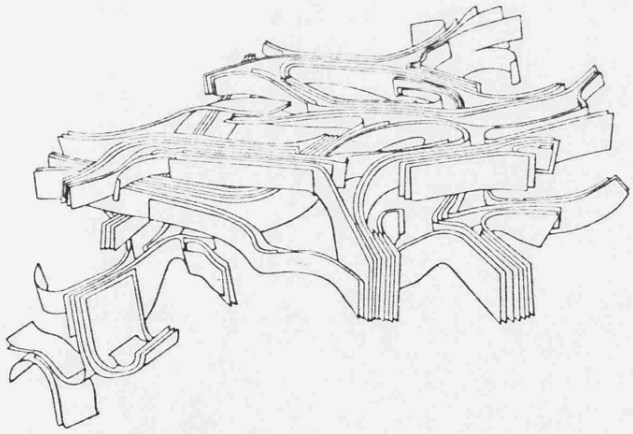

HTT 2973 K

Fig. 10.1 Structural Evolution of PVDC from 2223 K to 2973 K, from Ban et al (ref. 86)

APPENDICES

APPENDIX A

Preparation of Carbons

"The daintiest of distinguished learners,
His face is like a charcoal burner's
From nose to ears all black and deadened;
His eyes from blowing flames are reddened"

Faust (Goethe) 6677-6680

A(1)

Cellulose powder (Whatman's Chromedia 11, 98% α form) was compressed in a ½ inch diameter die under 500 MPa pressure for one minute, to form pellets. The effect of pelleting is supposed to be of secondary importance in the carbonisation reactions[223].

The pellets were carbonised by heating in a tube furnace under flowing nitrogen (Air Products, high purity) which had passed through 3 A molecular sieves. The temperature was increased at a linear rate of 3.5 K min^{-1} until 1173 K - at which point a relay switched off power and allowed the sample to cool naturally, whilst still under nitrogen. The heating rate was controlled by a Eurotherm 121 linear temperature programmer linked to a Eurotherm temperature controller.

The resultant carbon yield as 21.3 ± 0.5%. The pellets shrunk by ∿35% parallel to the axis of compression and ∿30% perpendicular to the compression axis. The apparatus is shown in figure A(1), page 199.

A(2) Activation of Carbon

The activation furnace (to the left of photograph) was a vertical tube furnace with gas inlet at its base. Samples (in the form of whole pellets) were held in a nickel foil tube which had a base made of three crossed wires. This allowed oxidant gas to pass up the holder and so avoid stagnation. The tube was suspended into the furnace to be level with a thermocouple - this showing no temperature difference from a thermocouple within the sample holder. The furnace was heated by the same controller as the carbonisation furnace.

The activation procedure was to heat the furnace to operating temperature (usually 1170 K but some low activations were done at 1120 K) and thoroughly flush through with CO_2. The samples were then quickly lowered into the furnace and a split plate replaced around the suspension wire. After a suitable time the gas was switched over to nitrogen and the power switched off. To enable rapid cooling the sample tube was raised to the top of the furnace - which was cooler. After a few minutes the samples could be removed, but this was done with a stream of nitrogen directed at them. When cool to touch, the samples were transferred to a glass phial and quickly weighed. The activation rate at 1170 K was about 7% for the first hour, reducing to about 5% per hour at higher burn-offs.

A(3) Heat-treatment

The heat-treatment apparatus is shown in figures 6.1 and 6.2. . It consisted of a graphite susceptor held vertically inside a water cooled pyrex tube. Sample(s) were placed inside the susceptor and heated by a Radyne C240B R.F. generator. Temperatures were measured by

viewing the top surface of the sample with a Foster Cambridge optical pyrometer. The pyrometer was calibrated by sighting a thermocouple placed in a high temperature resistance furnace. Corrections were made to the high temperature scale, which was found to overestimate by 100 - 200 K. Temperatures were estimated as accurate to $\pm$5K up to 1720 K and $\pm$ 20 K for higher temperatures. No problems were encountered with R.F. discharges when operating at atmospheric pressure.

Prior to heat-treatment all specimens were evacuated to $\sim$0.01 Torr to remove occluded air. This is important since flushing with inert gas may not remove air within pores and this can lead to partial activation on heating. The heat treatments were carried out under flowing argon which had been dried by passage through silica gel and molecular sieves. The whole gas line was evacuated prior to use.

A(4) Isochronal Heat-Treatments

The heating schedule for isochronal treatments was to raise the temperature gradually over 5 mins., hold at temperature for 10 mins., then reduce power over 5 mins. The samples then cooled under argon.

A(5) Isothermal Heat-Treatments

Isothermal heat-treatments required fast heating rates thus a "dummy" pellet was used to obtain the correct power setting for the particular temperature, and this setting was retained whilst the R.F. power was switched off (the generator remained on standby). The isothermal sample was then heated by switching on the R.F. power at that setting and starting a stopwatch when the required temperature was

reached (this was reproducible and free from "overshoot"). After the allotted time the R.F. power was switched off. This resulted in temperatures being reached within 2 - 3 mins - irrespective of final temperature - and initial cooling rates of about 1000 K min^{-1}, reducing exponentially.

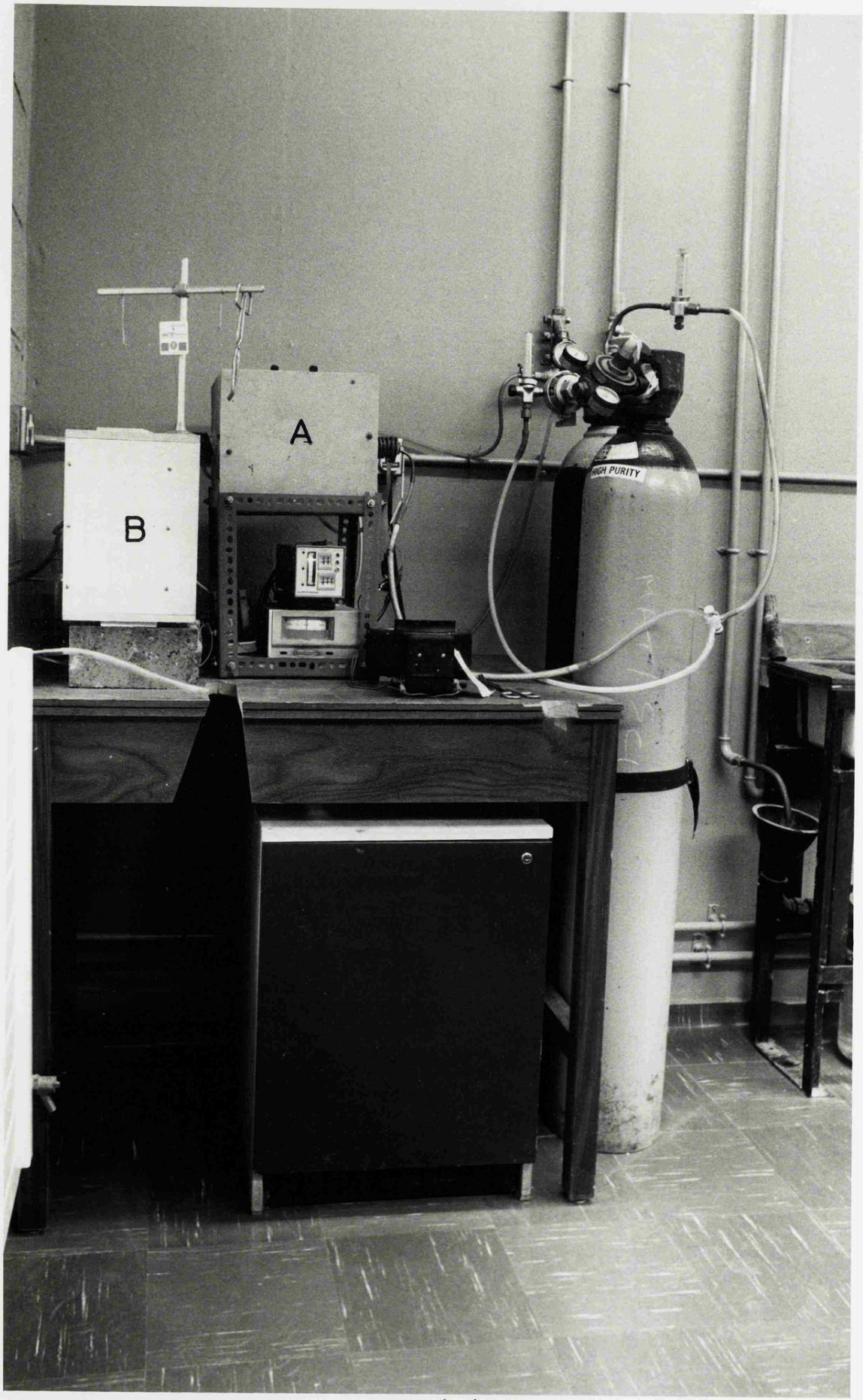

Fig. A1 Carbonisation (A) & Activation (B) furnaces.

APPENDIX B

X-Ray Correction Factors for Carbon/CuKα

$$y = \frac{I_{inc}}{R}\left(\frac{1 + \cos^2 2\theta}{2}\right) \qquad X = \frac{f^2 \sin^2\theta\cos\theta}{1 + \cos^2 2\theta}$$

(λ in Å)

$2\theta^o$	y	X x 10^3	$2\theta^o$	y	X x 10^3
9	0.40	0.094	23	1.40	0.968
10	0.47	0.118	24	1.47	1.097
11	0.53	0.146	25	1.54	1.244
12	0.59	0.178	26	1.61	1.40
13	0.65	0.215	27	1.67	1.59
14	0.72	0.256	28	1.73	1.77
15	0.78	0.303	29	1.78	1.99
16	0.85	0.357	30	1.84	2.23
17	0.92	0.419	31	1.87	2.48
18	1.00	0.483	32	1.93	2.79
19	1.08	0.563	33	1.97	3.11
20	1.16	0.645	34	2.02	3.46
21	1.24	0.746	35	2.05	3.85
22	1.32	0.851	36	2.09	4.29

APPENDIX C

Location of pivot point for D-R plots

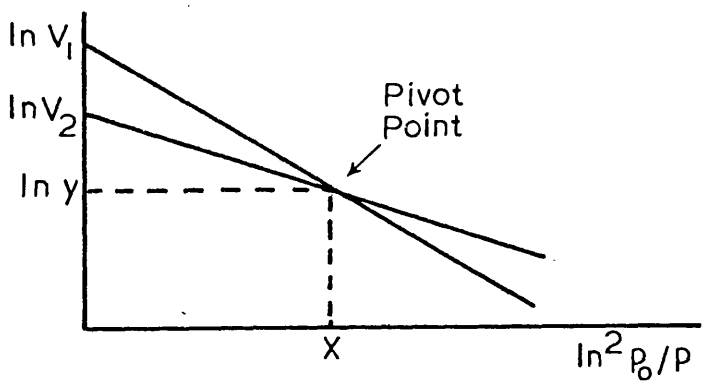

The gradients of the two D-R plots are given by

$$\frac{\ln y - \ln V_1}{x} = m_1$$

$$\frac{\ln y - \ln V_2}{x} = m_2$$

subtracting,

$$\frac{\ln V_2 - \ln V_1}{x} = m_1 - m_2$$

$$\therefore \quad x = \frac{\ln V_2 - \ln V_1}{m_1 - m_2}$$

then $\ln y = \ln V_1 + x m_1$

(or $\ln y = \ln V_2 + x m_2$)

REFERENCES

1. N.T. de Saussure, Gilbert's Ann., 47, 113, (1814).
2. P.L. Walker, T.G. Lamond and J.E. Metcalfe, 2nd Conf. on Industrial Carbon and Graphite, SCI, London p.7 (1966).
3. P.L. Walker, L.G. Austin and S.P. Nandi, Chem. and Phys. of Carbon, 2, p.257, Edward Arnold, London, (1967).
4. B. McEnaney and N.G. Dovaston, Carbon, 13, 515 (1975).
5. H.C. Howard and G.A. Hulett, J. Phys. Chem., 28, 1082, (1924).
6. W.F.K. Wynne-Jones, "Structure and Properties of Porous Materials", 10th Colston Symp. p.35, Butterworths, 1958.
7. J.J. Kipling, J.N. Sherwood, P.V. Shooter, N.R. Thomson, Carbon, 1, 315, (1964).
8. E. Greenhalgh, B.J. Miles, E. Redman, and S.A. Sharman ref.2, p.405.
9. Y. Toda, N. Yuki, S. Toyoda, Carbon 10,13, (1972).
10. K. Lonsdale, Am. Min., 56, 333, (1971).
11. F.P. Bundy and J.S. Kasper, J. Chem. Phys., 46, 3437, (1967).
12. V.R. Howes, Proc. Phys. Soc., 80(3), 648, (1962).
13. A.W. Hull, Phys. Rev., 20, 113, (1922).
14. O. Hassel and H. Mark, Z. Phys., 25, 317 (1924).
15. J.D. Bernal, Proc. Roy. Soc. (Lond.), A106, 749, (1924).
16. P. Debye and P. Scherrer, Phys. Z., 18, 291, (1917)
17. H. Lipson and A.R. Stokes, Proc. Roy. Soc. (Lond.), A181, 101, (1942).
18. H.P. Rooksby and E.G. Steward, Nature, 159, 638, (1947).
19. A. Kochanovska, Czech. J. Phys., 19, 383 (1951)
20. J. Hoerni and J. Weigle, Nature, 104, 1088, (1949).
21. J.S. Lukesh, Phys. Rev., 80, 226, (1950); 84, 1068, (1951)

22. J.S. Lukesh and L. Pauling, Amer. Min., 35, 125, (1950).

23. L. Pauling, Proc. Nat. Acad. Sci. U.S., 56, 1646, (1966).

24. R.W. Lynch and H.G. Drickamer, J. Chem. Phys., 44, 181, (1966).

25. S. Ergun, Nature, 241, 65, (1973).

26. J. Donohue, Nature, 255, 172, (1975).

27. H.G. Drickamer, Science, 156, 1183, (1967).

28. P. Trucano and R. Chen, Nature, 258, 136, (1975).

29. R. Chen and P. Trucano, Acta Cryst., A33, 823, (1977).

30. A. El. Goresy and G. Donnay, Science, 161, 363, (1968).

31. A.G.Whittaker, Carbon, 17, 21, (1979).

32. A.G. Whittaker and P.L. Kinter, Science, 165, 589, (1969).

33. J.R. Fryer, Pre-Prints of "Carbon '76", Deutsche Keramische Gesellschaft, Baden-Baden, p.22, (1976).

34. A.G. Whittaker and G.M. Wolker, Science, 178, 54, (1972).

35. A.G. Whittaker, Science, 200, 763, (1978).

36. V.I. Kasatochkin, V.V. Saoransky, B.N. Smirnov and V.M. Melnichenko, Dokl. Akad. Nauk. SSSR., 217, 796, (1974).

37. A.M. Stadkov and Yu. P. Koudrayatsev, Priroda, 5, 37, (1969).

38. V.I. Kasatochkin *et al*, Carbon, 11, 70, (1973).

39. M. Nakamizo and R. Kammereck, Abstracts of 11th U.S. Conf. on Carbon, Gatlinburg, Tenn. p.187, (1973).

40. M. Seal, Nature, 185, 522, (1960).

41. A.G. Whittaker, Abst. of 12th U.S. Conf. on Carbon, Pittsburgh, p.43, (1975).

42. R.E. Franklin, Proc. Roy. Soc. (Lond.), A209, 196, (1951).

43. B.P. Richards, J. Appl. Cryst. 1, 35, (1968).

44. S.J. Mitchell and C.R. Thomas, Carbon, 9, 253, (1971).

45. B.E. Warren, J. Chem. Phys., 2, 551, (1934).

46. U. Hoffman and D. Wilm, Z. Electrochem., 42, 504, (1936).

47. B.E. Warren, Phys. Rev., 59, 693, (1941).

48. J. Biscoe and B.E. Warren, J. Appl. Phys. 13, 364, (1942).

49. J.C. Bokros, Chem. and Phys. of Carbon 5, p.10, (1969).

50. J. Gibson, M. Holohan, H.L. Riley, J. Chem. Soc., 456, (1946).

51. H.L. Riley, Quart. Revs., 1, 59, (1947).

52. R.E. Franklin, Acta Cryst., 3, 107, (1950).

53. P.B. Hirsch, Proc. Roy. Soc. (Lond.), A226, 143, (1954).

54. R. Diamond, Acta Cryst. 11, 129, (1958).

55. R. Diamond, Phil. Trans. Roy. Soc. A252, 193, (1960).

56. S. Ergun and V.H. Tiensuu, Acta Cryst. 12, 1050, (1959).

57. W. Ruland, Chem. and Phys. of Carbon, 4, 72, (1968).

58. G.M. Jenkins and K. Kawamura, "Polymeric Carbons", p.197, Cambridge Univ. Press, (1976).

59. T. Noda and M. Inagaki, Bull. Chem. Soc., Japan, 37, 1534, (1964).

60. K. Furukawa, Nihon Kessho Gekkai Shi, 6, 101, (1964).

61. J. Kakinoki, Acta Cryst., 18, 578, (1965).

62. T. Noda, M. Inagaki and S. Yamada, Bull. Chem. Soc. Japan, 41 (12), 3024, (1968).

63. A.A. Khomenko, Yu. E. Sminov, V.P. Sosedov and V.I. Kasatochkin, Dokl. Akad. Nauk. SSSR, 206(5), 1112; Trans: Soviet Physics Doklady 17 (10), 956, (1973).

64. F.M. Wachi and D.E. Gilmartin, Carbon, 8, 141, (1970).

65. H.P. Klug and L.E. Alexander, "X-ray Diffraction Procedures 2nd Ed.", p.791, Wiley, New York, (1974).

66. J.R. Townsend and S. Ergun, Carbon, 6, 19, (1968).

67. R. Lovell, G.R. Mitchell, A.H. Windle, Acta Cryst. A35, 598, (1979).

68. G.D. Wignall and C.J. Pings, Carbon, 12, 51, (1974).

69. D.F.R. Mildner and J.M. Carpenter, 4th London Conf. on Carbon and Graphite, SCI, p.558, (1974).

70. R.R. Saxena and R.H. Bragg, Carbon, 12, 210, (1974).

71. A.A. McFarlane, Carbon, 11, 73, (1973).

72. F.R. McFeely *et al*, Phys. Rev. B. 9(12), 5268, (1974).

73. R. Diamond and P.B. Hirsch, 1st London Conf. on Carbon and Graphite, SCI, p.197, (1958).

74. J. Maire and J. Mering, Ibid, p.204.

75. S. Ergun, Phys. Rev. B1, 3371, (1970).

76. S. Ergun and R.R. Schehl, Carbon, 11, 127, (1973).

77. S. Ergun, Carbon, 11, 221, (1973).

78. W. Braun and E. Fitzer, Carbon, 16, 81, (1978)

79. F. Rousseaux and D. Tchoubar, Carbon, 15, 55, 63, (1977).

80. Y. Takahashi and E.F. Westrum Jr., J. Chem. Thermo., 2(6), 847, (1970).

81. M.K. Halpin and G.M. Jenkins, Nature, 218, 950, (1968).

82. G.M. Jenkins, K.Kawamura and L.L. Ban, Proc. Roy. Soc. (Lond.), A327, 501, (1972).

83. A. Fourdeux, R. Perret and W. Ruland, 10th U.S. Conf. on Carbon, Lehigh, Bethlehem, Paper FC-22, (1971).

84. A. Oberlin, F. Molleyre, M. Bastick, 13th U.S. Conf. on Carbon, p.371, (1977).

85. A. Oberlin, Carbon, 17, 7, (1979).

86. L.L. Ban, D. Crawford, H. Marsh, J. Appl. Cryst., 8, 415, (1975).

87. S. Ergun, Carbon, 6, 141, (1968).

88. E. Fitzer, K. Muller, W. Schafer, Chem. and Phys. of Carbon, 7, 237, (1971).

89. H. Marsh, 4th London Conf. on Carbon and Graphite, p.2, (1974).

90. B.T. Kelly, UKAEA, Springfields, Personal Communication.

91. M.M. Dubinin, Chem. and Phys. of Carbon, 2, 51, (1966).

92. D.H. Everett (Chairman), Pure and Applied Chem., 31 (4), p.585, (1972).

93. M.M. Dubinin, J. Colloid and Int. Sci., 46, 351., (1974).

94. D.H. Everett and J.C. Powl, J. Chem. Soc., Faraday I, 619, (1976).

95. W.F. Wolff, J. Phys. Chem. 62, 829, (1958).

96. J.J. Kipling and R.B. Wilson, Trans. Faraday Soc., 56, 562, (1960).

97. J.R. Dacey and D.G. Thomas, Trans. Faraday Soc., 50, 740, (1954).

98. H.F. Stoeckli, Helv. Chim. Acta. 57, (Fasc. 7), 2192,(1974).

99. H. Marsh, Fuel, 44, 253, (1965).

100. H. Marsh, B. Rand, 3rd London Conf. on Carbon and Graphite, p.172.

101. Supplied by LKB Instruments Ltd., LKB House, 232 Addington Road, Selsdon, S. Croydon, Surrey, CR2 8YD.

102. Supplied by Electrothermal Engineering Ltd., 270 Neville Road, London E7.

103. Supplied by Still and Cameron, 66 Rugby Avenue, Wembley, HAO 3DJ, Tel. 01 902 9030.

104. V. Chipallatti and C.H. Giles, Nature, 165, 735, (1950).

105. Supplied by Techne (Cambridge) Ltd., Duxford, Cambridge.

106. R.M. Dell and V.J. Wheeler, UKAEA, Harwell Research Report, AERE R3424, (1960).

107. I. Langmuir, J.A.C.S., 40, 1361, (1918).

108. S. Brunauer, L.S. Deming, W.E. Deming, E. Teller, J.A.C.S., 62, 1723, (1940).

109. S. Brunauer, P.H. Emmett and E. Teller, J.A.C.S., 60, 309, (1938).

110. J.H. de Boer and J.F.H. Custers, Z. Phys. Chem. B.25, 225, (1934).

111. D.A. Cadenhead and D.H. Everett, Ref. 73, p.272.

112. T.G. Lamond and H. Marsh, Carbon, 1, 293, (1964).

113. C. Pierce, J.W. Wiley, R.N. Smith, J. Phys. Chem., 53, 669, (1949).

114. R.V. Culver, N.S. Heath, Trans. Faraday Soc., 51. 1564, (1955).

115. K.S.W. Sing, Chem. Ind. (Lond.) (Nov.), 1520, (1968).

116. C. Pierce, J. Phys. Chem., 72, 3673, (1968).

117. M.M. Dubinin, Prog. in Surface and Membrane Sci., 9, 68, Academic Press, (1975).

118. H. Marsh and B. Rand, J. Coll. Inst. Sci., 33 (3), 479, (1970).

119. H. Marsh and B. Rand, J. Colloid and Int. Sci., 40(1), 121, (1972).

120. R.S. Mikhail, S. Brunauer, E.E. Bodor, J. Coll. Int. Sci., 26, 45, (1968).

121. M. Polanyi, Verh. Deut. Phys. Ges., 18, 55, (1916).

122. L. Berenyi, Z. Phys. Chem., 94, 628, (1920).

123, K.M. Nikolayev and M.M.Dubinin, Izv. Akad. Nauk. SSSR. p.1165, (1958).

124. W.K. Lewis *et al*, Ind. Eng. Chem., 42, 1326, (1950).

125. V.G. Fastovsky and A.E. Rovinsky, Kislorod, 9, 14, (1952).

126. M.M. Dubinin, O. Kadlec, A. Zukal, Coll. Czech. Chem. Comm., 31, 406, (1966).

127. D.M. Newitt *et al*, "Thermodynamic Functions of Gases (ed. F.Din), 1, p.123, Butterworth, London, (1962).

128. H. Marsh and B. Rand, J. Coll. Int. Sci., 33(1), 101, (1970).

129. W. Weibull, J. Appl. Mech., 18, 293, (1951).

130. B. Rand, J. Coll. Inst. Sci., 56(2), 337, (1976).

131. H.F. Stoeckli, J. Coll. Inst. Sci., 59(1), 184, (1977).

132. P.P. Ewald, Proc. Phys. Soc., (Lond.), 52, 167, (1940).

133. P. Debye and A.M. Bueche, J. Appl. Phys. 20, 518, (1949).

134. G. Porod, Kolloid Z., 124(2), 83, (1951).

135. G. Porod, IBID, 125(1), 51, 108.

136. P. Debye, H.R. Anderson and H. Brumberger, J. Appl. Phys. 28(6), 679, (1957).

137. H. Kuroda, J. Colloid Sci., 12, 496, (1957).

138. V. Gerold, Small Angle X-ray Scattering, Ed. Brumberger, p.277, Gordon and Beach, N. York, (1967).

139. John Allen Williams, Ph.D. Thesis, "SAXS of Nucleation in Glass", Penn. State Univ., Chem. Eng., (1970).

140. D.J. Johnson and C.N. Tyson, J. Phys., D., Appl. Phys., 3, 526, (1970).

141. D.P. Riley, "X-ray Diffraction by Polycrystalline Materials", Eds. H.S. Peiser, H.P. Rooksby, A.J.C. Wilson, p.452, Chapman and Hall, (Lond.)., (1955).

142. A. Guinier and G. Fournet, "Small Angle Scattering of X-rays", Wiley, New York, (1955).

143. O. Kratky, G. Porod and Z. Skala, Acta Phys. Austriaca, 13, 76, (1960).

144. A. Guinier, Ann. Physik, 12, 161, (1939).

145. W.S. Rothwell, J. Appl. Phys., 39, 1840, (1968).

146. R. Hosemann, Kolloid Z., 117, 13, (1950).

147. C.G. Shull and L.G. Roess, J. Appl. Phys., 18, 295,, (1947).

148. M.H. Jellinek and I. Fankuchen, Ind. Eng., Chem., 37, 158, (1945).

149. P.B. Elkin, C.G. Shull, L.C. Roess, Ind. Eng. Chem., 37, 327, (1945).

150. R. Hosemann and S.N. Bagchi, "Direct Analysis of Diffraction by Matter", North Holland Pub. Co., Amsterdam, p.600, (1962).

151. C.G. Vonk, J. Appl. Cryst., 8, 340, (1975).

152. C.G. Vonk, IBID, 9, 433, (1976).

153. J.I. Wang, R.G. Jenkins and P.L. Walker, 14th U.S. Conf., Penn. State, p.125, (1979).

154. M.A. Short and P.L. Walker, Carbon, 1, 3, (1963).

155. S. Ergun, W. Braun and E. Fitzer, Rev. Sci. Inst., 41, 1133, (1970).

156 S. Ergun and M. Berman, IBID, 41, 870, (1970).

157. G. Breit, Phys. Rev., 27, 362, (1926).

158. D.T. Keating and G.H. Vineyard, Acta Cryst., 9, 895, (1956).

159. S. Ergun, Chem. and Phys. of Carbon, 3, 219, (1968).

160. "International Tables for X-ray Crystallography", III, p.250, The Kynoch Press, Birmingham, England, (1962).

161. D.J. Johnson,(Univ. of Leeds), Personal communication.

162. R.R. Saxena and R.H. Bragg, Carbon, 16, 373, (1978).

163. E.R. Pike, Acta Cryst., 12, 87, (1959).

164. E.R.Pike and J. Ladell, IBID, 14, 53, (1961).

165. A.J.C. Wilson, "Mathematical Theory of X-ray Diffractometry", Philips Tech. Library, p.63, (1963).

166. Ref. 160, p.202.

167. L.G. Henry and R.H. Bragg, Abstracts of 14th U.S. Conf., Penn. State Univ., p.129, (1979).

168. Ref. 65, p.637.

169. P. Scherrer, Nachr. Ges. Wiss. Gottingen, 96, (1918).

170. N.G. Dovaston, Ph.D. thesis, CNAA (Sunderland Poly), pp.69 and 93, (1972).

171. N. Berkowitz and W. Den Hertog, Fuel, XLI(6), 507,(1962).

172. V. Luzzati "X-ray Optics and Microanalysis", 3rd Int. Symp. (Stanford), Eds. Pattee, Cosslett and Engstrom, p.133, (1962).

173. R.G. Jenkins and P.L. Walker, Carbon, 14, 7, (1976).

174. S. Bose, R. Saxena and R.H. Bragg, 13th U.S. Conf. (Irvine), 369, (1977).

175. R. Perret and W. Ruland, J. Appl. Cryst. 1, 308, (1968).

176. R. Perret and W. Ruland, IBID, 5, 183, (1972).

177. W. Ruland, IBID, 4, 70, (1971).

178. C. Schiller et J. Mering, C.R. Acad. Sci., (Paris), 264(3), 247, (1967).

179. R. Perret and W. Ruland, J. Appl. Cryst., 2, 209, (1969).

180. Ref. 150, pp.64 and 605.

181. W. Ruland, Pre-Prints of 8th U.S. Conf. (Buffalo), paper 159, (1967).

182. D.H.T. Spencer, M.A. Hooker, A.C. Thomas and B. Napier, Proc. 3rd Conf. on Carbon and Graphite, p.467, SCI, (London), (1971).

183. J.W. Edington, "Interpretation of Transmission Electron Micrographs", Monographs in Practical E.M. in Mat. Sci., 3, p.75, Philips Tech. Library.

184. J.W. Menter, Proc. Roy. Soc., A236, 119, (1956).

185. R.D. Heidenreich, L.L. Ban and W.M. Hess, J. Appl. Cryst., 1, 1, (1968).

186. E.L. Evans, J.L. Jenkins and J.M. Thomas, Carbon, 10, 637, (1972).

187. D. Crawford and D.J. Johnson, J. Microscopy, 94, 51, (1971).

188. D. Crawford and H. Marsh, Fuel, 55, 251, (1976).

189. K.J. Hanzen, Adv. in Optical and Electron Microscopy, 4, 1, (1971).

190. W. Hoppe, Acta Cryst., A26, 414, (1970).

191. J.M. Cowley and S. Iijima, Z. Naturforsch, 27A, 445, (1972).

192. L.L. Ban, Surface and Defect Properties of Solids, Eds. Roberts and Thomas, Chem. Soc., 1, 54, (1972).

193. G.R. Millward and D.A. Jefferson, Chem. and Phys. of Carbon, 14, 1, (1978).

194. D. Crawford, Univ. of Capetown, S.A., Personal Communication.

195. W.V. Kotlensky and P.L. Walker, Proceedings of 4th U.S. Conf. (Buffalo), 423, (1959).

196. J.D. Watt and R.E. Franklin, 1st London Conf. on Carbon and Graphite, SCI, 321, (1958).

197. M.M. Dubinin, 4th Int. Symp. Reactivity of Solids, Elsevier, Amsterdam, 643.

198. J.C. Arnell and W.M. Barss, Can. J. Res. 26A, 236, (1946).

199. A. Voet, J.B. Donnet, P.A. Marsh and J. Shultz, Carbon, 4, 155, (1966).

200. J.B. Donnet, J. Shultz and A. Eckhardt, Carbon, 6, 781, (1969).

201. P.A. Marsh, A. Voet, T.J. Mullens and L.D. Price, Rubber Chem. and Tech. 43(2), 470, (1970).

202. G.A. Robins, M.Sc. Thesis, Bath, (1974).

203. F.W. Jones, Proc. Roy. Soc., A166, 16, (1938); also ref.65, p.637.

204. D. Crawford and H. Marsh, "Developments in Electron Microscopy and Analysis", Ed. J.A. Venables, Academic Press, p.279, (1976).

205. J.R. Fryer, "Characterisation of Porous Solids", Eds. Gregg, Sing and Stoeckli, pub. SCI (London), p.41, (1979).

206. Ref. 150, p.302.

207. G. Halsey and H.S. Taylor, J. Chem. Phys., 15, 624, (1947).

208. M. Smisek and S. Cerny, "Active Carbon", Elsevier Pub. Co., Amsterdam, p.96, (1970).

209. N.G. Dovaston, B. McEnaney and C.J. Weedon, Carbon, 10. 277, (1972).

210. V.A. Astakhov and M.M. Dubinin, Izv. Akad. Nauk, SSSR, 17, (1971).

211. Ref. 117, p.52.

212. E.M. Freeman, T. Siemieniewska, H. Marsh and B. Rand, Carbon, 8, 7, (1970).

213. F.T. Meehan, Proc. Roy. Soc., A115, 199, (1927).

214. D.H. Bangham and N. Fakhoury, IBID, A130, 81, (1930).

215. M. Folman and D.J.C. Yates, Trans. Faraday Soc., 54, 429, (1958).

216. B. McEnaney, J.C.S. Faraday Trans. I, 70, 84, (1974).

217. B. McEnaney, 14th U.S. Conf., p.7, (1979).

218. A. Bailey, D.A. Cadenhead, D.H. Davies, D.H. Everett and A.J. Miles, Trans Faraday Soc., 67, 231, (1971).

219. H. Takahashi, K. Kuroda and H. Akamatu, Carbon, 2, 432, (1965).

220. H. Honda, K. Kobayashi and S. Sugawara, Carbon, 6, 517, (1968).

221. R.H. Bragg and S. Bose, 14th U.S. Conf. (Penn. State Univ). p.189, (1979).

222. M. Inagaki, K. Hosii, S. Naka, Carbon, 13, 97, (1976).

223. J.J. Kipling and B. McEnaney, Fuel, 43, 367, (1964).

224. A. Zukal, Thesis, Inst. of Phys. Chem. Prague, (1967); Ref. 117, p.17.